Estimating operational releases of 14C and 3H of the GE-Hitachi BWRX-300 & Rolls-Royce SMR using full-core modeling in Serpent 2

Brandt, Simon; Öhrlund, Fredrik; Eriksson Stenström, Kristina

2025

Document Version:
Publisher's PDF, also known as Version of record

Faculty of Science
Department of Physics
Division of Particle and Nuclear Physics
Biospheric and Anthropogenic Radioactivity (BAR) Group

Estimating operational releases of ^{14}C and ^{3}H of the GE-Hitachi BWRX-300 & Rolls-Royce SMR using full-core modeling in Serpent 2

List of authors

Simon Brandt	simon.brandt@fysik.lu.se
Fredrik Öhrlund	fredrik.ohrlund@fysik.lu.se

REVIEWED BY: Kristina Eriksson Stenström kristina.stenstrom@fysik.lu.se

Department of Physics
Professorsgatan 1
SE-223 63 Lund

Report BAR-2025/04
Lund 2025

Estimating operational releases of ^{14}C and ^{3}H of the GE-Hitachi BWRX-300 & Rolls-Royce SMR using full-core modeling in Serpent 2

Simon Brandt, Fredrik Öhrlund
Reviewed by Kristina Eriksson Stenström

August 2025

LUND
UNIVERSITY

Foreword

This paper was written as part of a project funded by the Swedish Radiation Safety Authority SSM, aiming to estimate the impact on operational releases of ^{14}C and ^{3}H due to new nuclear power installations in Sweden. This paper is the second part of the project, aiming to estimate the operational releases from new technology whereas the first part aimed to estimate the operational releases from proven technology. The paper was written by the project assistants Simon Brandt and Fredrik Öhrlund, with Kristina Eriksson Stenström acting as project lead. Christophe Demazière, professor in reactor physics, was brought in as an expert advisor.

Abstract

The purpose of this project was to find estimates of the operational releases of ^{14}C and ^{3}H from new SMR technology that is being considered in Sweden, namely the Rolls-Royce SMR and the GE-Hitachi BWRX-300. To achieve this goal, models of the reactors of interest were made in the continuous-energy Monte-Carlo neutron and photon transport code Serpent, where the production of ^{14}C and ^{3}H could then be directly calculated. However, due to a lack of publicly available information relating to the Rolls-Royce SMR and the BWRX-300, a method was devised in which models of 2 large conventional reactors, a PWR (AP1000) and BWR (ABWR), were created in Serpent to complement the former models where necessary. The four models were then compared to find estimates of operational releases. The results showed that the operational release rate of ^{14}C normalized to power output from the BWRX-300 was 533.2 GBq·GW(e)$^{-1}$·a^{-1}, approximately 3% higher than from the conventional BWR. For ^{3}H the corresponding increase was 11% with a normalized release rate of 1045 GBq·GW(e)$^{-1}$·a^{-1}. For the Rolls-Royce SMR the ^{14}C normalized operational release rate was 263.2 GBq·GW(e)$^{-1}$·a^{-1}, approximately 1.3% higher in the SMR compared to the large conventional PWR, and the ^{3}H normalized operational release rate was 1031 GBq·GW(e)$^{-1}$·a^{-1}, at least an order of magnitude lower in the SMR compared to the large conventional PWR. This difference was due to the Rolls-Royce SMR not utilizing boron for reactivity control in contrast to most conventional PWRs. This made the Rolls-Royce SMR more comparable to the BWRs in the case of ^{3}H operational releases, and compared to the large conventional BWR, the Rolls-Royce SMR had an approximately 1.7% higher operational release rate of ^{3}H.

Contents

List of Abbreviations

ABWR - Advanced Boiling Water Reactor
ARIS - Advanced Reactor Information System
BWR - Boiling Water Reactor
CSG - Constructive Solid Geometry
GRCA - Gray Rod Control Assembly
IFBA - Integral Fuel Burnable Absorber
LEP - Lower End Plug
LTG - Lower Tie Grid
LWR - Light Water Reactor
NPP - Nuclear Power Plant
PO - Power Operation
PWR - Pressurized Water Reactor
RCCA - Rod Cluster Control Assembly
RR - Rolls-Royce
SD - Shut-Down
SINCAD - Silver-Indium-Cadmium
SMR - Small Modular Reactor
SS - Stainless Steel
UEP - Upper End Plug
UTG - Upper Tie Grid

1 Introduction

^{14}C and ^{3}H are both released in small amounts from the normal operation of Nuclear Power Plants (NPPs), a type of emission known as operational releases. Such emissions are distinct from emissions originating from e.g. fuel reprocessing and decommissioning. ^{14}C and ^{3}H are both weak β-emitters and therefore do not constitute an external radiation hazard [1]. However, monitoring of ^{14}C and ^{3}H is always necessary, as is predicting their release rates. This is because both radionuclides are easily assimilated in organic matter, and because of their relatively long half-lives[1] they have time to move and spread far from their release point[1]. It is known that operational releases of ^{14}C and ^{3}H from NPPs contribute significantly to the effective dose as well as to the collective dose to members of the public after release [2].

The present authors recently conducted a literature study on operational releases from EU-based Pressurized Water Reactors (PWRs) and Boiling Water Reactors (BWRs), resulting in the publication of a report titled "*^{14}C and ^{3}H Discharges from Pressurized Water Reactors and Boiling Water Reactors*" [3]. This report compiles life-time measurement data of operational releases of ^{14}C and ^{3}H self-reported by the European NPPs, providing a baseline for the actual operational release rates of the NPP technologies currently in operation. The report also details typical production and release pathways for ^{14}C and ^{3}H within conventional large scale Light Water Reactors (LWRs), specifically PWRs and BWRs. The results of the previous study can be found in Table 1. For further clarification on these results, see the previous study [3]. Figures 66 67, 68 and 69 in section 6.3 show the yearly variation as well as the spread in data of the ^{14}C and ^{3}H normalized release rate from European reactors, as well as how the results of the present report compare.

Table 1: Median normalized release rates [GBq·GW(e)$^{-1}$·a^{-1}] (total) of European PWRs and BWRs during the period 1995-2023 [3]. The interquartile range is in square brackets. The number of reactors included in the data composition is in the first parenthesis. The second parenthesis shows the total number of data points included in the data composition [3].

Normalized release rate (1995-2023)	PWR	BWR
Liquid ^{3}H	$1.77{\cdot}10^{4}$ [$1.43{\cdot}10^{4}$-$2.5{\cdot}10^{4}$] (107) (1030)	765 [524-1264] (18) (235)
Atmospheric ^{3}H	583 [316-983] (107) (1030)	249 [129-547] (18) (235)
Total ^{3}H	$1.83{\cdot}10^{4}$ [$1.46{\cdot}10^{4}$-$2.59{\cdot}10^{4}$] (107) (1030)	1014 [653-1811] (18) (235)
Atmospheric ^{14}C	259.7 [167.8-363.4] (99) (629)	480.8 [369.8-625.2] (18) (206)

Currently, several countries around the world are considering building new nuclear power. Small Modular Reactors (SMRs) have become a potential candi-

[1] ^{13}H = 12.3 a and ^{14}C = 5730 a

date as a new nuclear power technology to be built. This includes Sweden, where GE-Hitachi's BWRX-300, a 300 MWe SMR, and Rolls-Royce's 470 MWe SMR (here simply referred to as RR SMR) are being considered in the near future [4].

As mentioned above, the operational releases of ^{14}C and ^{3}H of any nuclear power technology should be studied and estimated before it is used. This applies to any SMR design, given that few SMRs have yet been built. It is important to understand that this applies even for SMR designs which are essentially scaled-down versions of current NPP technologies, such as the two SMRs that Sweden is currently considering. The BWRX-300 is (as the name implies) a small BWR, whereas the RR SMR is a small PWR. The reason is that operational releases of ^{14}C and ^{3}H are not expected to scale linearly with reactor size (nor power output) in neither of the two LWR technologies, at least according to an argument provided by Krall et al [5]. In fact, Krall et al claim that it is to be excepted that operational releases of ^{14}C and ^{3}H in scaled-down LWRs will be higher than in conventional large-scale LWRs when normalized to the electrical energy output. With this expectation in mind, the main objective of this report is now stated.

The purpose of the current report is to obtain estimates of the operational release rates, normalized to energy production, of ^{14}C and ^{3}H in two SMRs, namely the BWRX-300 and the RR SMR.

These estimates are obtained using detailed 3D models of both reactors in Serpent 2, where the models are based on currently publicly available information wherever possible. In order to obtain trustworthy estimates from the Serpent simulations, a methodology had to be devised which is described in chapter 3. An essential component of the methodology relies on the generation of Serpent models of two large conventional NPPs with known typical production rates of ^{14}C and ^{3}H. The SMR simulation outputs are then compared with the corresponding large-scale LWR simulation outputs. The choice of large conventional BWR is the Advanced Boiling Water Reactor, i.e. the ABWR, whereas the choice of large conventional PWR is the AP1000.

In overview, this report is structured as follows:

- Chapter 1 - Section 1.1 describes the limitations of the work presented in this report.
- Chapter 2 discusses the background motivations of this project.
- Chapter 3 describes the methodology that has been developed and then employed to generate estimates of the operational releases of ^{14}C and ^{3}H in the BWRX-300 and the RR SMR.
- Chapters 4-5 provides detailed descriptions of each of the four Serpent 2 models, taking up the bulk of this report. Chapter 4 describes the PWR

models, i.e. the AP1000 and the RR SMR. Chapter 5 describes the BWR models, i.e. the ABWR and the BWRX-300. These two chapters have been written with the goal of providing enough detail so that each model can be reproduced in Serpent.

- Chapter 6 contains the main results, providing the obtained estimates of the operational releases of ^{14}C and ^{3}H of the two SMRs.
- Chapter 7 concludes the report.

1.1 Limitations

This project uses four detailed 3-dimensional full-core Serpent models to obtain estimates of operational releases of ^{14}C and ^{3}H. Specifically, models have been produced of the AP1000, the ABWR, the BWRX-300 and the RR SMR. Only the ABWR, BWRX-300 and RR SMR models are original since the AP1000 model was made using [6].

The production of such models is not a trivial task. It requires considerable proficiency with Serpent itself. It is time-consuming, with each model requiring several thousand lines of Serpent input code. It is also time-consuming to develop because the models soon become very computational demanding, requiring the use of an HPC-cluster node for essentially all simulations. Given this a decision was made early on to constrain the ambition of the project to within reasonable levels.

It was decided that performing full-core coupled thermal-hydraulics calculations was to be avoided, opting instead to provide Serpent with at most "fixed" spatial distribution information. Such fixed/uncoupled distributions have been used for the moderator density distribution, the moderator temperature distribution, and the fuel temperature distributions. What this means is that, while continuous distributions of density and temperature exist in the models, the shapes of these distributions are currently unaffected by the Serpent outputs since there can be no feedback effects. For instance, when inserting a control blade in one of the BWRs, the axial moderator distributions along the flow channels of the assemblies belonging to the 2x2 super-cell remains unchanged. To acquire the distributions which are currently in use, several different codes or methods are used[2]. When these codes require input values, the values are taken or derived from specification sheets from the manufacturer or similar. Thus, the assemblies of each model (including the AP1000 in this case) have the same moderator density and temperature distribution, regardless of where the assembly is positioned in the core.

Another limitation present in the original models must be pointed out, one which in no small part is related to the lack of coupling/feedback. In the ABWR, BWRX-300 and RR SMR models separately, only one kind of fuel assembly is used throughout their respective core lattices. This is unlike the AP1000, which uses 9 kinds of assemblies in the core lattice. Normally, a nuclear reactor core is loaded with fuel assemblies of several different types and also at different burnup levels. Such core loading patterns are optimized to achieve many different things simultaneously. One of these is to achieve a flat volumetric power density and therefore a mostly flat neutron flux distribution throughout the core. This flattening of the neutron flux in turn affects the total neutron leakage out of the core, and as is discussed at length in chapter 2, the total neutron leakage affects the total amount of operational releases of ^{14}C and ^{3}H from the reactors.

[2] See chapter 3, chapter 4, and chapter 5 for details

Therefore, in order to generate the estimates of operational releases of ^{14}C and ^{3}H, it is desirable that the models have a critical steady-state flux that is as realistic as possible, including being flat in the typical way just described. Attempts have been made to achieve this goal by running full-core burnup simulations with a very large number of depletion zones throughout the fuel[3]. The idea was then that the initial configuration was going to "burn itself flat". Now, even though such burnup simulations did indeed flatten the flux as expected, because of the aforementioned lack of feedback effects, the reactivity of the cores increased substantially over time, a result that eventually led to the abandonment of the full-core burnup methodology.

Based on certain theoretical principles (and influenced by certain numerical results), a method was devised for flattening the flux using certain combinations of control rods in place of full-core burnup simulations. In the end, the final simulations carried out using the created Serpent models are considered appropriate for the purposes of generating estimates of operational releases of ^{14}C and ^{3}H. The method of flattening the flux using control rod insertions is described in 3.3. The results of flattening the flux using the control rod methodology can be seen in the power plots and the flux plots provided in chapter 4 and chapter 5.

Due to the complexity of the reactor systems it was not deemed reasonable to individually account for all the different pathways of the ^{14}C and ^{3}H between production and release. The amount of produced ^{14}C and ^{3}H which is released operationally varies between reactors (even those of the same model), as well as on a yearly basis. Finding a value for this metric would be beyond the scope of this project. It was therefore deemed more appropriate to compare production values of ^{14}C and ^{3}H between the models to find if there would be an increase in release rate due to a smaller reactor size. This meant however that certain aspects of the reactor systems were not taken into account, such as for example the ion-exchange resins present in the water-loop, upon which some of the produced ^{14}C accumulates (in the range of 0.6-0.8 % for BWRs, and 6-10 % for PWRs [7]).

Another example is that some material compositions have been simplified, such as for example the reactor coolant. The coolant, which has been modeled as pure H_2O, could in reality have a complicated chemistry due to intentional additions of particulates besides H_2O, adsorption from structural materials, or diffusion or leakage from fuel- or control-rods which are here not taken into account. It is also possible that certain novel designs in the real reactors could

[3]As an example, full-core burnup simulations have been carried out for the ABWR using roughly a quarter million depletion zones throughout the fuel. The simulation was continued until the desired flatness had been achieved. Because it is highly relevant to the decision to abandon this methodology, it is pointed out that the runtime of this simulation was more a week. The compute node used was equipped with 2x Xeon Platinum 8358 (-omp 128) and 1 TB of RAM. In order for this simulation to be runnable at all on this compute node, Serpent's memory optimization had to be turned off using `set opti 1`. Even then, close to all available RAM was utilized.

affect the presence of nuclides such as ^{14}N or ^{13}C in the coolant, which would have a large impact on the production of ^{14}C.

2 Background, Theory and Motivation

This chapter starts in section 2.1 by reviewing the basic facts about operational releases of ^{14}C and ^{3}H in LWRs. Then, in section 2.2, a theoretical argument is made that the operational releases of ^{14}C and ^{3}H should increase in LWRs of smaller size. Finally section 2.3 gives a brief introduction to Serpent 2, the main tool used to achieve the main objective of this report.

Further details pertaining to the arguments made in chapter 2 can be found in Appendices A2 and A3.

2.1 Operational Releases of ^{14}C and ^{3}H in LWRs

This section is intentionally kept brief and as focused as possible on the details that matter for this report. More exhaustive information is available in the referenced sources.

This report is about a certain kind of emission known as operational releases of the two particular radioactive nuclides ^{14}C and ^{3}H from two specific types of LWR, the BWRX-300 and the RR SMR. Such emissions are now described in more detail.

As was mentioned in the introduction, for an emission of a nuclide from a NPP to be considered an operational release, the nuclide must somehow be released as a direct consequence of the normal operation of the NPP. In both common types of LWRs i.e. in PWRs and BWRs, for any radionuclide under consideration to be released during normal operation, the radionuclide must first reach the coolant water in the primary loop. The operational release itself then occurs either during venting of the primary loop or because of liquid leakages or controlled discharges to water or air from the primary loop [3].

Based on [1, p. 13, 31] it can be assumed that essentially all ^{14}C and ^{3}H that reach the primary loop coolant in both types of LWRs are eventually released into the environment. A crucial fact for this report as a whole is that the causes of operational release, i.e. the venting and the leaking of coolant, are both independent of the size of the reactor core, and are instead associated with the LWR-technology in general and the associated systems. Therefore, this fact is expected to be essentially unchanged in the two SMRs under consideration, i.e. in the BWRX-300 and the RR SMR, as compared to a conventional large-scale BWR and PWR, respectively.

In LWRs the production pathways of ^{14}C and ^{3}H are few and almost identical for both reactor types. The major sources of operationally released ^{14}C and ^{3}H are listed below. Note that this list constitutes the bare minimum of physical phenomena that must be faithfully captured in any numerical simulation that

purports to estimate the operational releases in typical LWRs.

1. The only non-shared production pathway that leads to significant operational releases is the production of ^{3}H in PWRs due to irradiation of boron which is typically dissolved in the reactor coolant. This production pathway contributes a large fraction of all operationally released ^{3}H from typical PWRs [1]. This production pathway is entirely absent in both the BWRX-300 and the RR SMR[4].

2. In both types of LWRs, one production pathway that leads to operationally released ^{3}H stems from ternary fission inside the nuclear fuel. Almost every other nuclide produced in fission is entirely contained inside the sealed fuel rod cladding. This is true for the vast majority of ^{3}H as well. However, as an isotope of hydrogen, the smallest nuclide that exists, it is therefore very hard to contain and a considerable amount of the ternary fission ^{3}H escapes the fuel rods by diffusing through the cladding and into the coolant water [8].

3. In both types of LWRs, a major production pathway that leads to significant amounts of operational releases of both ^{14}C and ^{3}H is by the direct irradiation of the coolant water. Molecules of water consist of two hydrogen nuclei and one oxygen nuclei. These elements appear in the water with their respective natural isotopic distribution. Crucially, a small fraction of the hydrogen is actually ^{2}H i.e. deuterium, and likewise, a small fraction of the oxygen is ^{17}O. In LWRs therefore, ^{3}H and ^{14}C will be produced directly in the coolant water itself when it is irradiated by neutrons, since such irradiation of ^{2}H and ^{17}O generates ^{3}H and ^{14}C with respective cross-sections of 0.506 mbarn [9] and 0.235 barn [7]. Note also that ^{2}H is produced when ^{1}H is irradiated, with a cross section of 0.333 barn [9]. In the coolant there are also trace elements of other nuclides present which contribute to the total production of ^{14}C, such as ^{14}N and ^{13}C. These nuclides, similar to ^{17}O, have a relatively high cross-section for producing ^{14}C when irradiated by neutrons, with thermal cross-sections of 1.82 barns and $1.37{\cdot}10^{-3}$ barns respectively [7] (see Table 2 for all stated cross-sections). The exact amount of these nuclides present in the coolant is difficult to establish, and as presented in [7], the vast majority of the ^{14}C production is due to irradtiation of ^{17}O, not ^{14}N or ^{13}C, see Table 3. For the sake of simplicity it was therefore decided to not include ^{14}N and ^{13}C in the reactor coolant.

[4]This absence is expected in the BWRX-300 as boron is typically not used in BWRs during normal operation. The absence of dissolved boron in the small PWR-style RR SMR is however more of a novelty.

Table 2: Thermal cross-sections the most important reactions taking place in the reactor coolant [7][9].

Neutron-induced reaction	Thermal cross-section (barn)
^{2}H(n, γ)^{3}H	$0.506{\cdot}10^{-3}$
^{1}H(n, γ)^{2}H	0.333
^{17}O(n,α)^{14}C	0.235
^{14}N(n, p)^{14}C	1.82
^{13}C(n, γ)^{14}C	$1.37{\cdot}10^{-3}$

Table 3: Calculated production rates of ^{14}C (Bq s^{-1}) in the a 2500 MW$_{th}$ BWR and PWR due to neutron irradiation of ^{17}O and ^{14}N. For the BWR a concentration of 0.1 ppm N_2 in the feedwater was used, and for the PWR a concentration of 0.54 ppm N_2 in the reactor coolant was used [7].

	BWR 2500 MW$_{th}$			PWR 2775 MW$_{th}$		
	Production rate (Bqs^{-1})			Production rate (Bqs^{-1})		
	Thermal	Epithermal	Fission	Thermal	Epithermal	Fission
^{17}O	$8.4{\cdot}10^{3}$	770	$6.5{\cdot}10^{3}$	$3.4{\cdot}10^{3}$	$1.1{\cdot}10^{3}$	$5.8{\cdot}10^{3}$
^{14}N	2.7	0.25	0.10	47	16	4.0
Fraction from ^{14}N	0.02%			0.65%		

Besides the listed production pathways, there is also a significant amount of ^{14}C produced in structural materials such as the reactor vessel of both types of LWR, and a significant amount of ^{3}H produced in the boron control rods used in BWRs. The diffusion of ^{14}C and ^{3}H into the coolant from these pathways is however expected to be small compared to what is listed above.

The production of ^{14}C and ^{3}H directly in the coolant is going to be the primary topic of discussion for the upcoming two sections. This is because it is this production pathway that is expected to increase substantially in the BWRX-300 and RR SMR in comparison to the same production pathway in conventional large-scale LWRs of the respective type.

2.2 Higher operational releases of ^{14}C and ^{3}H per unit energy production in scaled-down LWR type SMRs

The last item of the list in section 2.1 of sources of operationally released ^{14}C and ^{3}H from LWRs is expected to increase in importance when the size of the LWR is scaled down. This expected increase should occur because of a non-linearly increasing neutron leakage, resulting in correspondingly increasing irradiation of the coolant surrounding the LWR. This has been claimed by Krall et al and their argument can be found in [5, Appendix 01]. In this section, the result

of a new argument to the same effect is provided. The derivations underlying this result can be found in Appendix A2 which differs slightly in appearance but is very similar in spirit to that of Krall et al. The argument is based on basic reactor theory. Please keep in mind that to justify applying the argument provided here to the two SMRs under consideration, the production pathways listed in section 2.1 are essential, as are the following two premises:

- For several technical reasons, such as to avoid xenon-135 poisoning of the core, LWRs are typically operated in steady-state conditions at all times. It is assumed that the BWRX-300 and the RR SMR will be operated in steady-state conditions also.
- It is assumed that any SMR which is a scaled-down version of a conventional large-scale LWR will use the same kinds of fuel assemblies as would a corresponding large-scale LWR. This is true for both the RR SMR, which uses modified RFA 17x17 PWR fuel assemblies [10], and for the BWRX-300, which uses GNF2 assemblies [11]. Both the RFA 17x17 assembly and the GNF2 assembly are already in widespread use in operating PWRs and BWRs around the world. As a consequence, relevant material properties such as enrichment levels, spatial enrichment variations, coolant-moderator-fuel ratios and thermal-hydraulic properties should be comparable in the SMRs and LWRs.

In Appendix A3 it is found that the net leakage out of the system per unit (thermal) energy production can be expressed as a function of the geometric parameters α and R as

$$l(\alpha, R) \equiv \frac{Leakage(\alpha, R)}{Power(\alpha, R)} = \frac{D}{\kappa \Sigma_f} \left(j_0^2 + \frac{\pi^2}{\alpha^2} \right) \frac{1}{R^2} \tag{1}$$

Clearly, as long as the homogenized and condensed material properties D, κ and Σ_f are approximately constant in the core radius R, and for fixed height-to-radius ratio $\alpha := \frac{H}{R}$ of the core, the energy-normalized leakage grows quadratically with decreasing size. For instance we find that $l(\alpha, \frac{1}{x}R) = x^2 l(\alpha, R)$, where x can be interpreted quite naturally as the factor by which the reactor size is decreased.

The derivation provided in Appendix A2 leading to equation 1 is deemed to be overall sound. Based on this argument together with the argument by provided by Krall et al that reaches the same conclusion, the expectation of higher operational releases of ^{14}C and ^{3}H in LWR-SMRs due to higher energy-normalized irradiation of the coolant surrounding the reactor core is therefore considered to be well motivated.

In Appendix A3, a critique of the derivations provided in Appendix A2 is given, which thereby constitute a critique of the obtained result itself, namely equation 1. At the end of Appendix A3 the choice to use Serpent 2 to obtain the sought estimates of ^{14}C and ^{3}H is subsequently motivated.

2.3 On the use of Serpent 2 full-core model simulations to estimate operational releases of ^{14}C and ^{3}H from the BWRX-300 and RR SMR

Serpent is described on the official website as "a Continuous-energy Monte Carlo neutron and photon[5] transport code" and is used in this project to simulate the neutronics of the nuclear reactors under consideration.

The exact methodology using Serpent models to obtain estimates of the operational releases of ^{14}C and ^{3}H in the BWRX-300 and RR SMR is the topic of the next chapter, chapter 3. Here, a brief description of how Serpent works is provided. Emphasis is placed on certain aspects of Serpent that matter for physical accuracy and which have guided the creation of the models used in this report.

Serpent simulates individual neutrons as they move through a physical system. A neutron spawns with some position and velocity pair $(\vec{\mathbf{r}}, \vec{\mathbf{v}})$ corresponding to some neutron generating nuclear interaction, such as a fission event. The next neutron state is then found from a stochastic process where the total distance traveled until the next interaction is sampled. This sampling involves the nuclear cross section data of the materials filling the spatial regions traversed by the neutron. The new neutron state will be expressable as $(\vec{\mathbf{r}} + s\hat{\mathbf{\Omega}}, \vec{\mathbf{v}})$, where $\hat{\mathbf{\Omega}} = \hat{\mathbf{v}}$ is the standard notation. Then, the interaction itself takes place. The interaction type is stochastically sampled among the list of possible interactions with the material currently being traversed by the neutron. This could be some interaction which consumes the neutron, such as an absorption event. Another possibility could be a scattering interaction, where the neutrons velocity is changed. The neutron is then moved to the next sampled interaction position, and the loop begins anew, terminating whenever the neutron disappears, either due to being absorbed or by moving out of the boundaries of the system. Such an individual neutron life-time including all its interactions is referred to as a neutron history, and it is by generating many such neutron histories that Serpent can tally stochastically the physical properties of the physical system in question.

An important feature of the probabilistic results that Serpent outputs is that by simply simulating more neutron histories, it is always possible to increase the expected level of convergence of the results arbitrarily. Now, other than statistical convergence, what else could lead to erroneous results when trying to estimate operational releases of ^{14}C and ^{3}H using Serpent? It is assumed that Serpent models neutron physics with sufficient fidelity[6] to not produce errors of any relevance. This leaves two possible sources of error that the user can influence. The user must provide Serpent with a nuclear data library, and in

[5] No photon has been simulated when making this report.

[6] In this project, Serpent is set up with all options for maximum physical fidelity. Examples are `set ures 1` and `set egrid 0.0 1.0E-11 100.0`.

this project the choice has been JENDL-4.0. The reasons for using this nuclear data library can be found in Appendix A1.

The main way that the user can influence what level of physical accuracy Serpent can achieve is also what the user spends almost all their time doing when writing any Serpent input file: defining the geometric and material properties of the physical system to be simulated. As Serpent uses Constructive Solid Geometry, or CSG, the user could in principle provide arbitrary levels of geometric detail.

The goal when creating the models used in this report can be described as follows. By creating finely detailed models of the nuclear reactors under consideration, including the finely detailed geometry of the components directly surrounding the active fuel, the total irradiation of all the coolant in the nuclear reactor can be simulated in such a way that any geometric effect is automatically taken into account, resolving all of the issues brought up in Appendix A2 and A3.

Note how this naturally makes it possible to capture the absolute irradiation of the entirety of the coolant in an LWR, including any coolant surrounding the core. This is because a detailed model of a full core including structural components surrounding the core allows Serpent to simulate neutrons that move out of the active core and into the surrounding coolant, i.e. the neutron leakage. Any effects related to the size of the nuclear core will of course also be faithfully captured by such a simulation as an emergent effect, without the user having to do anything special other than ensure that the core geometry is physically accurate and detailed. This consideration has strongly influenced the level of detail of certain geometric components in the BWRX-300 and the ABWR, specifically lower and upper parts of the fuel assemblies (the same level of detail was not applied to the RR SMR and the AP1000).

As the last topic of chapter 2, the issue of estimating the operational releases of ^{3}H that originate from ternery fission in the fuel must be discussed. Serpent is able to simulate the amount of ^{3}H produced in the fuel using the built-in burnup routine. However, Serpent is not capable of simulating the diffusion of ^{3}H through fuel rod cladding. Such diffusion can however be obtained from only the production rate, as long as the typical fractional amount of ^{3}H that diffusses through the cladding is known. This is how such diffusion is calculated in this report. The diffusion fractions used in this report can be found in chapter 3, where the methodology employed to obtain these numbers is described as well.

3 Methodology

As stated in chapter 1, the main objective of this report is to generate estimates of the operational releases of ^{14}C and ^{3}H in the BWRX-300 and in the RR SMR. The purpose of this chapter, chapter 3, is to describe the methodology that has been developed in order to achieve this main objective.

As mentioned in the previous chapter, one way of achieving this objective is through high-resolution 3-dimensional full-core simulations in a software such as Serpent 2. Doing so requires making a model of the reactors that are to be simulated. Given that the publicly available information of the reactors of interest is incomplete, crafting a model of them without any further input would be a difficult task, and any results derived from such a model would be doubt-worthy.

It was thus deemed necessary to make models of not only the reactors of interest, the RR SMR and the BWRX-300, but also a typical large PWR and BWR. The reactors that were chosen, the AP1000 and the ABWR, both had some similarities to the reactors of interest, and could also be used to fill in the gaps in information. Since Serpent is unable to account for diffusion through the cladding or leakage of ^{14}C and ^{3}H from the primary loop, what was achievable then was to roughly estimate the production of ^{14}C and ^{3}H during a typical mode of operation. By comparing the results of the larger reactors to the reactors of interest it would then be possible to give an estimate of the increase in *production* of ^{14}C and ^{3}H due only to the smaller physical size of the reactor. Given that the release rate is proportional to the production rate (in this report it is assumed that the proportionality is 1, based on [1, p.13, 31], though this is a simplification), an estimate of the release rate could then be calculated.

The methodology is therefore given as follows:

- Make models in Serpent of the AP1000 and the ABWR based on publicly available information as well as previous studies, and ensuring that the criticality of the models is within 120 pcm of $k_{eff} = 1$.
- Make models of the RR SMR and the BWRX-300 based on publicly available information where it is possible, and fill in the gaps with information from the AP1000 and ABWR models, ensuring again that the criticality of the models is within 120 pcm of $k_{eff} = 1$.
- Perform a burnup simulation for each of the 4 models, which calculates the production of ^{14}C and ^{3}H in the coolant and fuel due to the neutron reactions taking place. A 1 second burnup step was chosen for this purpose to minimize ^{3}H decay. Burnup in Serpent is usually performed on the fuel materials in order to find the fuel composition after a certain amount of burnup cycles, but here it was done on the coolant as well. Since the models have a discreet 90° rotational symmetry, where each 90° section is made up of 2 identical (mirrored) 45° sections, the number of

simulated neutron histories can be increased eightfold by using reflective boundary conditions corresponding to these symmetries. This means that even though the transport and burnup simulations were performed using 125000 neutrons per cycle for 500 active cycles, for a total of $6.25 \cdot 10^7$ neutron histories, the total effective number of neutron histories is $5 \cdot 10^8$.

- Find the normalized production rate of ^{14}C and ^{3}H in all 4 models. The normalization was done by taking the activity of ^{14}C and ^{3}H that was produced during the 1 second burnup step and dividing with the power (energy produced during 1 second). The resulting value was then multiplied by the number of seconds in a year to get the production rate per energy unit per year, presented in the unit GBq$\cdot$GW(e)$^{-1}\cdot$a^{-1}.
- Compare the results of the previous step and calculate the increase of normalized production rate due to decreased reactor dimensions.
- Estimate the normalized release rate by applying the increase to known release rates of traditional large PWRs and BWRs from [3].

The models were created using Dell Latitude 7450 laptops, however all simulations were run on a cluster node with two Intel(R) Xeon(R) Platinum 8358 CPUs with 1 TB of RAM. All simulations were run using the JENDL-4.0 nuclear data library (see appendix A1 for motivation).

3.1 Fuel temperature gradients

The fuel material has a high gradient both axially and radially within a fuel rod. This can be seen for example by solving the heat conduction equation within the fuel pins. A MATLAB-script was provided by Christophe Demaziere [12] which did exactly this for a single fuel rod in an infinite lattice using the following inputs:

- Height fuel rod H.
- Number of axial regions N.
- The outer radius of the fuel material R_{fo}.
- The inner radius of the cladding R_{ci}.
- The outer radius of the cladding R_{co}.
- Fuel rod pitch p.
- Mass flow rate of coolant G_m.
- Coolant inlet/outlet temperature T_{in}/T_{out} (only for PWRs).
- Slip ratio s at the inlet and outlet (only BWRs).
- Void fraction at the outlet (only BWRs).

- Pressure of the coolant at the outlet P_{out}.

The script outputs the axial fuel temperature distribution at different radial distances from the fuel centerline, as well as the radial temperature distribution at half the height of the fuel rod. The script was further adjusted to calculate the radial temperature distribution at 26 points along the height of the fuel rod. These radial distributions were then averaged and normalized by area to obtain the radially averaged axial temperature distribution.

3.2 Diffusion of ^{3}H from fuel rods

It is assumed that some of the ^{3}H that is produced by ternary fission in the fuel rods diffuses out through the Zircaloy cladding. The exact amount of diffusion is difficult to determine as it depends on a number of factors such as the composition of the Zircaloy, the thickness, the temperature, the density and pressure of the system etc. Westerly and Philips [8] state that estimates of the diffusion through Zircaloy cladding in LWRs range from 0.013% to 1% of the ^{3}H from ternary fission. For PWRs which utilize boron as a burnable absorber in the coolant, the ^{3}H from ternary fission does not constitute a major part of the ^{3}H discharges, and so the amount of diffusion is not as important. For BWRs however, the ^{3}H from ternary fission constitutes the vast majority of the ^{3}H discharges.

In this project the factor of produced tritium which diffuses through the cladding was estimated by using the relationship between released ^{3}H and ^{14}C from BWRs which was found in [3], and which can be seen in Table 1. Since both radionuclides are discharged through the coolant, the ratio between them should be the same in the coolant as in the discharges. From European BWRs, the median release rate of ^{3}H during the period 1995-2023 was 1014 GBq·GW(e)$^{-1}$·a^{-1}, while the median release rate of ^{14}C during the same period was 480.8 GBq·GW(e)$^{-1}$·a^{-1}, meaning the release rate of ^{3}H was approximately 2.109 times the release rate of ^{14}C. By applying this factor to the results of the ABWR Serpent model, the total amount of produced ^{3}H that ends up in the coolant can be found by multiplying with the ^{14}C production in the coolant. By subtracting the ^{3}H that is produced in the coolant from the total, the amount of ^{3}H that needs to diffuse through the cladding can be found. By dividing this number with the production in the fuel, the diffusion factor for the ABWR model can be found. Since the ABWR and BWRX-300 models are very similar, the same diffusion factor likely applies. The above method can be summarized in equation 2.

$$D_{^3\mathrm{H},cladding} = \frac{\kappa \cdot P_{^{14}\mathrm{C}} - P_{^3\mathrm{H},coolant}}{P_{^3\mathrm{H,fuel}}} \tag{2}$$

where $D_{^3\mathrm{H},cladding}$ is the factor of tritium diffusing through the cladding into the coolant, κ represents the ratio between total ^{14}C and ^{3}H that ends up in the coolant, while $P_{^{14}\mathrm{C}}$ is the production of ^{14}C in the coolant, $P_{^3\mathrm{H},coolant}$ is

the production of ^{3}H in the coolant and $P_{^3\mathrm{H},fuel}$ is the production of ^{3}H in the fuel. The production values can be found with Serpent, while κ was found from previous data [3].

Unfortunately the same method could not be applied to the AP1000 Serpent model due to the fact that the coolant ^{3}H production was severely affected by the constant boron concentration that was used. Since the ^{14}C production is unaffected by the boron concentration, the ratio between ^{3}H and ^{14}C is not constant. Instead, the same diffusion factor as in the BWRs was also applied to the PWRs. This was not expected to impact the results from the AP1000 in a meaningful way, and in the RR SMR model there are likely larger uncertainties from other sources.

3.3 Method for power flattening

The loading pattern of any real nuclear reactor is always optimized to achieve (amongst other things) a flat volumetric power density throughout the core (see section 1.1). The way such flattening is achieved in the models in this report is not by designing several different fuel assemblies, but by the use of control rods. This applies to the ABWR, the BWRX-300 and the RR SMR, whereas the AP1000 doesn't require any adjusments to achieve flattness. Furthermore, the exact method to achieve flattness is different in the three reactors.

The ABWR is by far the largest reactor core that has been modeled, having 872 individual fuel assemblies, a diameter well over 5 meters, and 205 control rods that can be used. What this means in practice is that the shape of the radial component of the steady-state flux of the ABWR core with All Rods Out (ARO) is well approximated by $J_0(r)$, the zeroth order Bessel function of the first kind[7]. Furthermore, because of the large number of control rods present in the core, it is possible to insert radial groups/banks of control rods at many different radial coordinates sparsely, meaning every inserted rod is surrounded by 2x2 super-cells without any control rod present. The method to flatten the power in the ABWR is based on the idea that the relative amount of insertion of a bank of control rods as compared to the other control rod banks should depend on its radial coordinate r according to $J_0(r)$. This idea came from theoretical considerations, of course, but also from looking at the simulation outputs for the ABWR with ARO, where the $J_0(r)$-shape of the power and flux is very apparent. More could be said about this method, but for brevity this is left out. Instead it is pointed out that this method has worked quite well in the sense that it has made it very easy achieve both criticality and reasonably flat power simultaneously. The results of the method can be seen in the power and flux plots for the ABWR in chapter 5.

[7] This is well known within reactor physics. Relevant references can be found in Appendix A2.

The BWRX-300 has used the same method as the ABWR as a starting point. Because of the significantly smaller size of the BWRX-300 however, this method could only be used as a starting point. To obtain the final control rod insertion configuration, considerable amounts of manouvering of the rods by hand was necessary. The final results can be seen in the power and flux plots for the BWRX-300 in chapter 5.

The RR SMR control rod insertion configuration was arrived at entirely by hand. The results can be seen in the power and flux plots for the RR SMR in chapter 4.

4 PWRs

Due to the limited publicly available information on RR SMR, several assumptions regarding the geometry and materials used were necessary when constructing the RR SMR model. From the information that was available for the RR SMR (mainly in the document [10]) it was clear that it used fuel assemblies similar in design to the 17x17 RFA assembly developed by Westinghouse, but with a shorter length [10]. It was also stated that it took some design elements from the AP1000 reactor design, such as the inclusion of ZIRLO material for the fuel cladding [10]. Since the AP1000 reactor design also uses a fuel assembly which is similar to the 17x17 RFA assembly [13], it was thus assumed that the AP1000 and the RR SMR are also similar. A model of the AP1000 could be recreated from the work by a research team at the Warsaw University of Technology [6]. Several features of this model were then used to create a model of the RR SMR. The following chapters will therefore describe the common design elements used in both reactor models, as well as the ones that are unique to each reactor.

4.1 Materials

In Serpent, materials have to be defined by specifying at the very least their density and atomic composition. To take Doppler-broadening into account, also the temperature of the material should be included. For most materials in the AP1000 model, these parameters were specified in [6].

The fuel material in the AP1000 reactor is uranium dioxide (UO_2). The fuel material was assumed to have a density of 10.4668 g/cm^3, which is 95.5% of the theoretical density of 10.96 g/cm^3 (this decision was made by the authors of [6]). In the reactor there are fuel pellets with 5 different ^{235}U enrichments: 1.58%, 2.35%, 3.2%, 3.4% and 4.45%. In the paper [6], different compositions with or without ^{17}O and ^{234}U were given, but only the composition with both of these nuclides included has been used for the Serpent model in this project. Since ^{18}O data was not available in the nuclear data libraries, the authors of the paper [6] exchanged this nuclide for ^{16}O in the compositions (this was also done for the oxygen in the water). The ^{234}U content in the materials was assumed to be 0.8% of the ^{235}U content. The resulting compositions for the different ^{235}U enrichments is given in Table 4. The same fuel compositions were assumed for the RR SMR model.

Table 4: Isotopic composition of the UO_2 fuels in the AP1000 reactor model [6]. The same fuel compositions were assumed for the RR SMR model.

	Enrichment [wt% ^{235}U]				
	1.58	2.35	3.2	3.4	4.45
Isotope	Atomic density [atoms/barn-cm]				
^{234}U	3.00079049E-06	4.46314840E-06	6.07739953E-06	6.45721721E-06	8.45122188E-06
^{235}U	3.73498192E-04	5.55512910E–04	7.56433261E–04	8.03707877E–04	1.05189486E–03
^{238}U	2.29688057E–02	2.27873770E–02	2.25871035E–02	2.25399811E–02	2.22925932E–02
^{16}O	4.66728670E–02	4.66769622E–02	4.66814827E–02	4.66825463E–02	4.66881303E–02
^{17}O	1.77424316E–05	1.77439883E–05	1.77457068E–05	1.77461111E–05	1.77482338E–05

As the AP1000 and RR SMR are LWRs they use light water as coolant and moderator. In addition, in the AP1000 model, boron (in the form of boric acid, $B(OH)_3$)) is added to the water to compensate for excess reactivity and maintain the reactor in a critical state for a longer period of time. The isotopic composition of the water/boron that was used in the model can be found in Table 5 [6]. Serpent was used to find the optimal amount of boron in the water of the recreated model for the core to be critical (k=1), which we found to be 940 ppm boron. The water is pressurized at 15.5 MPa and according to [6] its temperature varies between 260-315°C between the inlet and outlet of the core for hot conditions. However, the source that is pointed to for this statement [13] does not agree with the temperature range. Instead, the range 535-616.4°F (280-325°C) is stated. Therefore this range has been used for the Serpent model used in this report.

Table 5: Isotopic composition of the water/boron used in the AP1000 reactor model, given as an atomic fraction per atom of element/molecule [6].

Atomic fraction of isotope per atom of element/molecule		
Isotope	Water	Boron
^{1}H	1.999688520	-
^{2}H	0.000311480	-
^{16}O	0.9996210	-
^{17}O	0.0003790	-
^{10}B	-	0.1990
^{11}B	-	0.8010

In some fuel rods in the AP1000 model there is an addition of Integral Fuel Burnable Absorber (IFBA) coated on the UO_2 fuel pellets to compensate for excess reactivity in the beginning of a new fuel cycle. The IFBA material is made of ZrB_2 with a density of 5.42 g/cm^3. Another material which serves the same function but in another form is the borosilicate glass tubes (B_2O_3-SiO_2) used in the Pyrex rods. The Pyrex rods are inserted into the reactor in the same positions as the control rods, but are not moved during operation. The Pyrex

rod material has 12.5 wt% of B_2O_3 and a density of 2.299 g/cm^3. The IFBA and Pyrex rod materials can be found in Table 6. The RR SMR was assumed to not contain any IFBA or Pyrex rods.

Table 6: IFBA and Pyrex material compositions in terms of weight fraction of each isotope/element [6]. In the cases where only the element is given, the natural abundance of each isotope of that element is used.

	IFBA	Pyrex
Isotope/Element	Weight fraction	
^{10}B	0.0187	0.00699
^{11}B	0.1713	0.03207
^{90}Zr	0.416745	-
^{91}Zr	0.090882	-
^{92}Zr	0.138915	-
^{94}Zr	0.140778	-
^{96}Zr	0.02268	-
O	-	0.53902
Al	-	0.01167
Si	-	0.37856
K	-	0.00332
Na	-	0.02837
Density [g/cm^3]	5.42	2.299

Instead, some fuel rods in the RR SMR model contain the burnable absorber gadolinium in the form Gd_2O_3. It was assumed that only fuel rods with the ^{235}U enrichment 4.45 % contained gadolinium (in the BWR models, only the rods with the highest level of enrichment contained gadolinium so the same was assumed for RR SMR). No information could be found for the density of Gd_2O_3 at 900K, which was the assumed fuel temperature. Therefore Serpent was used to mix the constituents at this temperature. This way a composition and density for Gd_2O_3 could be found, though in hindsight this may not have been the best way of doing so. The resulting Gd_2O_3 composition, which had a density of 7.48 g/cm^3, was mixed with the fuel described above in the ratio 6 wt% Gd_2O_3 and 94 wt% UO_2 to yield the composition in Table 7.

Table 7: Isotopic composition of the Gd poisoned fuel material used in the RR SMR model.

Isotope	Atomic density [atoms/barn-cm]
^{16}O	3.84947E-02
^{17}O	1.46336E-05
^{18}O	2.53946E-07
^{152}Gd	4.18017E-06
^{154}Gd	4.55637E-05
^{155}Gd	3.09335E-04
^{156}Gd	4.27842E-04
^{157}Gd	3.27100E-04
^{158}Gd	5.19179E-04
^{160}Gd	4.56895E-04
^{234}U	6.94573E-06
^{235}U	8.64511E-04
^{238}U	1.83214E-02
Atomic density [atoms/barn-cm]	5.97926E-02

Surrounding the UO_2 fuel pellets in the fuel rods is a cladding made of ZIRLO^{TM} material designed by Westinghouse. It is a modification to the traditional Zircaloy-4 alloy often used as fuel cladding, which includes Niobium in the composition. Besides fuel cladding, the ZIRLO material is also used for instrumentation- and guide-tubes. The density of the ZIRLO material was in the paper [6] assumed to be the same as Zircaloy-4 which has a density of 6.55 g/cm^3. The composition of the ZIRLO material can be found in Table 8. The ZIRLO material is also used in the RR SMR [10].

Table 8: Composition of the ZIRLO material given as elemental weight fractions [6]. The natural abundance of each element isotope was used.

Element	Weight fraction
Sn	0.0067
Fe	0.001
Nb	0.01
O	0.0012
Zr	0.9811
Density [g/cm^3]	6.55

Also acting as neutron absorbers in the reactor are the control rods. In the AP1000 reactor the absorbing material in the control rods is Ag-In-Cd (Silver-Indium-Cadmium) also known as SINCAD. It has an assumed density of 10.159 g/cm^3, and composition found in Table 9 [6]. The RR SMR model also contained control rods with the SINCAD material, but it also has an additional control rod type which instead uses boron-carbide (B_4C) as neutron absorber. This is a

standard material available in Serpent which uses the composition and density given in [14]. The composition can be found in Table 10.

Table 9: Isotopic composition of the SINCAD material used in control rods in the AP1000 model [6], given in terms of atomic density.

Isotope	Atomic Density [atom/b-cm]
^{107}Ag	2.3523E-02
^{109}Ag	2.1854E-02
^{113}In	3.4291E-04
^{115}In	7.6504E-03
^{106}Cd	3.4019E-05
^{108}Cd	2.4221E-05
^{110}Cd	3.3991E-04
^{111}Cd	3.4835E-04
^{112}Cd	6.5669E-04
^{113}Cd	3.3257E-04
^{114}Cd	7.8188E-04
^{116}Cd	2.0384E-04
Density [g/cm^3]	10.159

Table 10: Material composition of the B_4C material used in the RR SMR model.

Isotop	Weight fraction
^{10}B	1.44242E-01
^{11}B	6.38368E-01
^{12}C	2.14872E-01
^{13}C	2.51831E-03
Density [g/cm^3]	2.52

Two types of structural steel have been used in the AP1000 and RR SMR models. Type 304 SS (Stainless Steel) was used for cladding in control- and Pyrex-rods as well as neutron absorbing material in some control rods. It was also used for the core shroud and core barrel. The assumed density of SS-304 was 7.889 g/cm^3, and the isotopic composition can be found in Table 11.

Table 11: Isotopic composition of Type 304 SS structural steel material used in the AP1000 and RR SMR models [6], given in terms of number density.

Isotope	Number density [atom/b-cm]
^{28}Si	9.5274E–04
^{29}Si	4.8400E–05
^{30}Si	3.1943E–05
^{50}Cr	7.6778E–04
^{52}Cr	1.4806E–02
^{53}Cr	1.6789E–03
^{54}Cr	4.1791E–04
^{55}Mn	1.7604E–03
^{54}Fe	3.4620E–03
^{56}Fe	5.4345E–02
^{57}Fe	1.2551E–03
^{58}Fe	1.6703E–04
^{58}Ni	5.6089E–03
^{60}Ni	2.1605E–03
^{61}Ni	9.3917E–05
^{62}Ni	2.9945E–04
^{64}Ni	7.6261E–05
Density [g/cm^3]	7.889

The low carbon steel type SA-508 Cl. 3 was used as the material for the reactor pressure vessels, with an assumed density of 7.85 g/cm^3. The elemental composition of this material can be found in Table 23.

Table 12: Elemental composition of the low carbon SA-508 Cl. 3 structural steel material used in the AP1000 and RR SMR models [6] given as weigth fraction of each element. The natural abundance of each isotope was used in the model.

Element	Weight fraction
C	0.0019
Si	0.0008
Mn	0.0135
P	0.00006
S	0.00002
Ni	0.0082
Cr	0.0017
Mo	0.0051
Fe	0.96872
Density [g/cm^3]	7.85

Lastly, air and helium gas was used to model gaps in the geometries (inside control- and fuel-rods). For air, the natural composition seen in Table 13 was

used [6], and the density was calculated for the pressure 15.5 MPa and temperature 576.55K (approximate temperature of the water) to be approximately 0.09230 g/cm^3. The helium was modeled as consisting of only ^{4}He with mass density 0.001598 g/cm^3.

Table 13: Elemental composition of the air used in the AP1000 and RR SMR reactor models, given as a weight fraction [6]. The natural abundance of each isotope was used for each element in the table.

Element	Weight fraction
C	0.000124
N	0.755268
O	0.231781
Ar	0.012827
Density [g/cm^3]	0.09230

4.2 Fuel Rods

The fuel assembly geometries were modeled in Serpent by first defining axially infinite 2D pins described as circularly symmetric cylinders with annular regions made of different materials. These were then stacked on top of each other to create the 3D rods, and arranged in assemblies. Below, the pin definitions are first described, followed by an explanation of how these were stacked to create the different rods in the fuel assembly.

4.2.1 Pin Geometries

In the AP1000 model there are 2 different types of fuel pins; regular and IFBA coated. The regular fuel pins are made up of a central circular core of UO_2 which has a radius of 0.409575 cm, surrounded by a 0.008255 cm layer of helium. The outermost annular region is made up of ZIRLO cladding with a thickness of 0.05715 cm [6]. The basic pin geometry and dimensions, which in the Serpent model is surrounded by water, can be seen in Figure 1. Since there are 5 levels of ^{235}U enrichment in the UO_2 pellets, there are 5 variations of the basic fuel pin. The same fuel pin geometries were assumed for the RR SMR model.

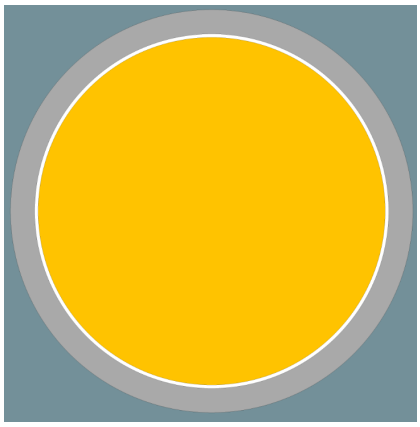

Material	Radius (cm)
UO_2 fuel	0.409575
He gap	0.417830
ZIRLO cladding	0.474980

Figure 1: AP1000 and RR SMR fuel rod geometry and dimensions.

The IFBA fuel pins are similar to the basic pins, except that outside the central UO_2 region there is an additional annular region with thickness 0.002580 cm made of the IFBA coating previously described. The helium gap thickness is thus decreased to 0.005675 cm. The IFBA fuel pin geometry and its dimensions can be seen in Figure 2. For the IFBA pins, only 3 of the ^{235}U enrichments are used, meaning there are 3 variations of this pin.

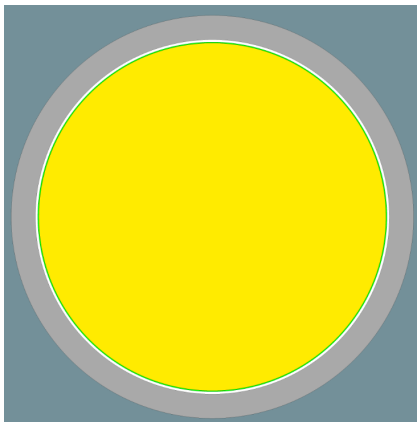

Material	Radius (cm)
UO_2 fuel	0.409575
IFBA coating	0.412155
He gap	0.417830
ZIRLO cladding	0.474980

Figure 2: AP1000 IFBA rod geometry and dimensions.

Each fuel assembly contains 24 guide tubes, which may in turn contain a neutron absorbing rod of some kind. The guide tubes can be described as a tube filled with water, with an inner radius of 0.56134 cm, and an outer radius of 0.61214 cm. Figure 3 shows the guide tube and its dimensions.

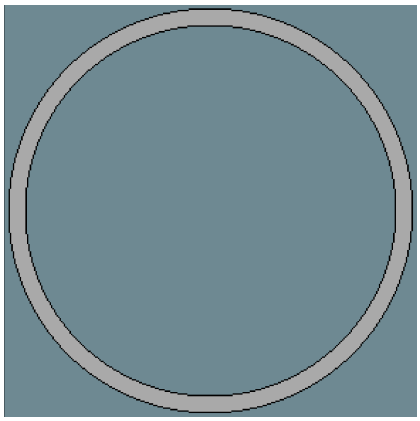

Material	Radius (cm)
H_2O	0.56134
ZIRLO	0.61214

Figure 3: AP1000 and RR SMR guide tube geometry and dimensions.

The Pyrex rods can be inserted into the guide tubes, but unlike control rods they are not moved during operation. They are best described as a small tube filled with air inside of a large tube filled with the Pyrex material described above. Figure 4 shows the Pyrex pin geometry (Pyrex rod inside a guide tube) and dimensions. The Pyrex rods are only included in the AP1000 model and not the RR SMR model.

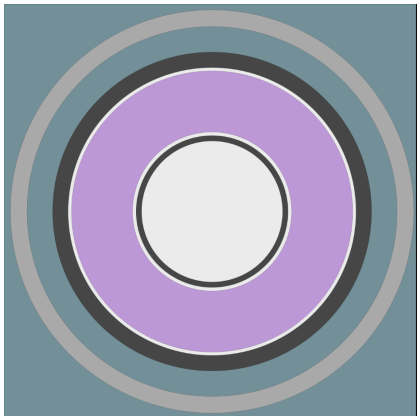

Material	Radius (cm)
Air	0.213995
SS-304	0.230505
Air	0.241300
Pyrex	0.426720
Air	0.436880
SS-304	0.483870

Figure 4: AP1000 Pyrex pin inside guide tube, and dimensions.

In the AP1000 and RR SMR models there are 3 types of control rod pins which are arranged in either a Rod Cluster Control Assembly (RCCA) or Gray Rod Control Assembly, each consisting of 24 control rods inserted into an assembly simultaneously. An RCCA consists of 24 identical pins with the geometry and dimensions seen in Figure 5. In the RR SMR model there is an additional variation to the RCCA pin which instead uses the B_4C material. This type of rod is mainly used in shut-down scenarios. In the figure, the RCCA pin is inside

a guide tube.

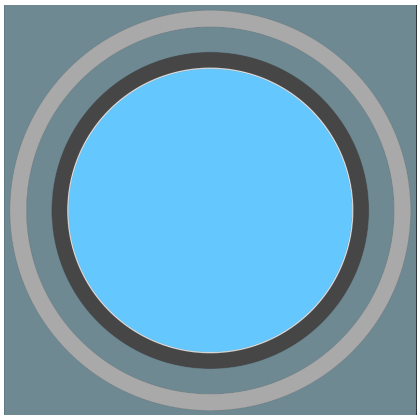

Material	Radius (cm)
SINCAD/B_4C	0.43307
Air	0.43688
SS-304	0.48387

Figure 5: AP1000 and RR SMR RCCA pin inside guide tube, and dimensions.

The GRCAs consist of 24 pins with similar geometry as the RCCA pins, except that the neutron absorbing material has a smaller radius, and 12 out of the 24 rods contain the SS-304 material instead of SINCAD. The GRCA pin geometries and dimensions can be seen in Figure 6. In the figure, the GRCA pin is inside a guide tube.

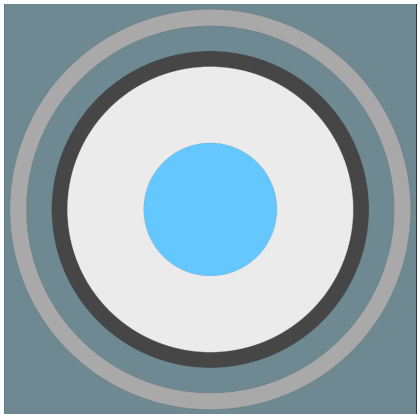

Material	Radius (cm)
SINCAD or SS-304	0.20320
Air	0.43688
SS-304	0.48387

Figure 6: AP1000 and RR SMR GRCA pin geometry and dimensions.

4.2.2 Rod Geometries

The previously described pin geometries were axially limited and stacked on top of each other to create fuel-, IFBA-, Pyrex-, control- and water-rods. The AP1000 fuel- and IFBA-rods consist of a 386.08 cm long central fuel region with normally enriched fuel/IFBA material. At the top and bottom of these

is an axial blanket 20.32 cm thick, consisting of lower enriched fuel (1.58%) in the case of regular fuel-rods, and 3.2 % enriched fuel for IFBA-rods. These two regions form the active fuel region, 426.72 cm in length. The rods are pressurized with helium which forms a 12.16 cm high layer above and below the active fuel region with the outer radius 0.417830 cm, and which is encapsulated by the same ZIRLO cladding as the rest of the rod. At both ends of the rods there is a ZIRLO cap of 1.27 cm in thickness and the same outer radius as the rest of the fuel rod. The control rods consist of an absorbing region with the same length as the active fuel region, i.e. 426.72 cm, above and below which is water (denoted as "guide tube" in Figure 7). The Pyrex rods consist of a 368.3 cm long region of Pyrex material, surrounded at the top and bottom with 30.48 cm of helium. At the top of the Pyrex rods is 19.05 cm of stainless steel, and the bottom 11.77 cm is water. All the AP1000 rod geometries can be seen in Figure 7 (not to scale). The Pyrex- and control-rods are in the geometry inserted into guide tubes.

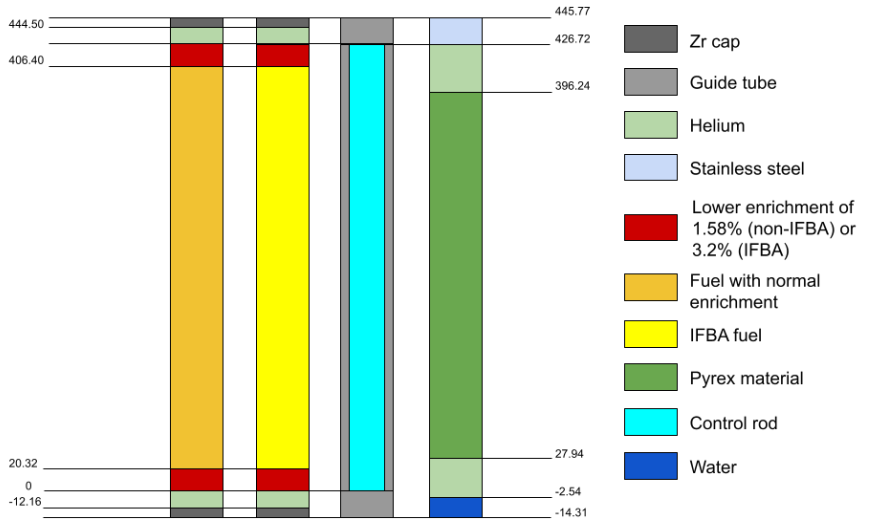

Figure 7: AP1000 rod geometries (not to scale). Figure created with inspiration from [6].

As previously stated the RR SMR is assumed to not contain any IFBA- or Pyrex-rods, but the fuel rods are also assumed to be different. The fuel rod in the RR SMR fuel assembly is according to [10] a shorter version of a 17x17 RFA which has an active fuel height of 365.7 cm, while the RR SMR active

fuel height is only 280 cm. The AP1000 is a longer version of the same fuel assembly (so called 17x17 XL RFA). According to a OECD proposal from 1994 [15], the RFA 17x17 assembly has a different axial geometry than what was used in the AP1000 model. Instead of just having 3 axial regions of different fuel enrichments as in the AP1000 model, the fuel rod in [15] has 9 axial fuel regions. To compromise between these two models and account for the shorter fuel-rods, and since there are 4 different fuel enrichments available from the AP1000 model (discounting the 3.2% enriched fuel used in the axial blanket of IFBA-rods), the RR SMR fuel rods were modeled as 7 axial fuel regions, with lower enrichments at the ends and the higher enrichments towards the center of the rod. At the ends of the fuel rod were ZIRLO caps, but the RR SMR fuel rod was not assumed to have a helium gap between the fuel and the caps.

The RR SMR fuel rod geometry can be seen in Figure 8, where the left rod contains Gd-poisoned fuel and the right rod contains regular fuel. The fuel-rods are axially symmetric, and from the bottom of the rod to the middle (the top half can be obtained by mirroring the rod about the xy-plane in the middle of the rod) the fuel-rod consists of: 1.75 cm ZIRLO cap, 5 cm of 1.58% enriched fuel, 5 cm of 2.35 % enriched fuel, 10 cm of 3.4 % enriched fuel and 120 cm of 4.45 % enriched fuel.

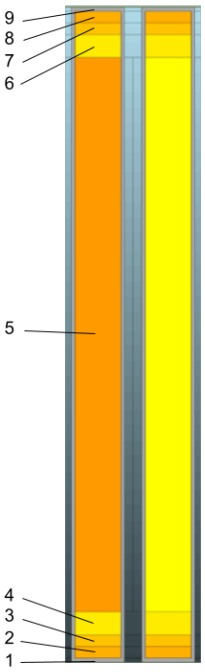

Region from the bottom	Material	Thickness [cm]
1	ZIRLO	1.75
2	1.58 % ^{235}U enriched UO_2	5
3	2.35 % ^{235}U enriched UO_2	5
4	3.40 % ^{235}U enriched UO_2	10
5	4.45 % ^{235}U enriched UO_2	240
6	3.40 % ^{235}U enriched UO_2	10
7	2.35 % ^{235}U enriched UO_2	5
8	1.58 % ^{235}U enriched UO_2	5
9	ZIRLO	1.75

Figure 8: RR SMR rod geometries. Left) Regular fuel rod. Right) Gd-poisoned fuel rod.

Serpent allows for the temperature and density of a material to be specified in different spatial regions with a so called "ifc-card". Since both the fuel and the coolant have an axial temperature gradient (the fuel also has a radial temperature gradient), this was accounted for in the Serpent model. The fuel temperature spatial dependence was found for each reactor by utilizing the MATLAB code provided by Christophe Demazière [12], assuming the coolant mass flow rate of 3255 kg/m^{2}s for the AP1000 [13]. The coolant mass flow of the RR SMR was derived from heat balance. With thermal power output 1358 MW_{th}, heat capacity of water $C_v \approx 5.4$ kJ/kg.K, 27K temperature increase of the coolant along the height of the core (295 - 322 °C) and the same effective coolant flow area per assembly as in the AP1000 [13] with 121 assemblies instead of 157, the coolant mass flow rate of the RR SMR was approximated to be 3112 kg/m^{2}s. The radial temperature distribution at the fuel half-height can be seen in Figure 9 where the top figure shows the distribution for the AP1000 and the bottom figure for the RR SMR. Figure 10 instead shows the axial temperature distribution at different radial distances from the fuel center-line, as well as the radially averaged distribution along the height of the fuel rod. The corresponding values are listed in Table 14 [12]. The density of the fuel was approximated to be constant with temperature.

Table 14: Axial temperature distribution in the fuel rods of the AP1000 and the RR SMR [12].

Height [cm]	Temp. AP1000 [K]	Height [cm]	Temp. RR SMR [K]
0.0	553.15	0.0	568.15
17.06880	618.89	11.2	627.24
34.13760	683.98	22.4	685.63
51.20640	747.39	33.6	742.38
68.27520	808.11	44.8	796.61
85.34400	865.18	56.0	847.46
102.4128	917.68	67.2	894.11
119.4816	964.80	78.4	935.84
136.5504	1005.78	89.6	971.96
153.6192	1039.96	100.8	1001.93
170.6880	1066.80	112.0	1025.27
187.7568	1085.88	123.2	1041.58
204.8256	1096.88	134.4	1050.64
221.8944	1099.65	145.6	1052.31
238.9632	1094.12	156.8	1046.52
256.0320	1080.41	168.0	1033.40
273.1008	1058.72	179.2	1013.18
290.1696	1029.42	190.4	986.12
307.2384	992.95	201.6	952.70
324.3072	949.94	212.8	913.44
341.3760	901.03	224.0	868.98
358.4448	847.02	235.2	819.98
375.5136	788.79	246.4	767.24
392.5824	727.25	257.6	711.60
409.6512	663.37	268.8	653.93
426.7200	598.15	280.0	595.15

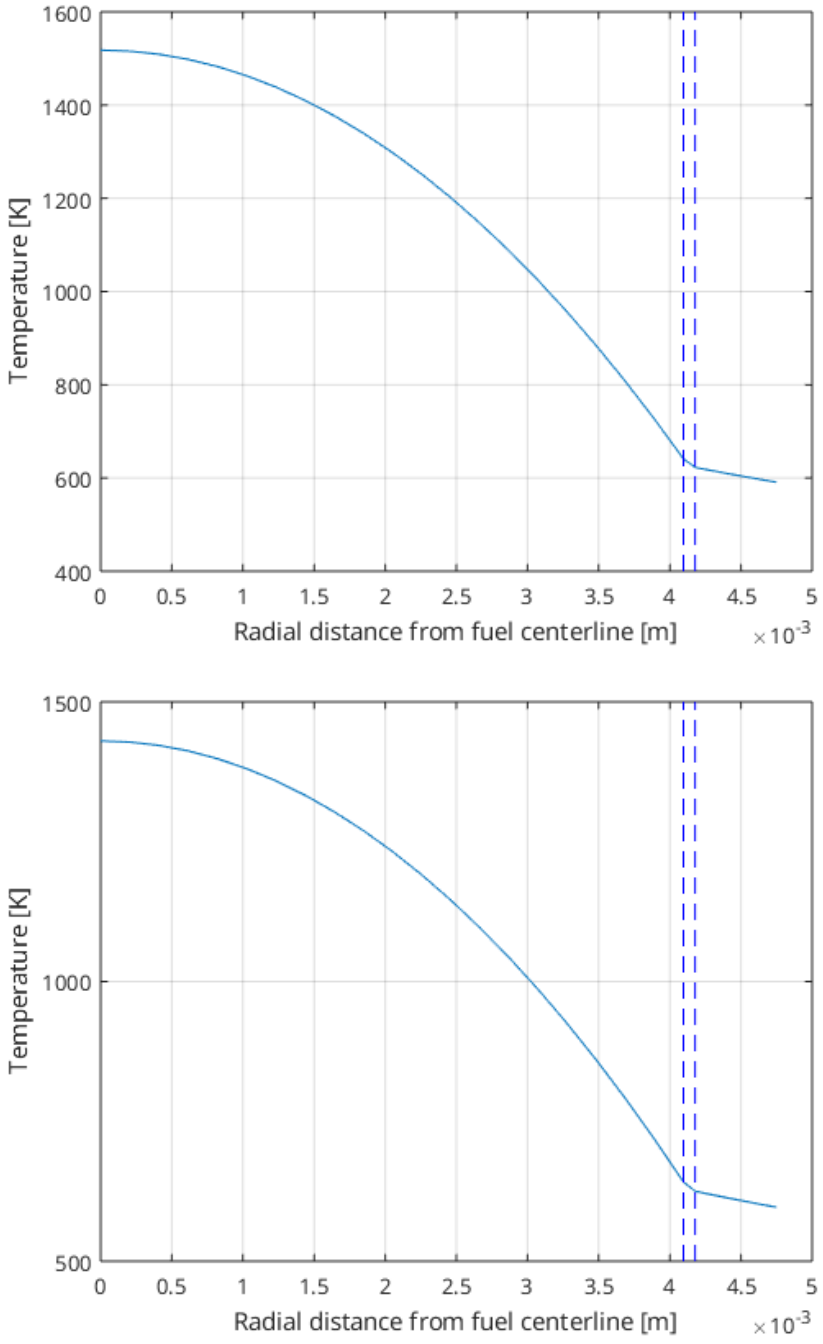

Figure 9: Radial temperature distribution at the fuel half-height. Top) AP1000. Bottom) RR SMR [12].

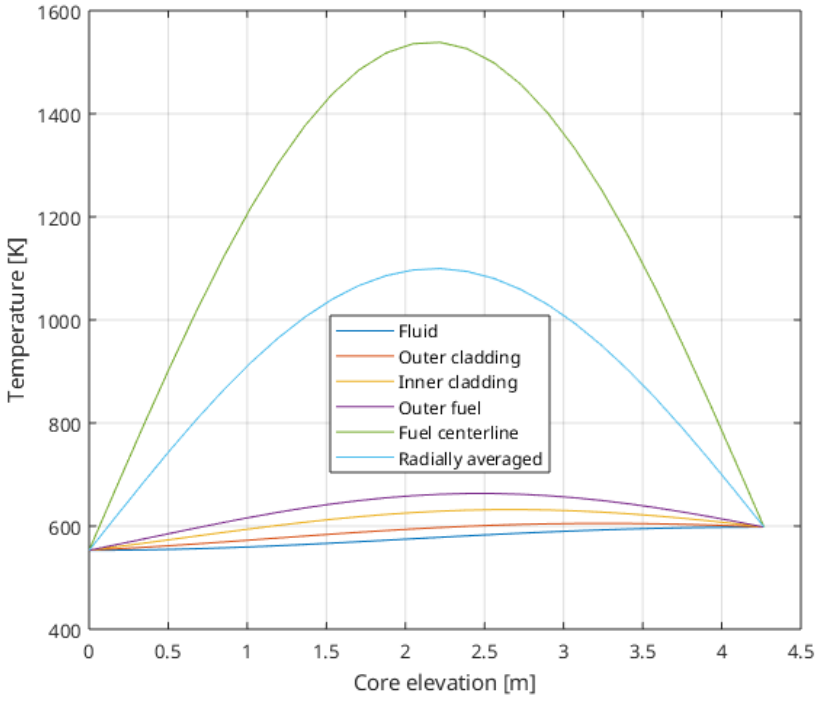

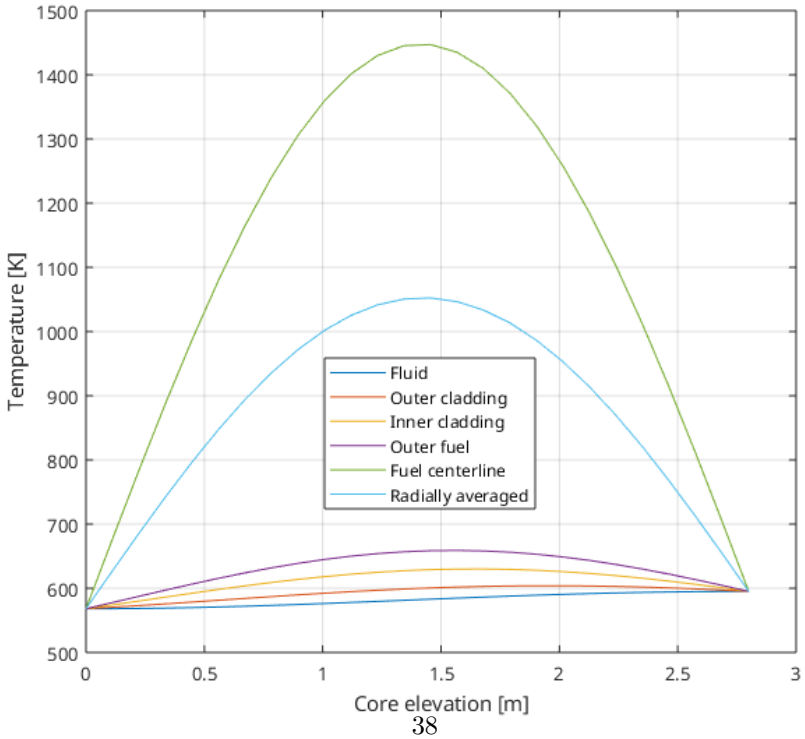

Figure 10: Axial temperature distribution in different parts of the fuel as well as radially averaged. Top) AP1000. Bottom) RR SMR [12].

As for the coolant, due to the high pressure in the system not allowing for water to boil, it was approximated that the temperature of the water increased linearly along the active fuel height in the reactor core. The density of the water was calculated in 25 discrete steps along the reactor height. This was achieved using the IAPWS-IF97 implementation of X-Steam in MATLAB [16]. The resulting water densities in the AP1000 and RR SMR along the height of the core can be seen in Table 15. The same distribution was applied throughout the entire core.

Table 15: Axial density and temperature distribution in the coolant of the AP1000 and the RR SMR [16].

AP1000			RR SMR		
Height [cm]	Dens. [g/cm^3]	Temp. [K]	Height [cm]	Dens. [g/cm^3]	Temp. [K]
0.0	0.7643	553.15	0.0	0.7366	568.15
17.067	0.7611	554.95	11.2	0.7344	569.23
34.138	0.7579	556.75	22.4	0.7323	570.31
51.206	0.7547	558.55	33.6	0.7301	571.39
68.275	0.7514	560.35	44.8	0.7279	572.47
85.344	0.7481	562.15	56.0	0.7257	573.55
102.413	0.7447	563.95	67.2	0.7234	574.63
119.482	0.7413	565.75	78.4	0.7212	575.71
136.550	0.7378	567.55	89.6	0.7189	576.79
153.619	0.7342	569.35	100.8	0.7165	577.87
170.688	0.7306	571.15	112.0	0.7142	578.95
187.757	0.7269	572.95	123.2	0.7118	580.03
204.826	0.7232	574.75	134.4	0.7094	581.11
221.894	0.7194	576.55	145.6	0.7070	582.19
238.963	0.7155	578.35	156.8	0.7045	583.27
256.032	0.7115	580.15	168.0	0.7020	584.35
273.101	0.7075	581.95	179.2	0.6994	585.43
290.170	0.7034	583.75	190.4	0.6969	586.51
307.238	0.6992	585.55	201.6	0.6943	587.59
324.307	0.6948	587.35	212.8	0.6916	588.67
341.376	0.6904	589.15	224.0	0.6889	589.75
358.445	0.6859	590.95	235.2	0.6862	590.83
375.514	0.6812	592.75	246.4	0.6834	591.91
392.582	0.6765	594.55	257.6	0.6806	592.99
409.651	0.6716	596.35	268.8	0.6778	594.07
426.720	0.6665	598.15	280.0	0.6748	595.15

4.3 Fuel Assemblies

The rods which were defined in the previous section were then arranged in a lattice to form the fuel assemblies. The assemblies for the AP1000 were defined in [6], and there are in total 9 different assembly types. Each assembly is

assumed to consist of a fuel-pin lattice with a pitch of 1.25984 cm, which is surrounded by a 0.04318 cm layer of coolant, meaning each assembly has a side-length of 21.50364 cm. The different assemblies can be seen in Figure 11. In the figure, the assemblies are numbered from left to right 1-3 in the top row, 4-6 in the middle row and 7-9 in the bottom row.

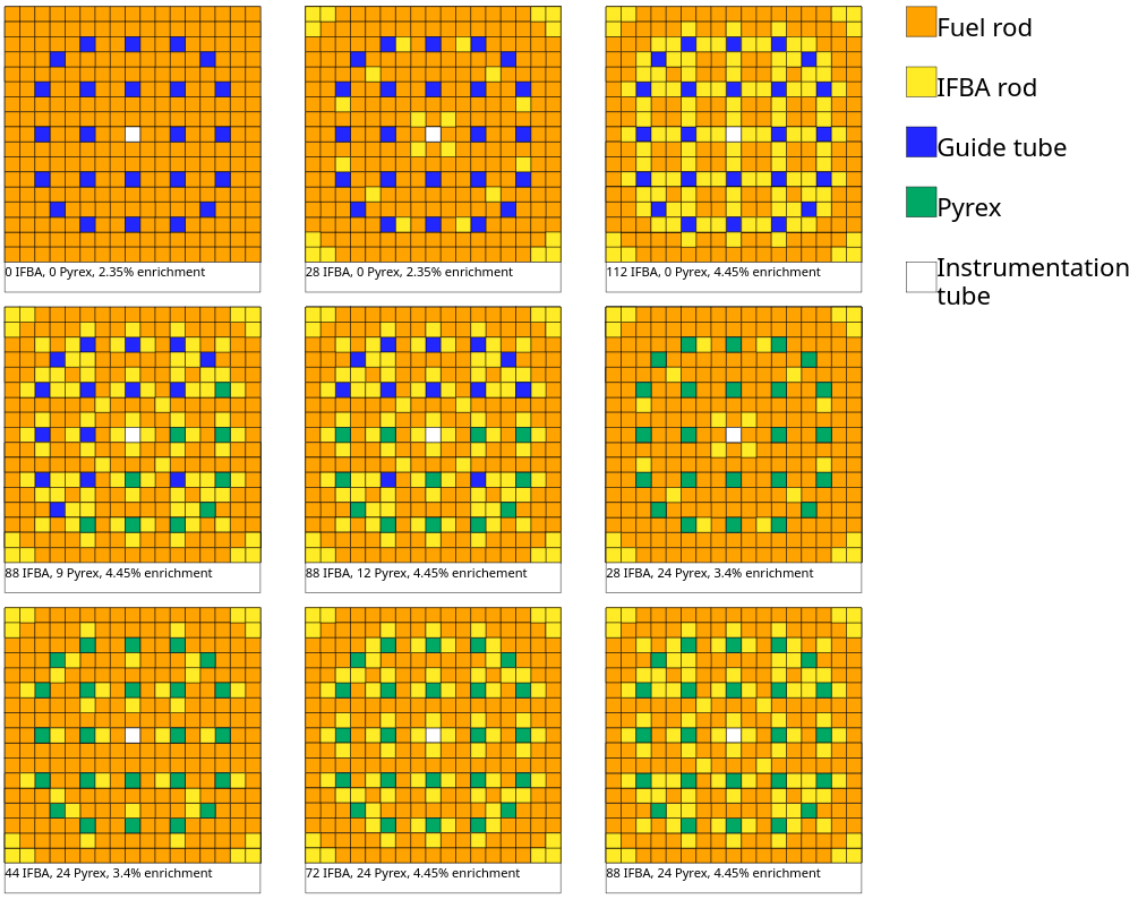

Figure 11: AP1000 assemblies, corresponding to Figure 8 in [6].

Figures 12 and 13 show a top-view and side-view of an AP1000 assembly in the Serpent model.

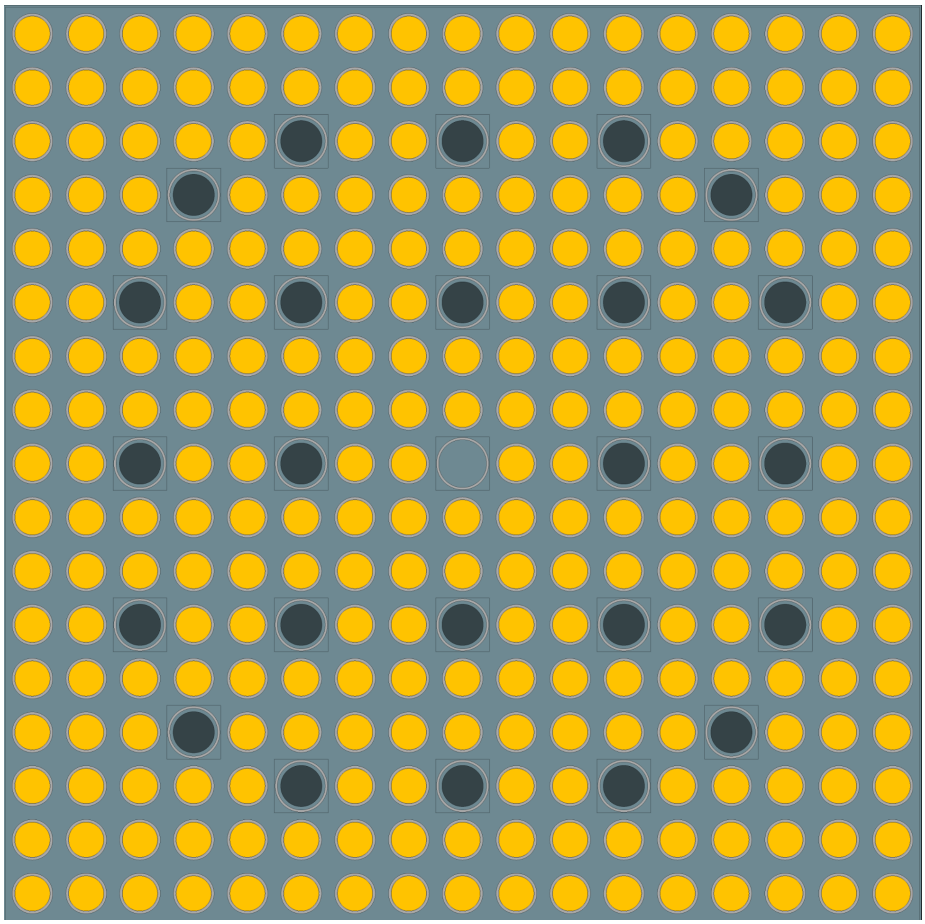

Figure 12: AP1000 assembly in Serpent, top-view.

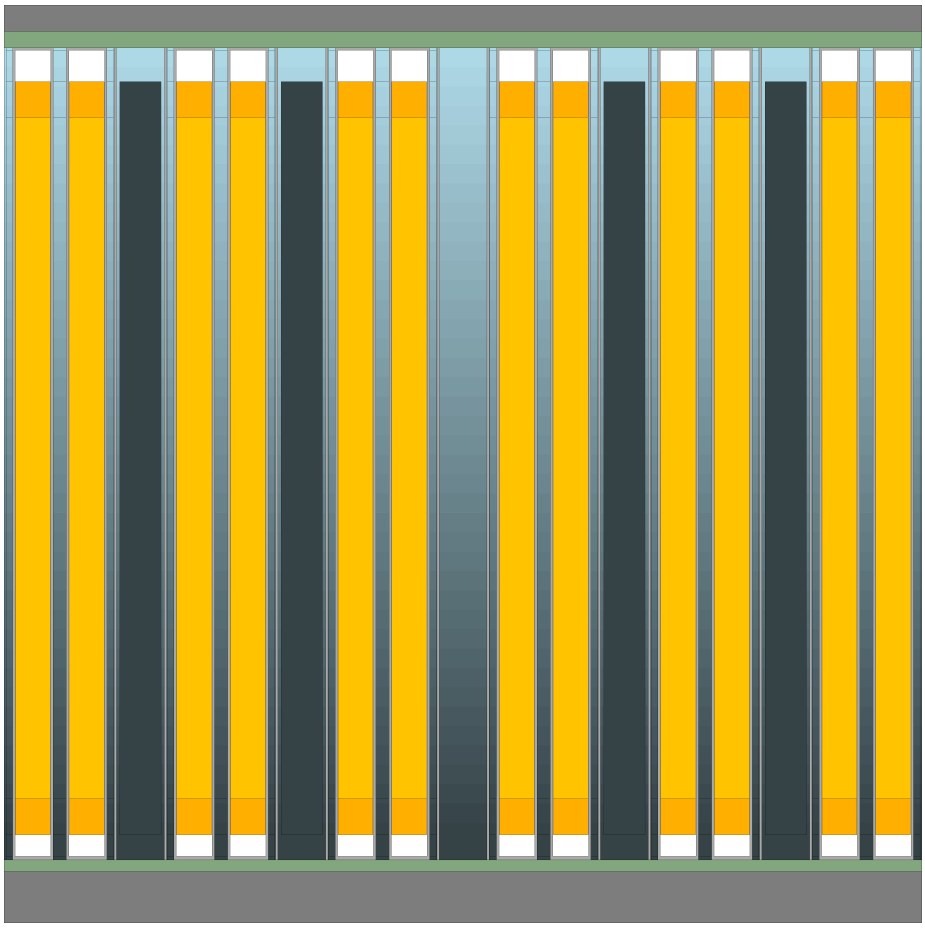

Figure 13: AP1000 assembly in Serpent, side-view.

In the model of the RR SMR model there is only one type of assembly. It is assumed to have the same size, pin-pitch, and number of guide tubes in the same positions as in the AP1000 assembly, i.e. 24 guide tubes and one instrumentation tube per assembly. In [10] it is stated that there are 40 Gd-poisoned fuel rods per assembly, but that there are no poisoned fuel rods adjacent to a guide tube/control rod. This rules out many of the central fuel rod positions. In the left of Figure 14 are the allowed positions of poisoned fuel-rods. To the right is the chosen configuration of poisoned/un-poisoned rods.

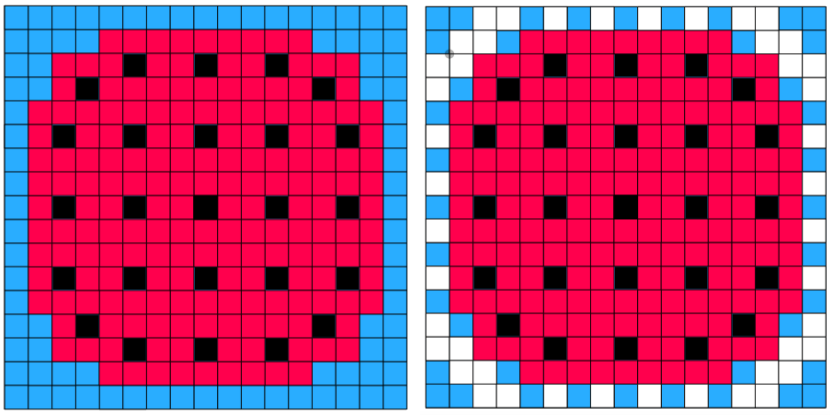

Figure 14: RR SMR Assemblies: Guide/instrumentation tube (black); Rods without Gd-poisoned fuel rod (red/white); Rods with Gd-poisoned fuel rod (blue). Left) Possible positions for poisoned rods. Right) Chosen configuration of poisoned/un-poisoned rods.

As stated previously, the AP1000 and RR SMR models have two types of control rod clusters which are inserted into certain assemblies when necessary, the RCCAs and the GRCAs. The clusters look the same in both models, and irregardless of material. In the RCCA, all 24 guide tubes are filled with the same type of control rod, which was defined previously and shown in Figure 5. The GRCAs contain 12 control rods of each material (SINCAD/SS-304), configured as shown in Figure 15 [6]. In the AP1000 model, only the assemblies of type 1-3 contain control rods.

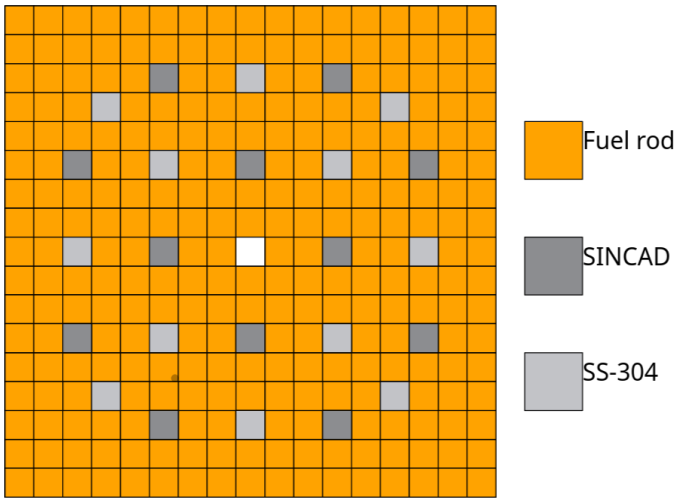

Figure 15: AP1000 and RR SMR GRCA configuration, corresponding to Figure 11 in [6].

4.4 Core

The assemblies of each respective model were then arranged into the full core models. Figure 16 shows the configuration of the AP1000 model, which was given in [6]. The numbers and color of each square respectively represents the assembly type and type of control rod cluster (if any) used in that position.

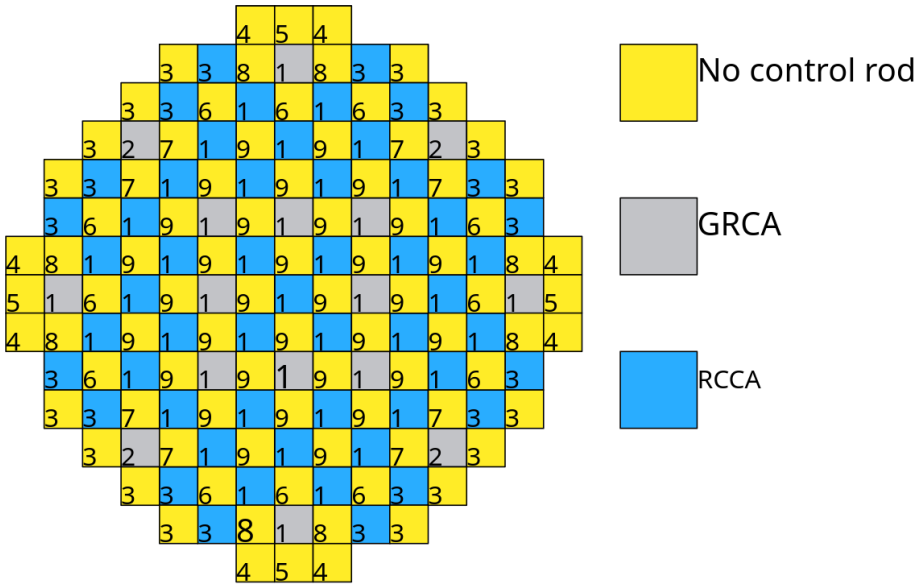

Figure 16: AP1000 core configuration. The numbers represent assembly type, and color represents the type of control rod cluster (if any) included in the assembly, inspired by Figures 12 and 13 in [6].

Since the AP1000 assembly- and core configuration was made with a flat power- and flux-distribution in mind, no additional measures had to be taken for the model other than to adjust the boron concentration to lower the reactivity to k=1. This can be confirmed by looking at Figures 17, 18 and 19 which respectively show the AP1000 power distribution, thermal flux-, and fast flux-distributions in each assembly. Each square in the xy-plane represents one quarter of an assembly, integrated over its entire height, and the z-axis is the resulting value of the power/flux.

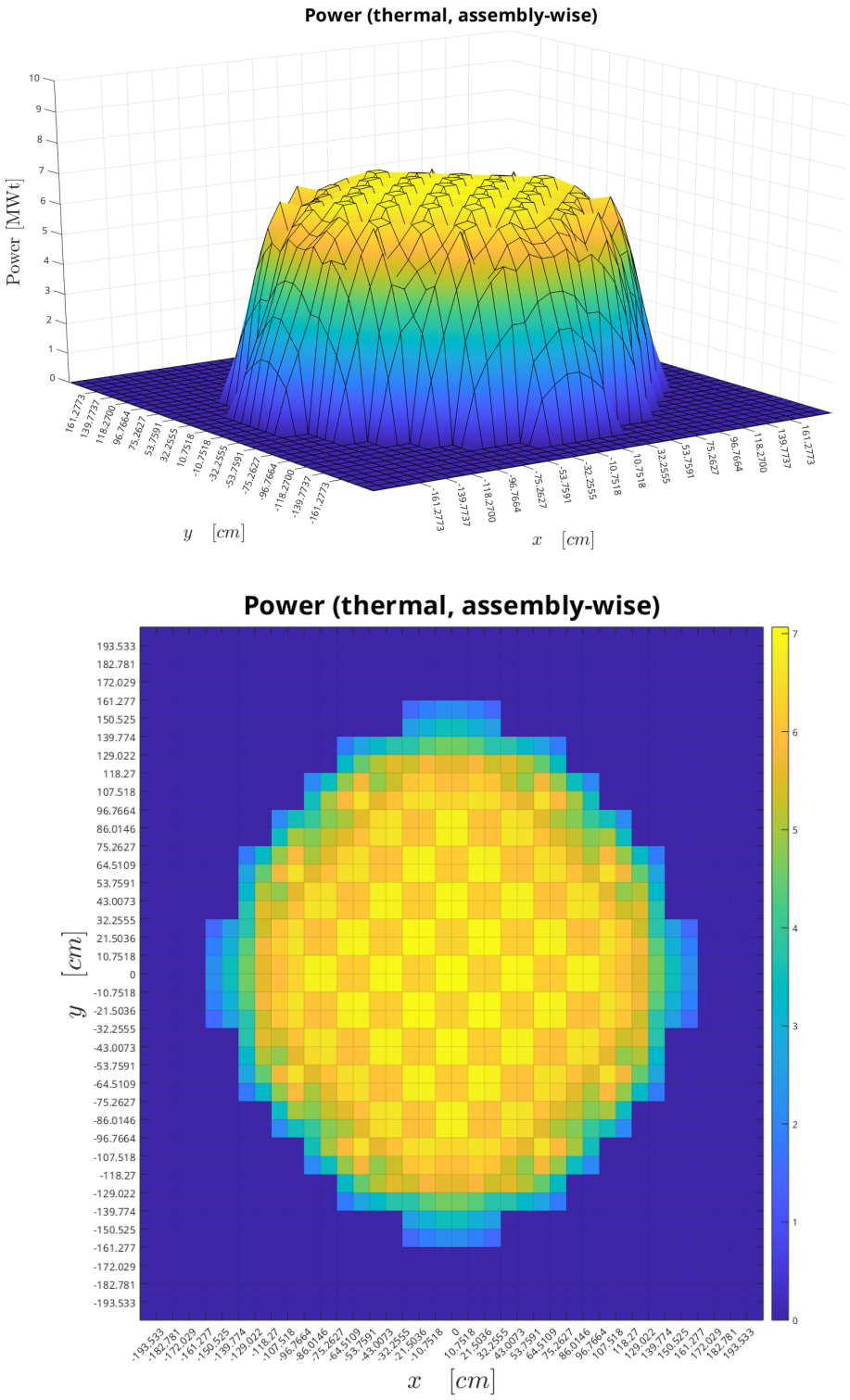

Figure 17: AP1000 power distribution in the Serpent model.

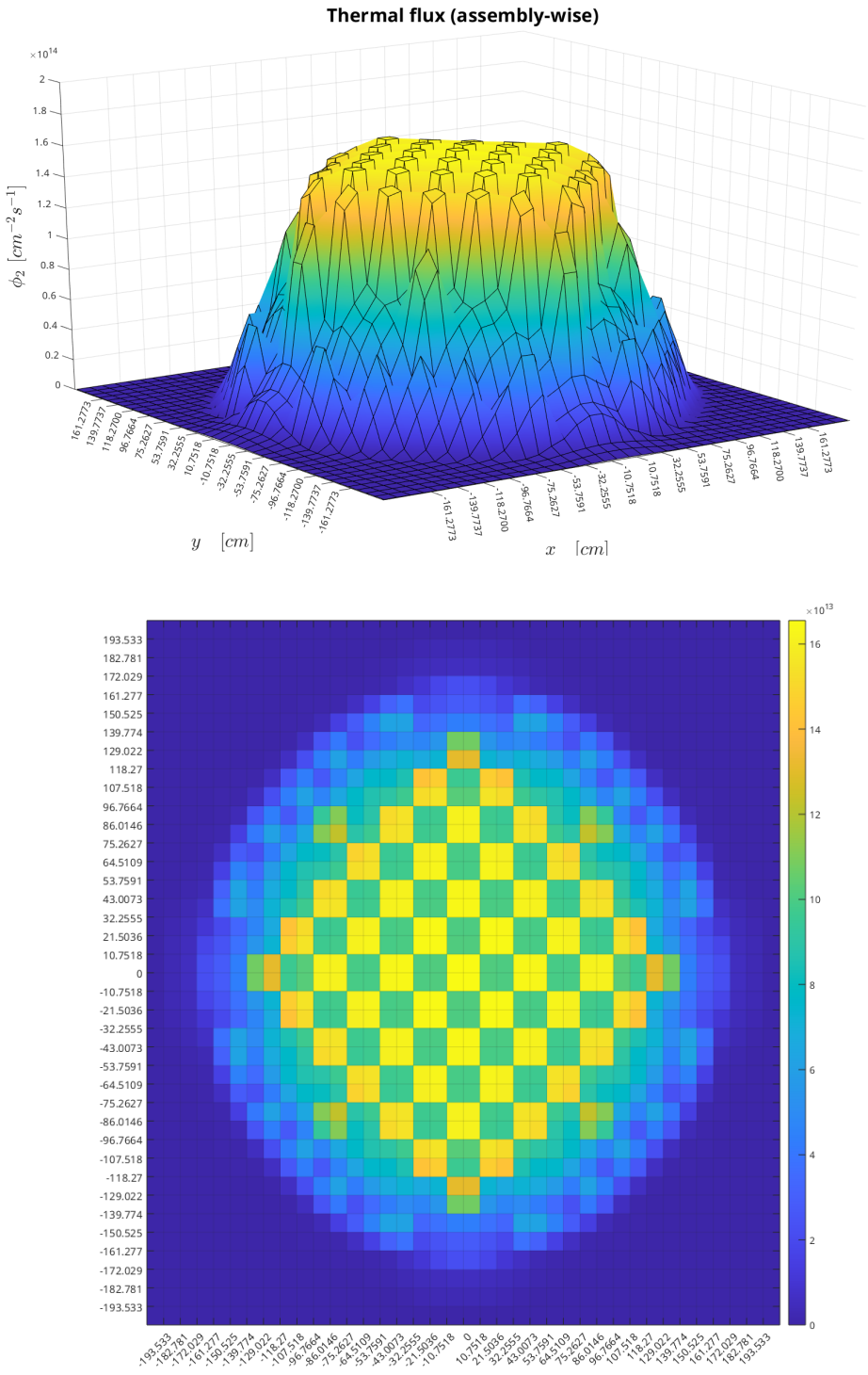

Figure 18: AP1000 thermal flux distribution in the Serpent model.

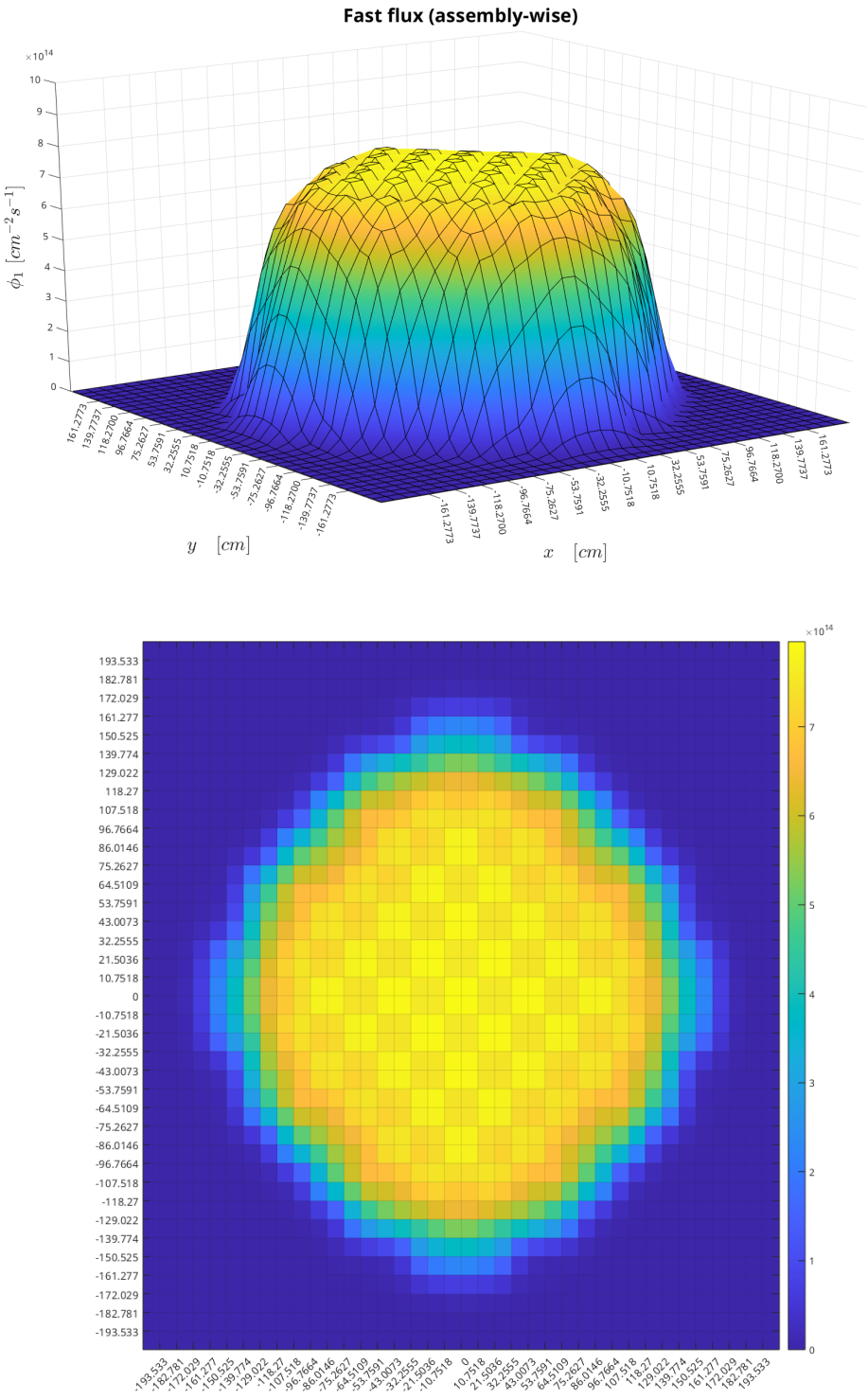

Figure 19: AP1000 fast flux distribution in the Serpent model.

For the RR SMR model on the other hand, there is no reference, neither

for the shape of the core other than that it is circular, nor for the position or amount of control rod clusters. What is given is the total number of assemblies being 121 compared to the 157 of the AP1000. Some qualified guesses therefore had to be made about the RR SMR core model. It was assumed that the number of control rod clusters per fuel assembly was the same in both the RR SMR and the AP1000. This number was approximately 0.439 for the AP1000. Furthermore, it was assumed that the fraction of control rod clusters of each type was the same (or as close to it as possible).

For the AP1000 the number of GRCAs and RCCAs per assembly in the core was approximately 0.102 and 0.338 respectively. Some of the RCCA clusters were to be used during power operation (PO RCCA), but some were to be reserved to exclusively be used during shut-down scenarios (SD RCCA). Using these assumptions, the number of GRCAs in the RR SMR model should be 12 (0.099 GRCAs per assembly) and the total number of RCCAs should be 41 for a total of 53 control rod clusters in the core (0.438 control rod clusters per assembly). The position of the different control rod clusters (and the number of shut-down rods) was chosen in order to flatten out the centrally-peaking power- and flux-distribution resulting from the singular assembly type used in the core. The total number of PO RCCAs was chosen to be 33, and the number of SD RCCAs was chosen to be 8. The resulting core configuration can be seen in Figure 20, where the colors of each cell represent the type of control rod cluster (if any) used in that assembly (the PO rods are divided into 2 banks, B1 and B2, which can be moved individually).

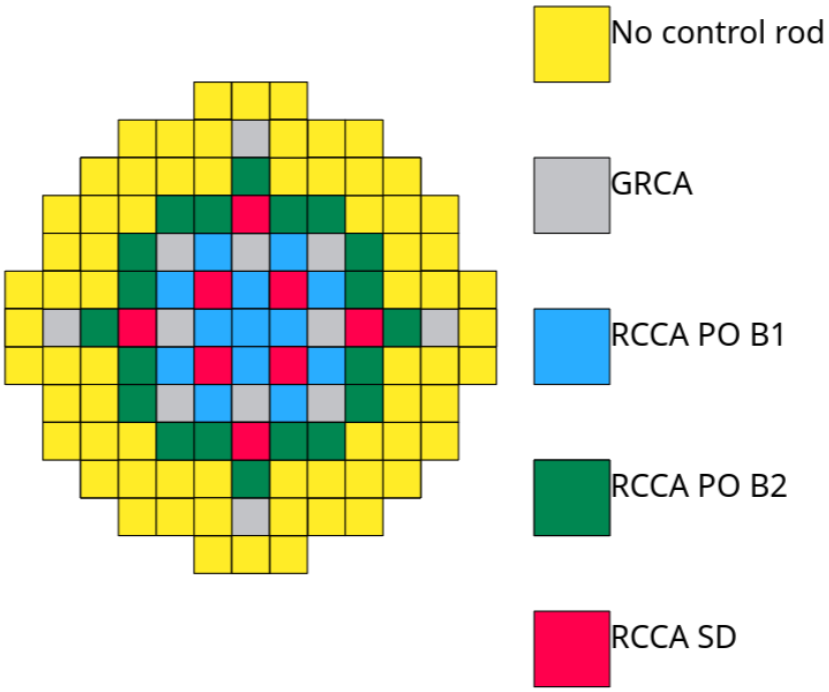

Figure 20: Assumed core configuration for the RR SMR.

The insertion level for each control rod cluster can be seen in Table 16.

Table 16: Insertion level for the different types of control rod clusters in the RR SMR model. 0 cm represents fully extracted and 280 cm represents fully inserted into the core.

Control rod cluster	Insertion level [cm]
GRCAs	140
RCCA PO B1	251
RCCA PO B2	251
RCCA SD	0

The resulting power, thermal flux, and fast flux-distributions in the RR SMR core can be seen in Figures 21, 22 and 23 with each square in the xy-plane representing one assembly, and the z-axis represents the values of the power/flux integrated over the entire height of the assembly.

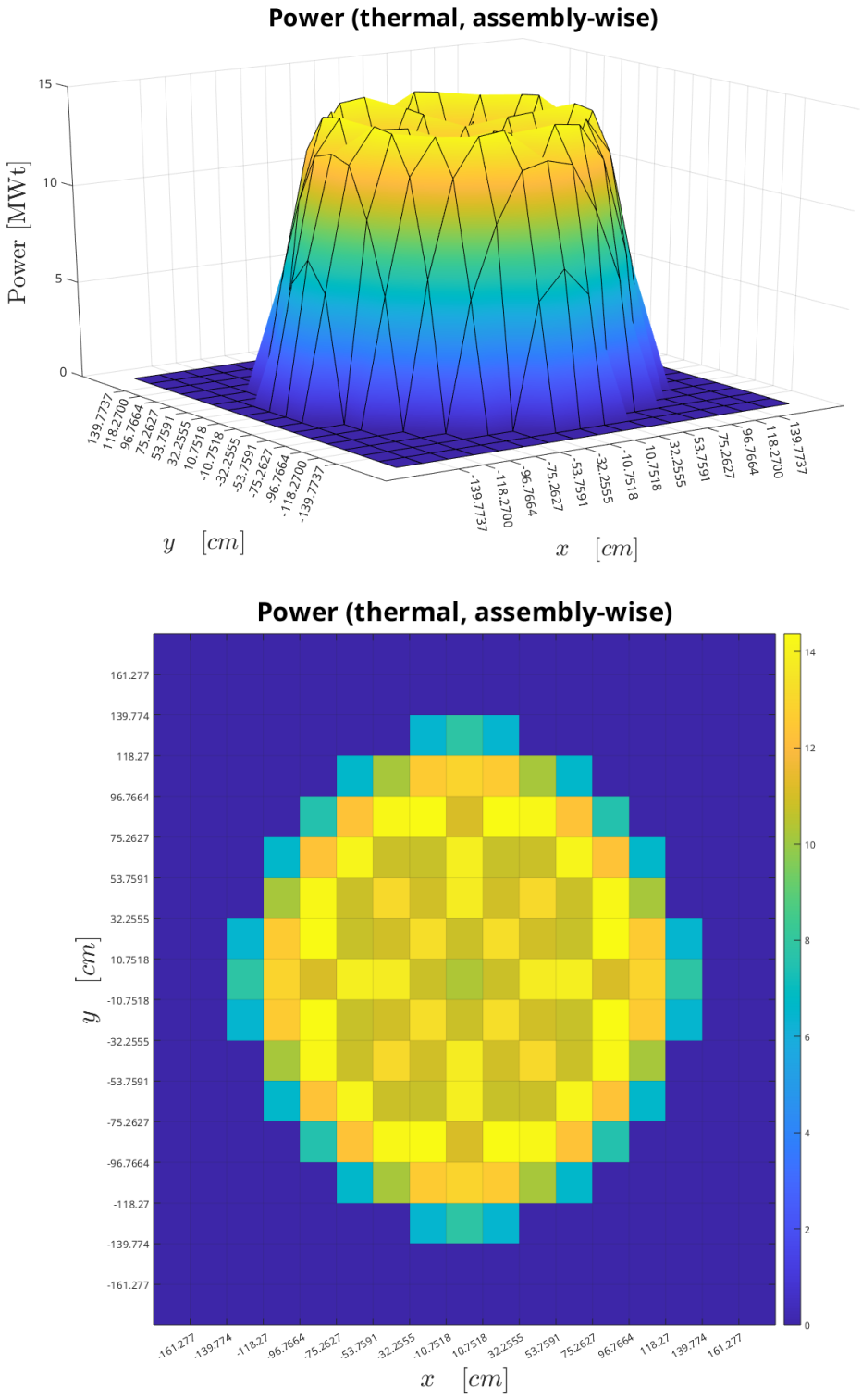

Figure 21: RR SMR power distribution in the Serpent model.

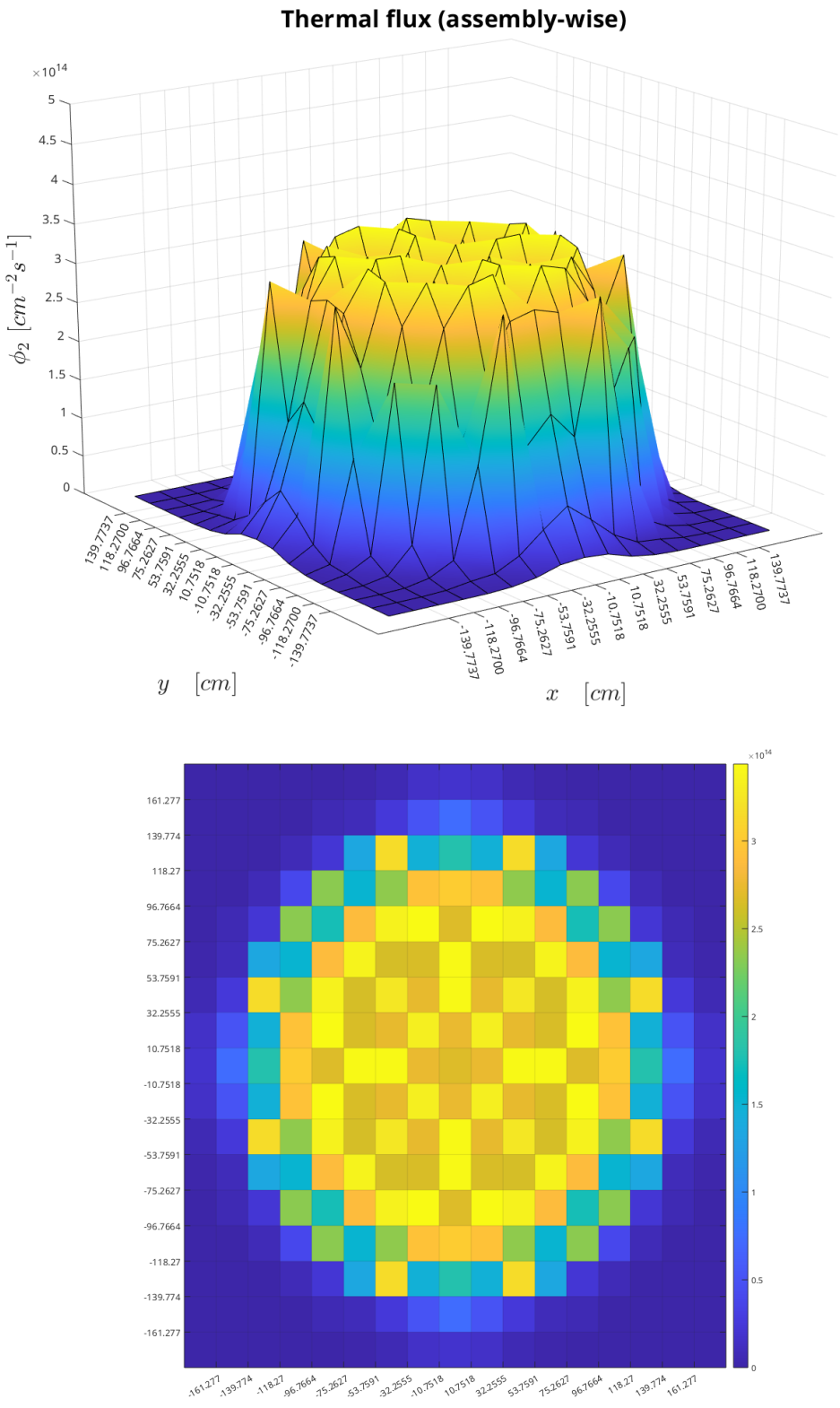

Figure 22: RR SMR thermal flux distribution in the Serpent model.

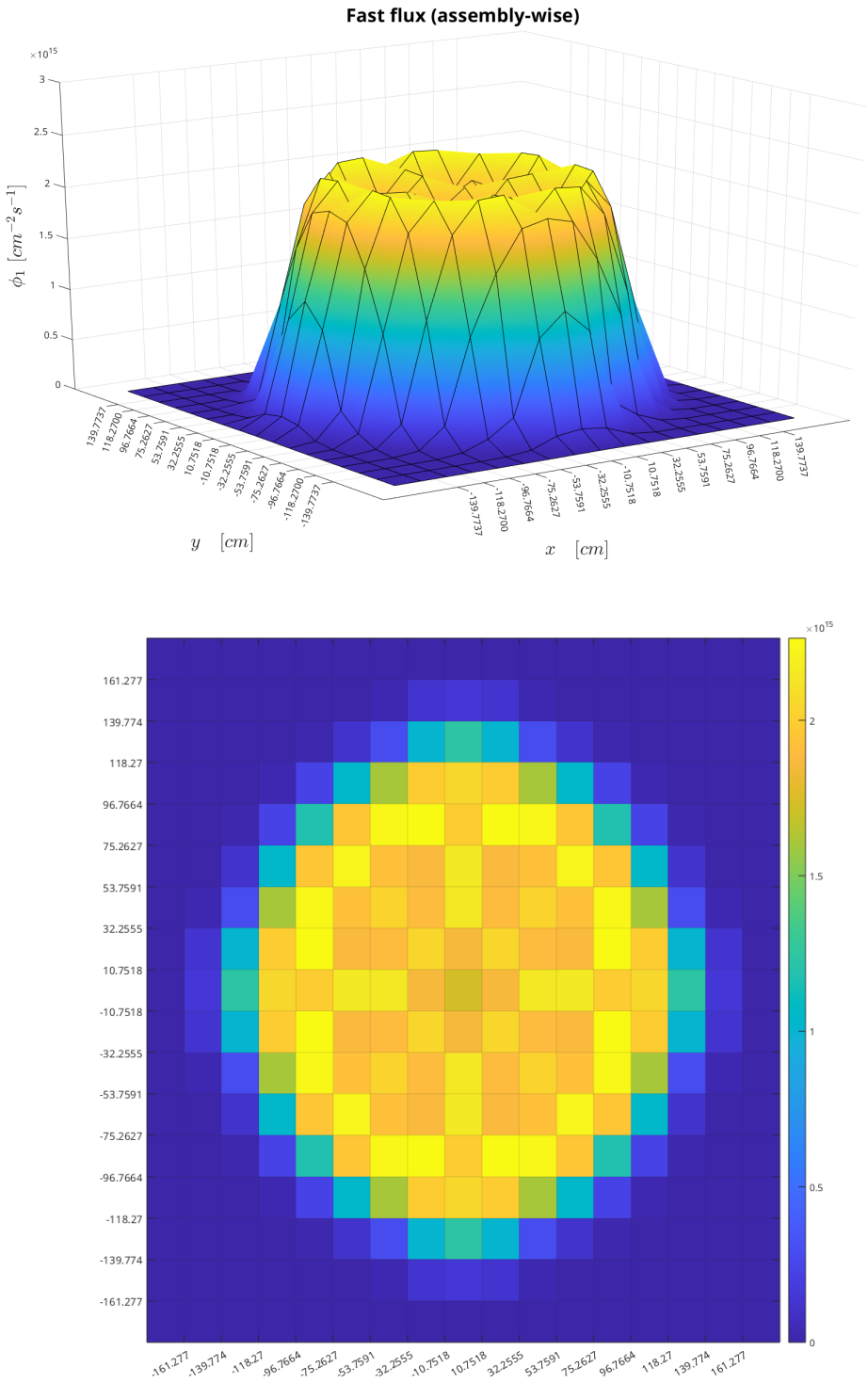

Figure 23: RR SMR fast flux distribution in the Serpent model.

4.5 Full model

In the full models there are a number of structures outside the core. Above and below the cores is a 6.44 cm thick axial nozzle, which is modeled as 50% water and 50% stainless steel (SS-304), followed by a 29.25 cm thick axial reflector modeled as 70% water and 30% stainless steel [6]. Radially there is a 2.54 cm thick baffle directly outside the core [6]. Outside the baffle is the cylindrical core shroud, with an inner radius of 167.531 cm in the AP1000 model (different to what is given in [6], smallest radius for which the shroud and baffle did not intersect) and 146.5061 cm in the RR SMR model, and a thickness of 2.163 cm. Further out from the shroud is the cylindrical core barrel, which has an inner radius of 172.863 cm in the AP1000 model (also different from [6], distance between the shroud and barrel was kept the same as in [6]), 152.2155 cm in the RR SMR model, and a thickness of 5.08 cm. Furthest out from the core is the RPV, with an inner radius of 201.930 cm in the AP1000 model, 189.68 cm in the RR SMR model, and a thickness of 20.32 cm [6]. Between the baffle, shroud and barrel is water. Figures 25 and 24 show the AP1000 Serpent model side-view and top-view respectively, while Figures 26 and 27 show the RR SMR Serpent model.

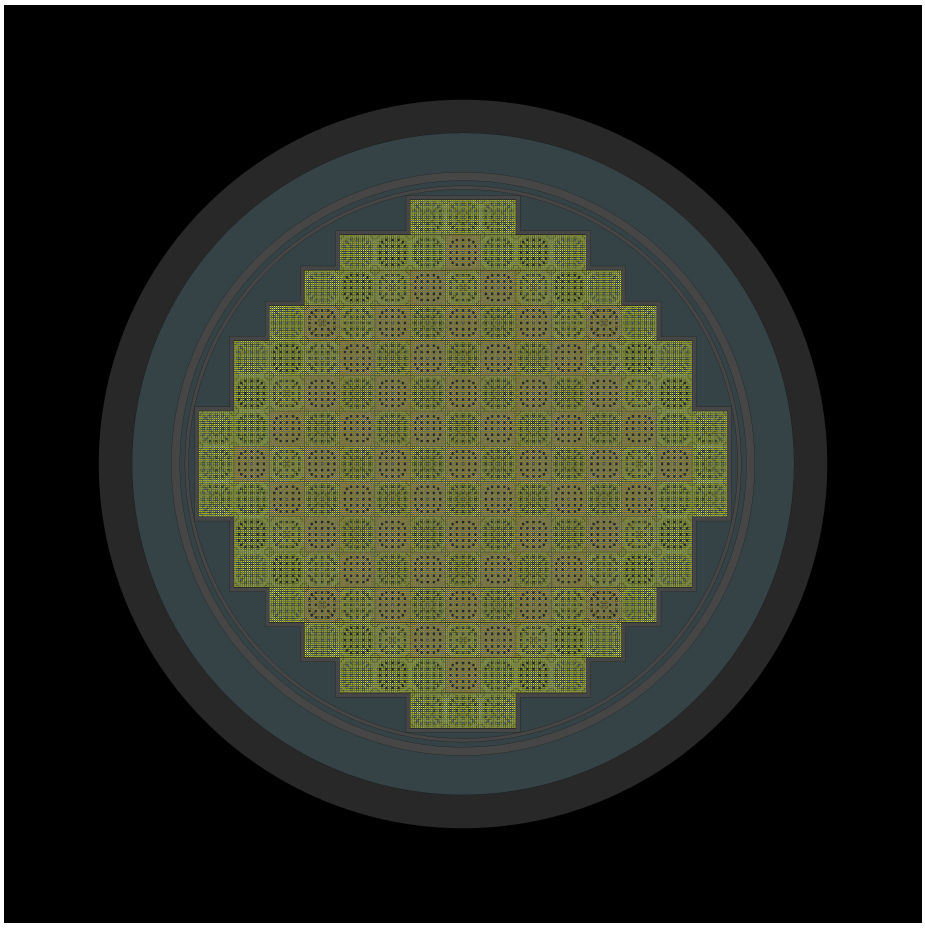

Figure 24: AP1000 full core model, top-view. The squares represent different assemblies, where the yellow and orange circles are fuel rods, while the dark or blue circles are either pyrex rods, control rods or empty guide tubes. Surrounding the core are some metal structures such as the core baffle, shroud, barrel, and furthest out from the core, the RPV.

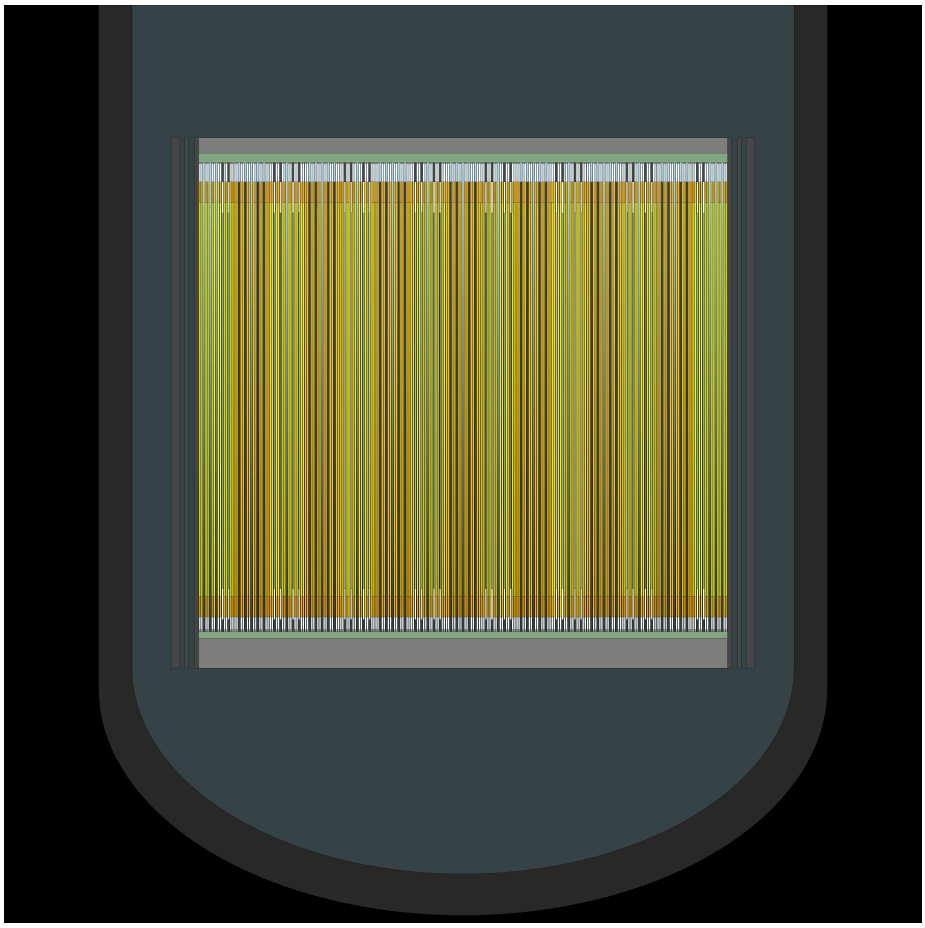

Figure 25: AP1000 full core model, side-view. Rods of different types can be seen. Yellow and orange rods are fuel rods, while blue and dark rods are either pyrex rods, control rods or empty guide tubes. The white part at the upper and lower end of the rods is helium. The green and gray blocks at the top and bottom of the core are homogenized regions containing a mix of steel and water (50/50, and 30/70) which represent the axial reflectors and inlet/outlet nozzles respectively.

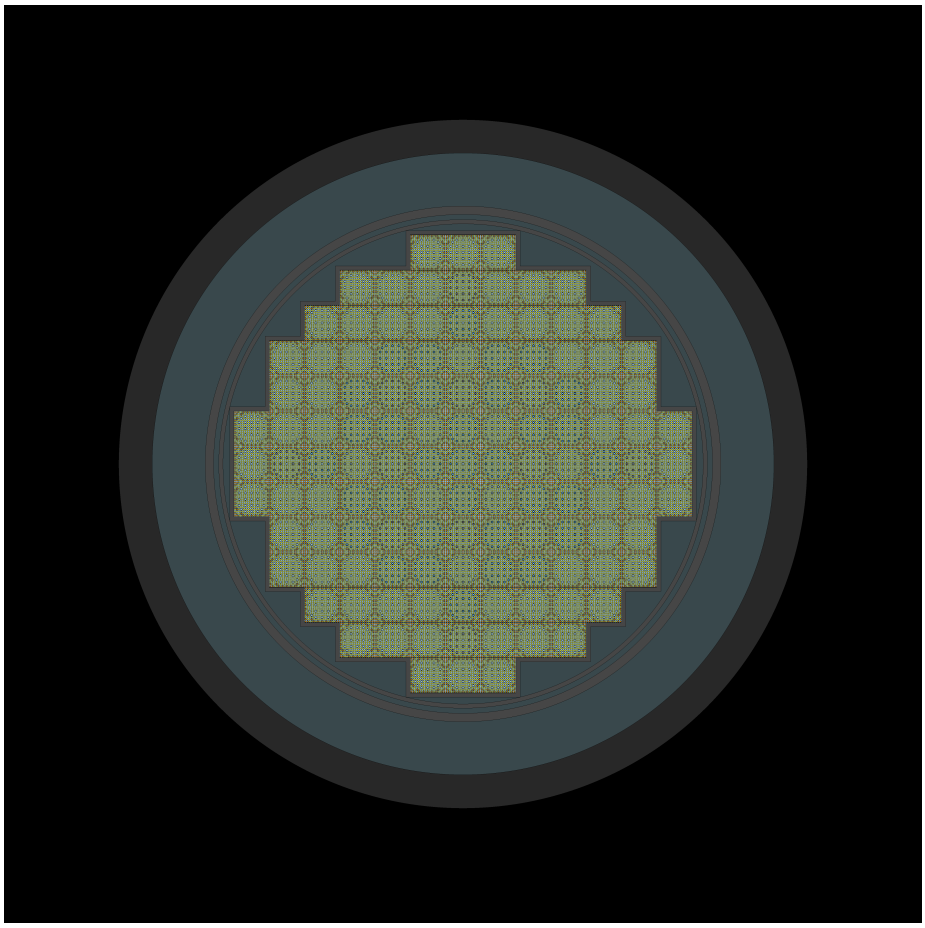

Figure 26: RR SMR full core model, top-view. The squares represent different assemblies, where the yellow and orange circles are fuel rods, while the dark or blue circles are either pyrex rods, control rods or empty guide tubes. Surrounding the core are some metal structures such as the core baffle, shroud, barrel, and furthest out from the core, the RPV.

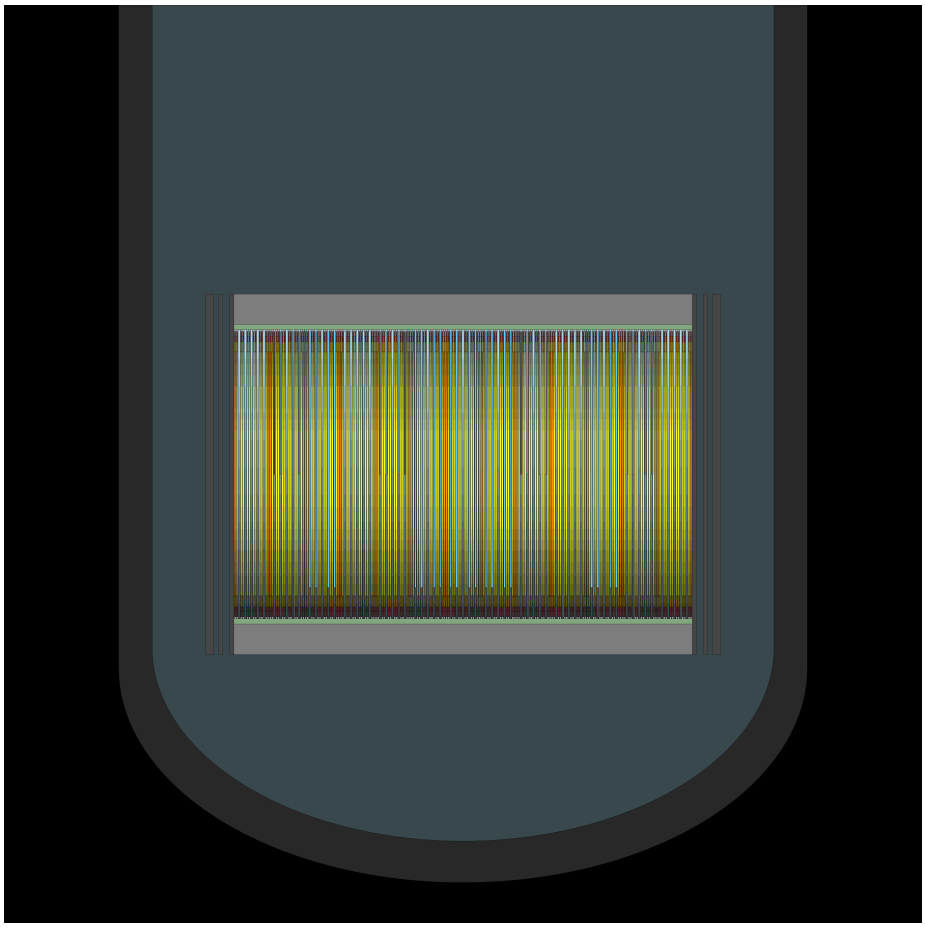

Figure 27: RR SMR full core model, side-view. Rods of different types can be seen. Yellow and orange rods are fuel rods, while blue and dark rods are either pyrex rods, control rods or empty guide tubes. The white part at the upper and lower end of the rods is helium. The green and gray blocks at the top and bottom of the core are homogenized regions containing a mix of steel and water (50/50, and 30/70) which represent the axial reflectors and inlet/outlet nozzles respectively.

5 BWRs

A model of the BWRX-300 was developed in a similar manner to the PWRs. While there is more information available for this reactor than the RR SMR, mainly in the "BWRX-300 General Description" document published by GE-Hitachi in 2023 [11] as well as in the "Small Modular Reactor Catalogue" published by IAEA in the Advanced Reactor Information System (ARIS) database in 2024 [17] (this information was also given by GE-Hitachi), there is still some information missing that is required to model the reactor. In both of the sources above it is stated that the BWRX-300 uses fuel assemblies of the type GNF2, with a description of the assembly and figures given in [11]. Upon comparison, the GNF2 assembly is similar in many ways to the GE14 assembly used in the ABWR, with the main differences outlined in Appendix 2 in [18] and Table 1-X in [19].

Differences mainly pertain to small variations in fuel rod dimensions, as well as the fact that the GNF2 assembly contains both short and long part-length rods (137.16 cm and 259.08 cm active height respectively) [19], while the GE14 only has part-length rods of one length (213.36 cm) [20]. The choice was therefore made to make a model of the ABWR for which there is more documentation available [20] [21] [22], and re-use the aspects from that model which were missing in the BWRX-300 description. It would then also be possible to compare the results from the BWRX-300 model to those of the ABWR model and thus relate the simulated production rates to a real reactor. The following sections describe the common and individual elements of the BWRX-300 and ABWR used in the Serpent model.

5.1 Materials

Most of the materials in the BWRX-300 model are identical to the ones in the ABWR model. The composition of the coolant that was used in the models was taken directly from Serpent, which uses the composition given in [14]. This can be found in Table 17 [14].

Table 17: Composition of the coolant used in the BWR models [14].

Isotope	Mass fraction
^{1}H	1.11868E-01
^{2}H	2.57129E-05
^{16}O	8.85699E-01
^{17}O	3.58568E-04
^{18}O	2.04818E-03

The fuel rod gaps were modelled as ^{4}He with density 0.001598 g/cm^{3}. The Boron carbide in the control rods used for reactivity control was the same as

previously defined in Table 10 [14].

The fuel materials used in the ABWR model was taken from [20]. Five different enrichment levels of UO_2 were specified, 0.71 wt% (natural uranium), 2.4 wt%, 3.1 wt%, 3.9 wt% and 4.9 wt%. Fourteen of the fuel rods with 4.9 wt% enrichment also contain burnable absorber in the form of Gd_2O_3, to the amount of 6 wt%. The total average enrichment in the ABWR core is approximately 3.7845 wt%. The compositions of the fuel materials are specified in Table 18.

Table 18: Composition of the UO_2 fuels in the ABWR model [20].

	Enrichment [wt% ^{235}U]					
	0.71	2.4	3.1	3.9	4.9	4.9 + 6 wt% Gd_2O_3
Isotope	Mass fractions					Atomic fractions
^{235}U	6.25863E-3	2.11559E-2	2.73264E-2	3.43784E-2	4.31934E-2	9.54439E-04
^{238}U	0.875238	0.860341	0.854171	0.847119	0.838304	1.82899E-02
^{16}O	1.18181E-01	1.18181E-01	1.18181E-01	1.18181E-01	1.18181E-01	3.84987E-02
^{17}O	4.78448E-05	4.78448E-05	4.78448E-05	4.78448E-05	4.78448E-05	1.46652E-05
^{18}O	2.73294E-04	2.73294E-04	2.73294E-04	2.73294E-04	2.73294E-04	7.91148E-05
^{152}Gd	-	-	-	-	-	4.19106E-06
^{154}Gd	-	-	-	-	-	4.56824E-05
^{155}Gd	-	-	-	-	-	3.10141E-04
^{156}Gd	-	-	-	-	-	4.28957E-04
^{157}Gd	-	-	-	-	-	3.27952E-04
^{158}Gd	-	-	-	-	-	5.20532E-04
^{160}Gd	-	-	-	-	-	4.58085E-04

For the BWRX-300, the same fuel materials were initially used as the average enrichment was also stated to be 3.8 % for this reactor [11]. Initial testing, however, indicated that these fuel enrichment levels were not sufficient to reach criticality in the core. The 4.9 wt% fuel was first increased to the maximum enrichment of 4.95 wt% (also in the Gd-doped fuel material), which was still not sufficient. Each of the other fuel materials (excluding the natural uranium) were then successively increased to reach a supercritical state (which allowed for control rod insertion). The final fuel enrichments that were used were 0.711 wt%, 2.5 wt%, 3.2 wt%, 4.1 wt% and 4.95 wt%. The average enrichment was thus increased from the initial 3.765 wt% to 3.832 wt%. The corresponding compositions can be found in Table 19.

Table 19: Composition of the UO_2 fuels used in the BWRX-300 model.

	Enrichment [wt% ^{235}U]					
	0.711	2.5	3.2	4.1	4.95	4.95 + 6 wt% Gd_2O_3
Isotope	Mass fraction					Atomic fraction
^{235}U	6.26745E-3	2.2037E-2	2.82079E-2	3.61414E-2	4.36341E-2	9.66440E-04
^{238}U	0.875230	0.85946	0.853290	0.845356	0.837864	1.83232E-02
^{16}O	1.18181E-01	1.18181E-01	1.18181E-01	1.18181E-01	1.18181E-01	3.85890E-02
^{17}O	4.78448E-05	4.78448E-05	4.78448E-05	4.78448E-05	4.78448E-05	1.46996E-05
^{18}O	2.73294E-04	2.73294E-04	2.73294E-04	2.73294E-04	2.73294E-04	7.93004E-05
^{152}Gd	-	-	-	-	-	4.20089E-06
^{154}Gd	-	-	-	-	-	4.57895E-05
^{155}Gd	-	-	-	-	-	3.10868E-04
^{156}Gd	-	-	-	-	-	4.29962E-04
^{157}Gd	-	-	-	-	-	3.28721E-04
^{158}Gd	-	-	-	-	-	5.21753E-04
^{160}Gd	-	-	-	-	-	4.59159E-04

There are two different types of Zirconium alloy used in the BWR models. Zircaloy-2 is used for fuel rod cladding (including lower and upper end plugs [23, figure 2.2-3]) and for the water rods, whereas Zircaloy-4 is used for the flow channel wall [24, p. 130]. The compositions used were those available in [14], and are specified in Table 20.

Table 20: Composition of the Zircaloy materials used in the BWR models.

Material ⟶	Zircaloy-2	Zircaloy-4
Isotope	Mass fraction	
^{16}O	1.19376E-03	1.19276E-03
^{17}O	4.83282E-07	4.82878E-07
^{18}O	2.76056E-06	2.75825E-06
^{50}Cr	4.16117E-05	4.16117E-05
^{52}Cr	8.34483E-04	8.34483E-04
^{53}Cr	9.64457E-05	9.64457E-05
^{54}Cr	2.44600E-05	2.44600E-05
^{54}Fe	5.62862E-05	1.12572E-04
^{56}Fe	9.16258E-04	1.83252E-03
^{57}Fe	2.15389E-05	4.30778E-05
^{58}Fe	2.91667E-06	5.83334E-06
^{58}Ni	3.35317E-04	-
^{60}Ni	1.33612E-04	-
^{61}Ni	5.90496E-06	-
^{62}Ni	1.91358E-05	-
^{64}Ni	5.03067E-06	-
^{90}Zr	4.98111E-01	4.97862E-01
^{91}Zr	1.09835E-01	1.09780E-01
^{92}Zr	1.69731E-01	1.69646E-01
^{94}Zr	1.75753E-01	1.75665E-01
^{96}Zr	2.89183E-02	2.89038E-02
^{112}Sn	1.27668E-04	1.27604E-04
^{114}Sn	8.84175E-05	8.83732E-05
^{115}Sn	4.59485E-05	4.59255E-05
^{116}Sn	1.98205E-03	1.98105E-03
^{117}Sn	1.05596E-03	1.05543E-03
^{118}Sn	3.35857E-03	3.35688E-03
^{119}Sn	1.20129E-03	1.20069E-03
^{120}Sn	4.59450E-03	4.59220E-03
^{122}Sn	6.63830E-04	6.63497E-04
^{124}Sn	8.43778E-04	8.43355E-04

There are a number of structural materials used. Stainless steel 304 (SS-304) is by far the most common structural material and is used for control rods, fuel supports[8], lower and upper tie plates, the core shroud and the top guide [25][24]. This material is available in Serpent with composition from [14]. The density was taken from [26]. The composition is specified in Table 21.

For the large structural component called the core plate, the steel material

[8]both orificed and peripheral fuel supports.

XM-19 was used [24]. The composition used for this material was taken from [27] and is specified in Table 22. The natural isotopic abundance of each element was used for the composition in Serpent.

One additional material was included in the BWRX-300 model, which is the stainless steel of the SA508 variety used for the RPV (unlike ABWR which used SS304). The material composition was taken from [28] and is shown in Table 23. For the elements which were given as less-than-or-equal-to a certain value, the maximum was used.

In addition, the material temperatures and densities were changed to align with the operating temperature and pressure of each reactor. In the ABWR, the temperature of the coolant varies between 278.3-291.5 °C from inlet to outlet, and the average pressure is 7.27 MPa. In the BWRX-300 the temperature of the coolant varies between 270-288 °C from inlet to outlet, and the average pressure is 7.17 MPa [17].

Table 21: Composition of the SS304 material used in the BWR models [14].

Isotope	Weight fraction
^{12}C	3.95366E-04
^{13}C	4.63372E-06
^{28}Si	4.59332E-03
^{29}Si	2.41681E-04
^{30}Si	1.64994E-04
^{31}P	2.30000E-04
^{32}S	1.42073E-04
^{33}S	1.15681E-06
^{34}S	6.75336E-06
^{36}S	1.68255E-08
^{50}Cr	7.93000E-03
^{52}Cr	1.59029E-01
^{53}Cr	1.83798E-02
^{54}Cr	4.66139E-03
^{55}Mn	1.00000E-02
^{54}Fe	3.96166E-02
^{56}Fe	6.44901E-01
^{57}Fe	1.51600E-02
^{58}Fe	2.05287E-03
^{58}Ni	6.21579E-02
^{60}Ni	2.47678E-02
^{61}Ni	1.09461E-03
^{62}Ni	3.54721E-03
^{64}Ni	9.32539E-04

Table 22: Composition of the XM-19 structural material used for the core plate in the BWR models [27].

Element/Isotope	Mass fraction
Carbon	0.0003
Nitrogen	0.0040
Silicon	0.0060
Phosphorous	0.0004
Sulphur	0.0001
Vanadium	0.0030
Chromium	0.2350
Manganese	0.0600
Iron	0.5232
Nickel	0.1350
Niobium	0.0030
Molybdenum	0.0300

Table 23: Material composition wt% of Low Alloy Steel SA508 [28]

Element	Content (%)
Carbon (C)	0.25
Manganese (Mn)	1.20
Silicon (Si)	0.60
Phosphorus (P)	0.035
Sulfur (S)	0.035
Nickel (Ni)	0.25
Chromium (Cr)	0.25
Molybdenum (Mo)	0.08
Copper (Cu)	0.35
Vanadium (V)	0.05
Boron (B)	0.003
Iron (Fe)	Balance (96.897)

5.2 Fuel Rods

As with the PWR models, the fuel rods in the BWR models are made up of axially infinite pin universes[9] that are stacked axially to create the axially limited fuel rods. The geometric properties of the individual pin universe are identical within the ABWR model and within the BWRX-300 model separately. All enrichment levels used for the fuel rods can be found in Table 18 for the ABWR and table 19 for the BWRX-300.

[9]The word "universe" is the terminology used in Serpent. More information about this can be found at https://serpent.vtt.fi/mediawiki/index.php?title=Universe-based_geometry_type_in_Serpent

5.2.1 Pin Geometries

Radially, the fuel rods are made of a cylindrical fuel region containing one of the ^{235}U fuel types with a radius of 0.4380 cm for the ABWR and 0.4440 cm for the BWRX-300. Outside the fuel region is a small gap filled with helium that stretches to a radius of 0.4470 cm for the ABWR and 0.4530 cm for the BWRX, outside of which is the fuel rod cladding. The cladding has a thickness of 0.066 cm for the ABWR and 0.06 cm for the BWRX-300, meaning the outer radius of the fuel rod is 0.5130 cm for both reactors. Surrounding the fuel rod is the coolant/moderator. The radius of the outer perimeter of each region in the fuel rod can be found in the table in Figure 28.

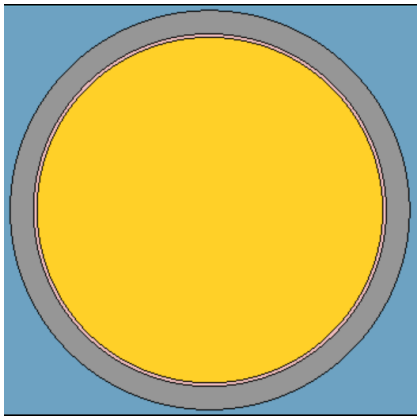

Material	Radius ABWR/BWRX-300 (cm)
UO_2 fuel	0.4380/0.4440
He gap	0.4470/0.4530
Zr cladding	0.5130
H_2O coolant	> 0.5130

Figure 28: Picture showing the radial pin dimensions used in the BWRX-300 model. The yellow at the center is fuel material, surrounded by a thin layer of helium, outside of which is the Zircaloy cladding. Surrounding the perimeter of the fuel rod (outside the cladding) is H_2O. At this scale the ABWR pins look essentially identical.

In each fuel assembly there are two water rods with larger radial dimension than the fuel rods. Each water rod occupies four slots in the assembly lattice meaning the water rods occupy a total of 8 slots per assembly. The central region of the water rods allow for water to easily pass through the assembly for increased moderation. The water rods are made of Zircaloy-2 and have an inner radius of 1.161 cm and a thickness of 0.1 cm in the ABWR [22, p. 71] and an inner radius of 1.169 cm and a thickness of 0.076 cm in the BWRX-300 [18]. All water rods are surrounded by coolant. The radius of the outer perimeter of each region in the water rods are also tabulated in Figure 29. In Figure 30 the moderating water is shown in different colors on the inside and on the outside of the water rod, reflecting the fact that in the model the moderator is approximated to be unheated inside the water rods and therefore remain at inlet conditions throughout the axial height of the fuel assemblies. The water with darker color represents water with lower temperature and higher density,

while water with lighter color represents a higher temperature and lower density.

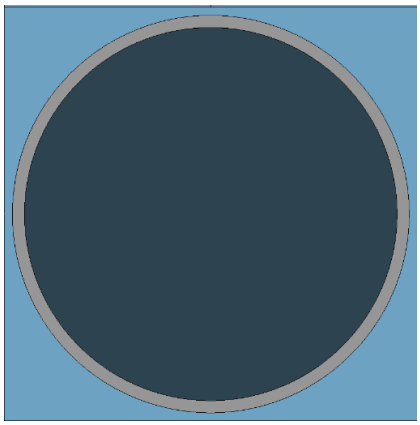

Material	Radius ABWR/BWRX-300 (cm)
H_2O coolant	1.161/1.169
Zr cladding	1.261/1.245
H_2O coolant	$>$ 1.261/1.245

Figure 29: Picture showing the radial water rod dimensions used in the BWRX-300 model. The rod is made of Zircaloy cladding (gray), at the center of which is water (darker color since in Serpent this water has the lowest temperature and highest density of water in the model). Outside the rod is also water (with a higher temperature/lower density than inside the rod). At this scale the ABWR water rods look essentially identical.

5.2.2 Rod Geometries

In each assembly there are a number of part-length fuel rods, in the positions which can be seen in Figure 33 [20] for the ABWR and in Figure 34 [11] for the BWRX-300. The part-length rods in the ABWR model are all of the same length, having an active fuel height of 213.36 cm and a total length of 243.84 cm [19] while in the BWRX-300 model they are either short, being only 137.2 cm long, or longer with a length of 259.1 cm [19]. All part-length rods were assumed to have fuel with a ^{235}U enrichment of 4.9 wt% (or 4.95 wt% in the case of the BWRX-300). The full length rods are 381.0 cm [19]. Axially the fuel rods have 3-4 regions. At the bottom, all rods have a 15.24 cm long axial blanket consisting of fuel with a lower ^{235}U enrichment of 0.71 wt% (0.711 wt% in the BWRX-300). Following that is a fuel region with ^{235}U enrichment as previously described, with different lengths depending on if it is a part length, or full-length rod. Above the fuel region, full length rods also have a 30.48 cm long axial blanket with the same enrichment as in the bottom axial blanket. Directly below the active fuel there is a lower end plug (LEP), and above the active fuel height there is a gas plenum followed by an upper end plug (UEP) [29, Figure 11.5-3]. Figure 30 shows a side-view of a BWRX-300 assembly where the different axial regions can be seen for both part-length and full-length rods.

In regards to the exact dimensions used for the LEPs, the UEPs and the

gas plenum regions found in all fuel rods in the BWR models, it must be noted that no definitive numbers have been found throughout the publicly available documentation. However, based on a number of sources, including [25] and [29] to name two, these numbers have been estimated to be the following for the BWR models. The LEPs extend 4.1776 cm below the active fuel. The gas plenum regions extend 25.40 cm above the active fuel height in all fuel rods. The UEPs extends 6.83 cm above the gas plenum regions.

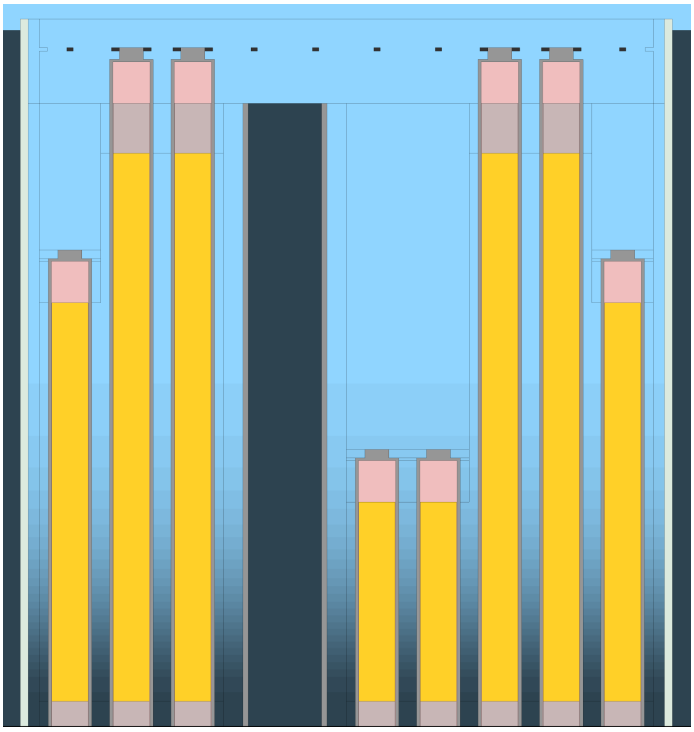

Figure 30: BWRX-300 assembly, with differing fuel rod lengths as well as a water rod - side-view. The yellow parts of the rods is the enriched fuel, while the gray part on the ends is the axial blanket of natural uranium. The enriched fuel and the axial blankets make up the active fuel region, 381 cm in height. At the top of each rod is a helium gas plenum (pink), above which is the end cap (gray). The end caps of the full length rods fit into the top grid. The water rod, which is the darker rod in the middle of the assembly, has approximately twice the diameter of a fuel rod. The water in the water rod has the same temperature and density as the coolant at the inlet of the core. The water surrounding the rods in the assembly in contrast has a gradient, due to it's temperature increase and density decrease along the height of the core. The walls of the assembly are made of zircaloy (white), outside of which is more water.

As was done previously for the PWRs, the axial fuel temperature distribution

was estimated with the code provided by Christophe Demazière [12]. The mass flow rate of BWRX-300 was given in [11] as 1530 g/m^{2}s. The mass flow rate of ABWR was calculated from [21] to be 1644 kg/m^{2}s. The resulting radial temperature distributions in the fuel can be seen in Figure 31, and the axial temperature distributions including the radially averaged distribution can be seen in Figure 32, with corresponding values listed in Table 24.

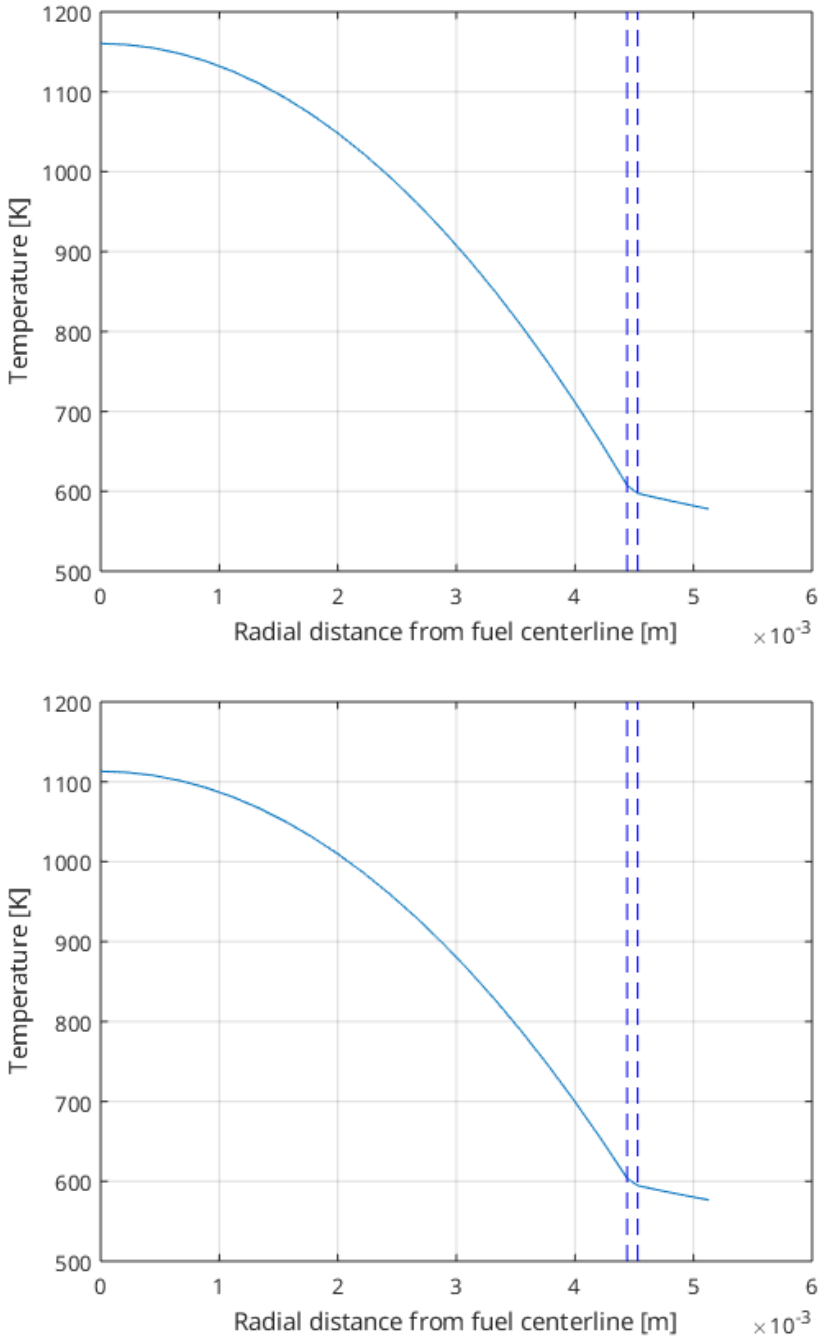

Figure 31: Radial temperature distribution at the fuel half-height [12]. Top) ABWR. Bottom) BWRX-300.

Table 24: Axial fuel temperature distribution in the ABWR and the BWRX-300 [12].

Height [cm]	Temperature [K]	
	ABWR	BWRX-300
0.0	561.55	560.61
15.24	604.38	600.23
30.48	646.54	639.25
45.72	687.39	677.04
60.96	726.29	713.03
76.20	762.42	746.48
91.44	794.08	775.70
106.68	821.83	801.30
121.92	845.35	822.98
137.16	864.34	840.47
152.40	878.58	853.57
167.64	887.89	862.11
182.88	892.15	865.99
198.12	891.30	865.17
213.36	885.39	859.67
228.60	874.50	849.58
243.84	858.80	835.06
259.08	838.54	816.33
274.32	814.03	793.69
289.56	785.64	767.47
304.80	753.81	738.08
320.04	719.03	705.97
335.28	681.83	671.62
350.52	642.78	635.58
365.76	602.48	598.38
381.00	561.55	560.60

The axial density and temperature distribution of the coolant along the flow channel for the ABWR were obtained from [22, Table 3.A2] in the case of the density distribution and from [22, Figure 3.20 (Serpent/CTF Average)] in the case of the temperature distribution. In order to be able to produce values for the coolant temperature at any arbitrary height along the flow channel, a function was fitted using extracted values from the referenced graph. The function[10] chosen was

$$T_{fit}(z;\tau) = T_{inlet} + (T_{outlet} - T_{inlet})\left(1 - \left(1 + \frac{z}{\tau}\right)e^{-\frac{z}{\tau}}\right)$$

For the BWRX-300, the code provided by Christophe Demazière [12] was used to estimate the density and temperature. The resulting distributions can

[10] This is the step-response of a second order linear time-invariant system, a kind of function normally encountered within control theory. The Serpent/CTF Average graph closely resembles such a step-response, a fact which upon being noticed led to the choice.

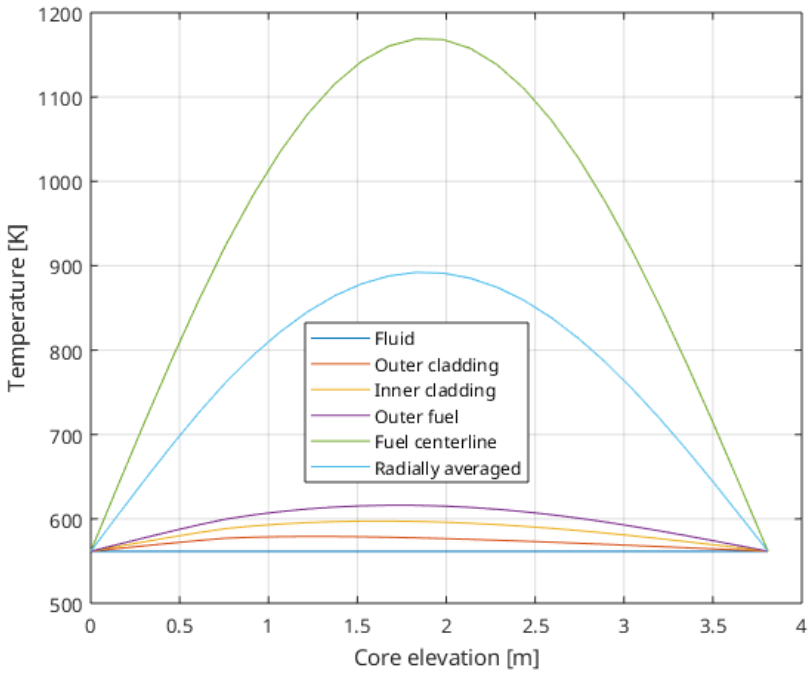

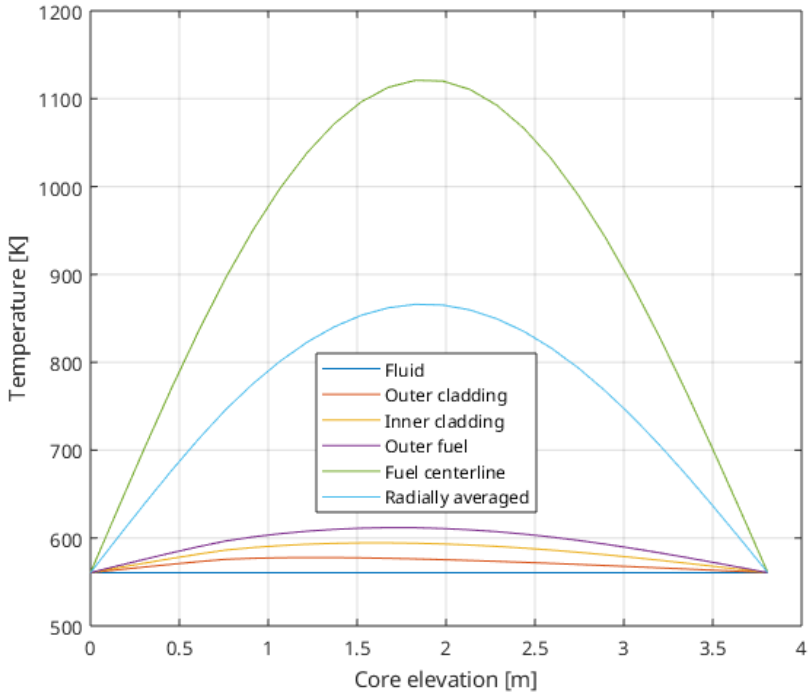

Figure 32: Axial temperature distribution in different parts of the fuel as well as radially averaged [12]. Top) ABWR. Bottom) BWRX-300.

be seen in Table 25.

Please note that the density and temperature distributions are the same along every assembly in the ABWR and in the BWRX-300 separately. This is a significant inaccuracy in all of the models which is especially detrimental to the two BWR models. This inaccuracy was pointed out and discussed section 1.1.

Table 25: Axial density and temperature distribution of the coolant in the ABWR [22] and the BWRX-300 [12].

Height [cm]	Density [g/cm^3]		Temperature [K]	
	ABWR	BWRX-300	ABWR	BWRX-300
0.0	0.7552	0.7367	551.4500	543.0000
15.24	0.7552	0.7268	551.4500	543.0000
30.48	0.7500	0.7002	554.0110	544.1079
45.72	0.7309	0.6623	555.9320	546.4417
60.96	0.6956	0.6185	557.7290	549.0727
76.20	0.6433	0.5730	559.2460	551.5512
91.44	0.5903	0.5288	560.6020	553.6919
106.68	0.5395	0.4877	561.7840	555.4481
121.92	0.4993	0.4503	562.7700	556.8406
137.16	0.4598	0.4170	563.5150	557.9184
152.40	0.4194	0.3877	564.0380	558.7376
167.64	0.3958	0.3621	564.3090	559.3516
182.88	0.3670	0.3399	564.5130	559.8066
198.12	0.3357	0.3208	564.6920	560.1408
213.36	0.3225	0.3044	564.7930	560.3844
228.60	0.3002	0.2905	564.8650	560.5607
243.84	0.2764	0.2787	564.9070	560.6877
259.08	0.2717	0.2689	564.9170	560.7787
274.32	0.2506	0.2609	564.9170	560.8436
289.56	0.2398	0.2546	564.9360	560.8898
304.80	0.2380	0.2498	564.9610	560.9225
320.04	0.2159	0.2465	564.9710	560.9457
335.28	0.2164	0.2447	564.9810	560.9620
350.52	0.2095	0.2442	564.9890	560.9734
365.76	0.1961	0.2450	564.9950	560.9814
381.00	0.2020	0.2473	565.0000	560.9871

5.3 Fuel Assemblies

Fuel and water rods were arranged in assemblies as seen in Figure 33 for the ABWR [20] and 34 for the BWRX-300 [11]. The pin pitch was taken to be 1.295 cm [18]. The placement of the different fuel rod types was taken to be the same in the GNF2 assembly in the BWRX-300 as in the GE14 assembly used

in ABWR model [20], with the exception of part-length rods. The assembly is encapsulated by a flow channel wall with rounded corners with an inner side-length of 13.42 cm an outer side-length of 13.75 cm. Coolant flows between the assemblies in the core, and including this the BWR assembly pitch is 15.24 cm. The ABWR and BWRX-300 assemblies in the Serpent model can be seen in Figures 35 and 36 (note that the colors in the Serpent models may not exactly match those used in Figures 33 and 34).

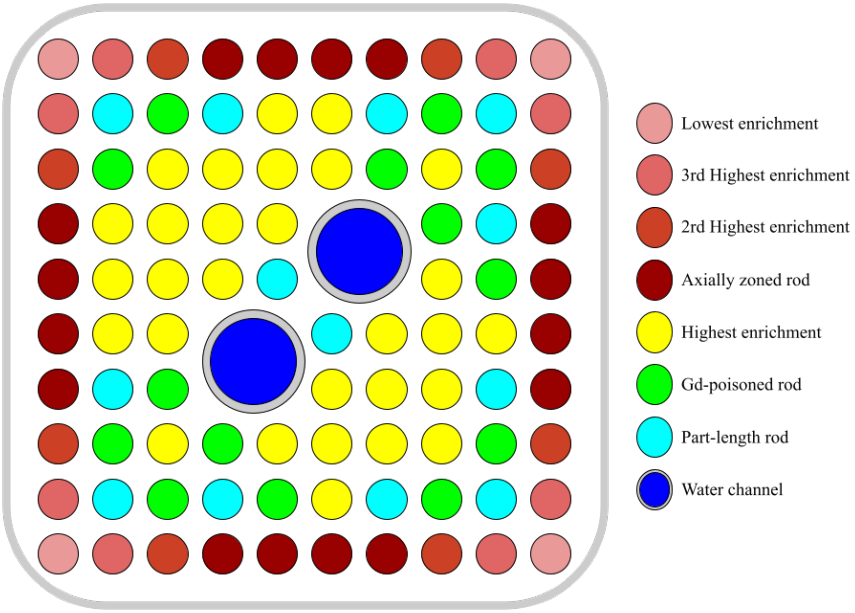

Figure 33: ABWR fuel assembly with part-length rod locations. Inspired by [20].

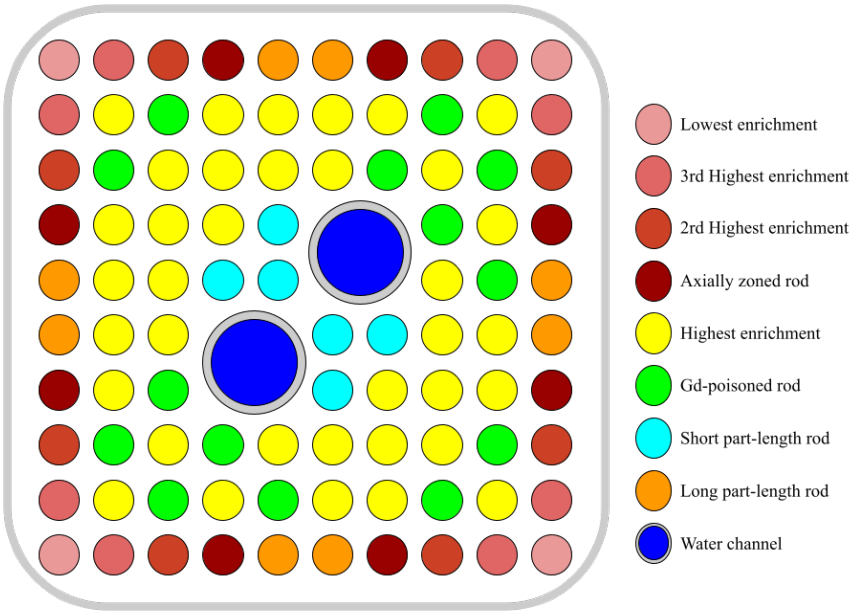

Figure 34: BWRX-300 fuel assembly with part-length rod locations. Certain elements of the assembly were inspired by [11] and [20].

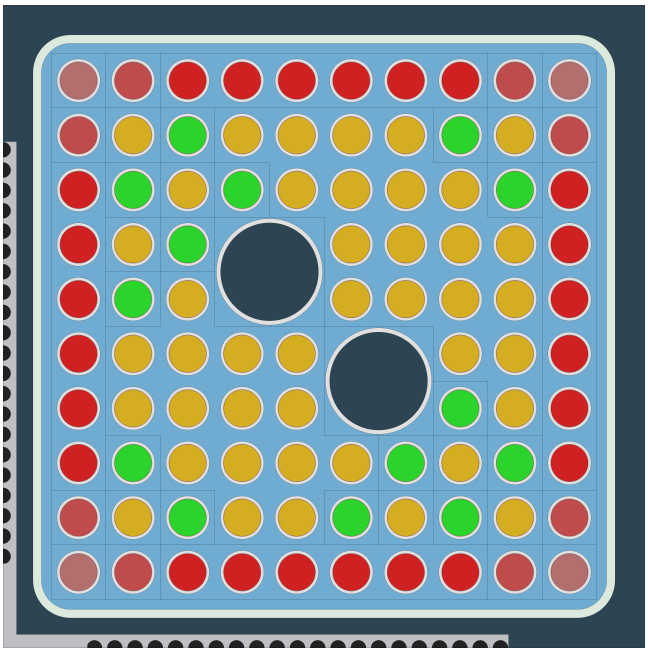

Figure 35: ABWR fuel assembly in the Serpent model, including a control blade insertion.

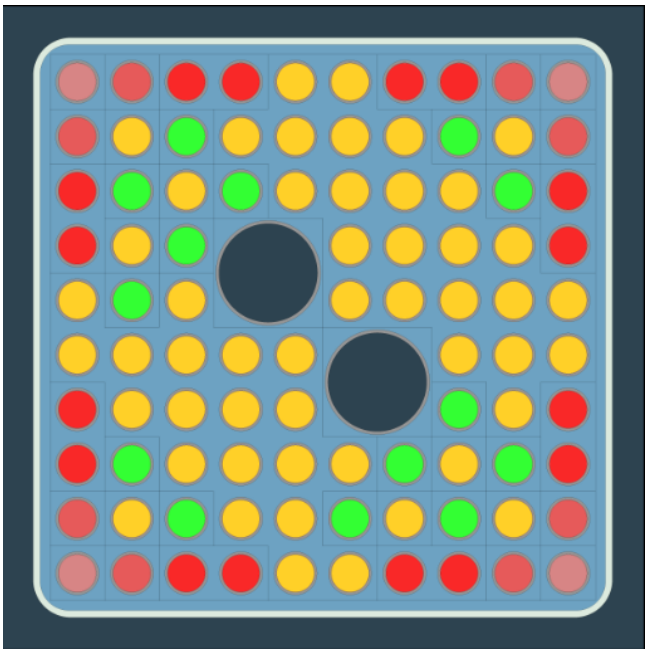

Figure 36: BWRX-300 fuel assembly in the Serpent model.

5.4 Core

Assemblies were arranged into 2-by-2 super-cells with control rods in-between them, which for the BWRX-300 can be seen in Figure 37. The control rods in the Serpent model were based of the simplified definition in [26]. Each rod is composed of a cruciform stainless steel structure with 21 tubes of B_4C in each blade.

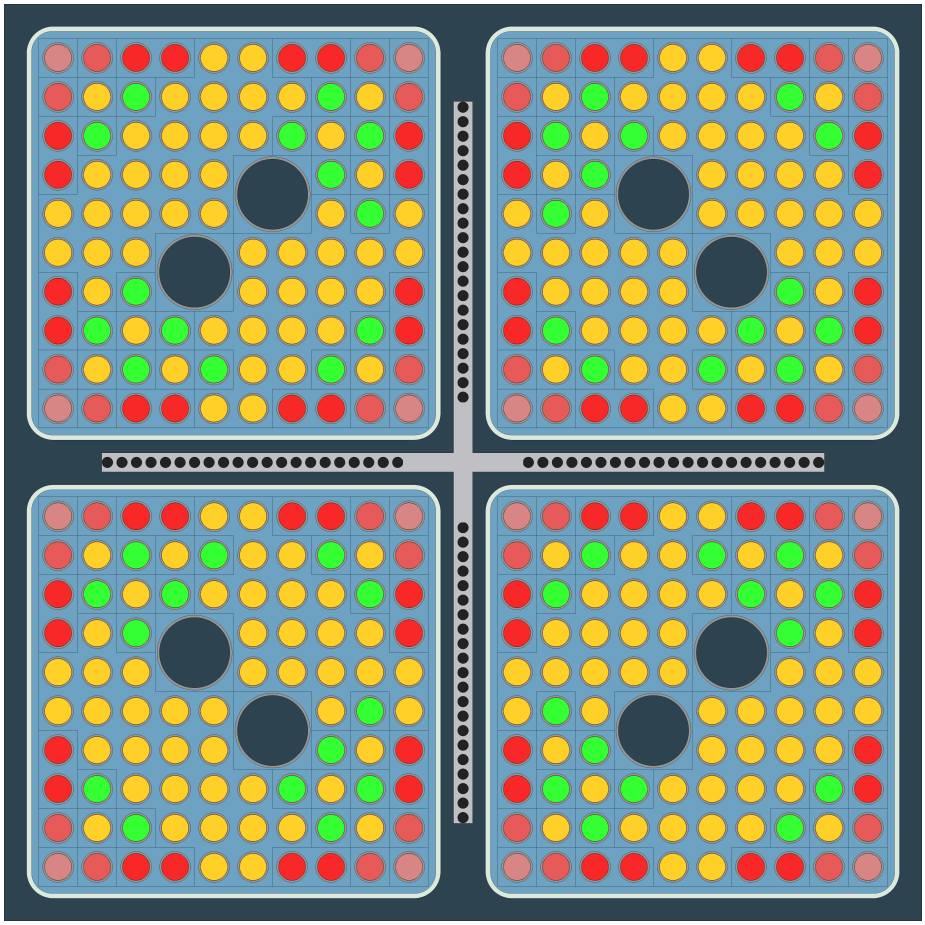

Figure 37: BWRX-300 2x2 supercell.

These supercells were then arranged according to the scheme in Figure 38 for the ABWR and 39 for the BWRX-300 [11]. As can be seen, some additional lone assemblies, also called peripheral assemblies are also added at the periphery of the core of both the ABWR and the BWRX-300. Note that the peripheral assemblies in both BWR models have different fuel supports between the active fuel and the core plate.

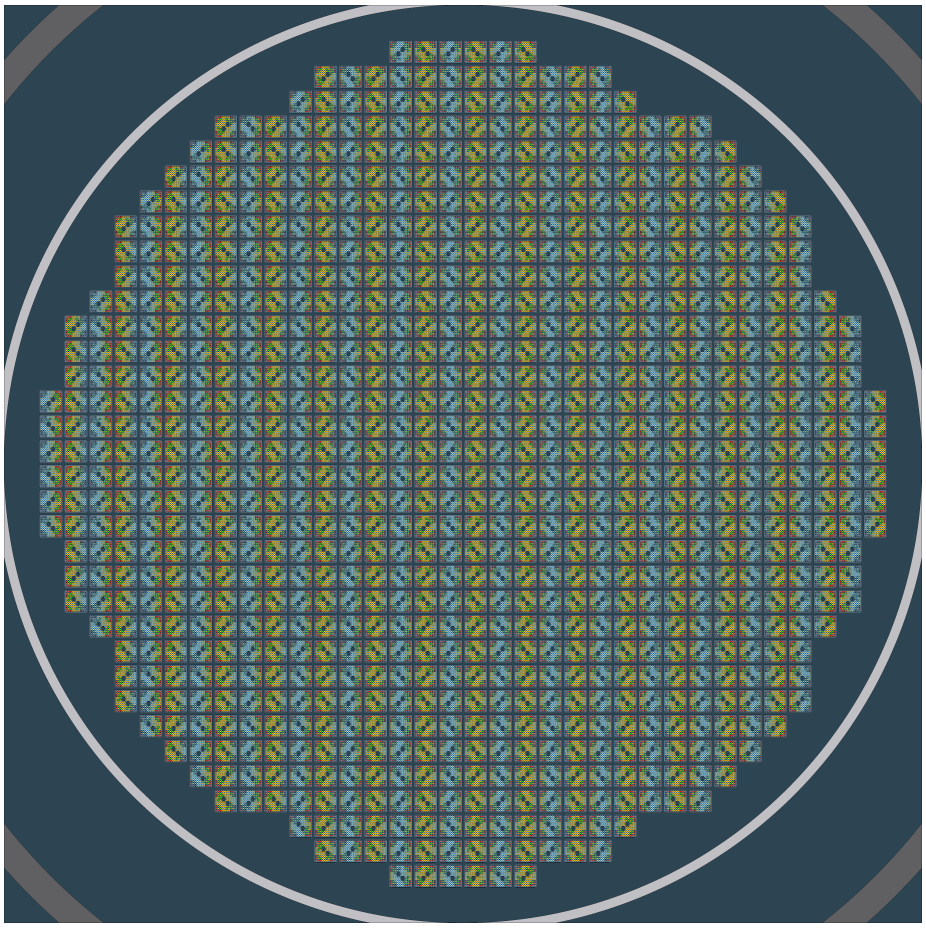

Figure 38: ABWR core lattice, top view. Surrounding the fuel assembly lattice is water coolant, followed by the shroud which is in white/light grey. The region outside the shroud is filled with more water. This region is bounded by the RPV which is in dark grey and which is only visible in the corners of the figure. The body of water filling the region between the shroud and the RPV is called the downcomer.

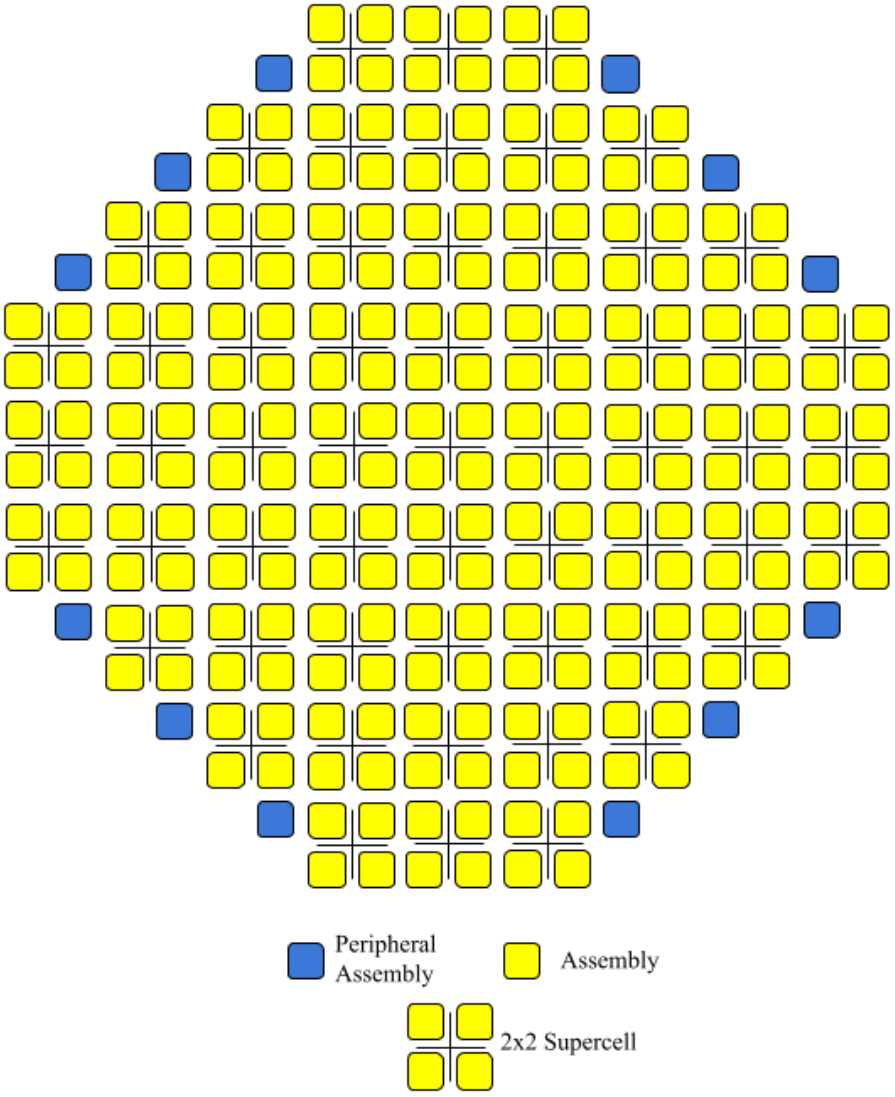

Figure 39: BWRX-300 core model [11].

The resulting model of the BWRX-300 in Serpent can be seen in Figure 40.

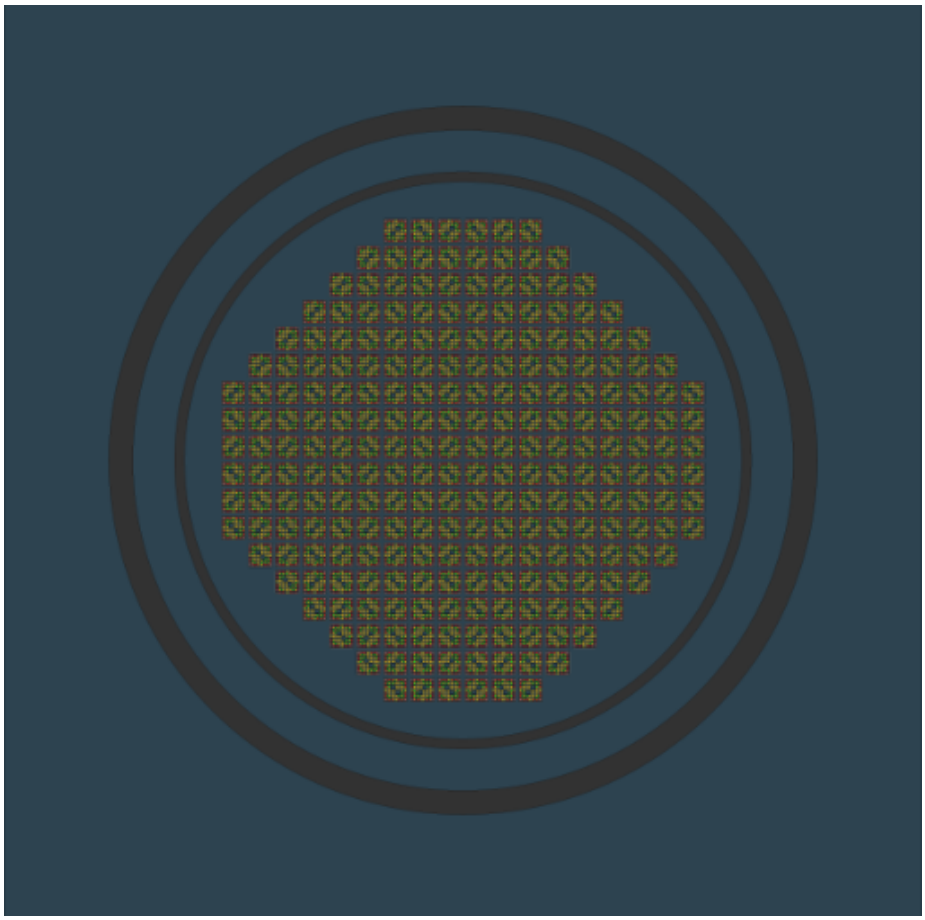

Figure 40: BWRX-300 core lattice, top view. Surrounding the fuel assembly lattice is water coolant, followed by the shroud which is in dark grey. The region outside the shroud is filled with more water. This region is bounded by the RPV which is also in dark grey. The body of water filling the region between the shroud and the RPV is called the downcomer. Outside the RPV is more water, which corresponds to the water of the pool in which the RPV sits.

As was described earlier, the singular fuel assembly type in both of these models results in the power and flux distributions having a bessel-function shape with a peak in the middle of the core. To flatten out the distributions control rods were inserted according to the scheme described in Chapter 3. In the ABWR model this worked very well since the size of the core is considerable. For the BWRX-300 however, some additional adjustments had to be made by hand. The final insertions can be seen in Table 26. The position of each control rod bank can be seen in Figure 41 for the ABWR and Figure 42 for the BWRX-300.

Table 26: Control rod insertions by bank in the ABWR and BWRX-300 models.

	ABWR	BWRX-300
CR bank	Insertion [cm]	
0	0.0	0.0
1	117.3480	80.96
2	108.1415	60.96
3	99.3010	60.96
4	82.6792	0.0
5	74.8790	0.0
6	53.4122	32.5547
7	46.8718	29.54
8	40.6248	26.6354

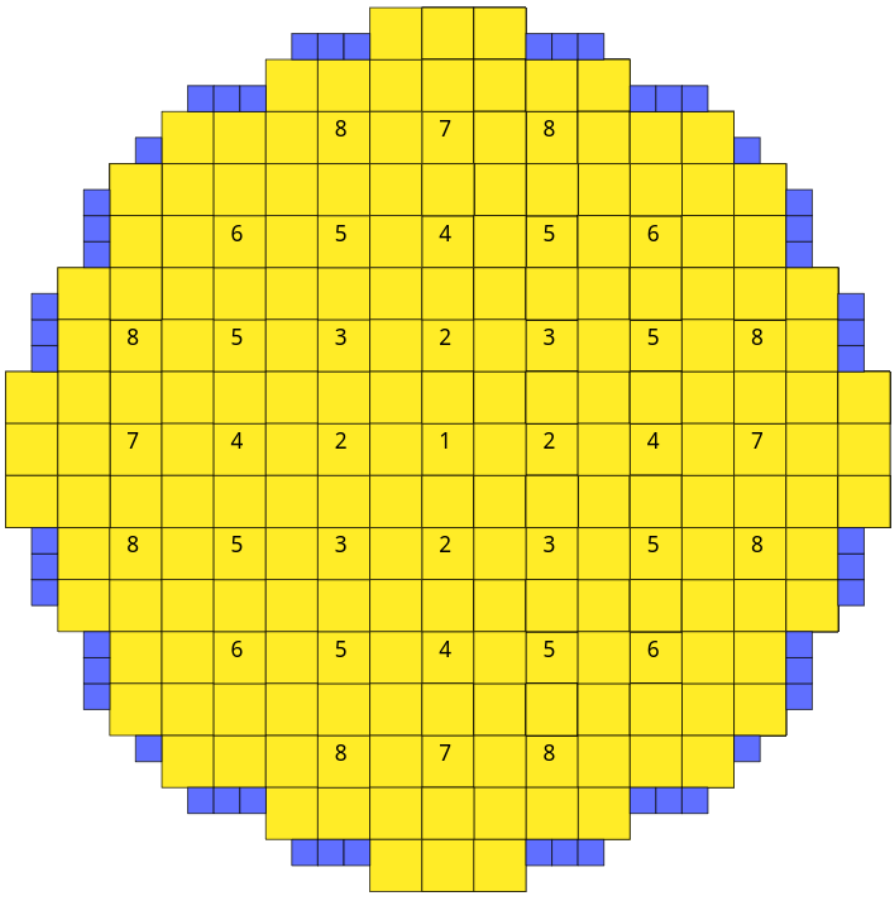

Figure 41: ABWR control rod banks. Yellow squares represent 2x2 supercells, while blue squares represent peripherial assemblies.

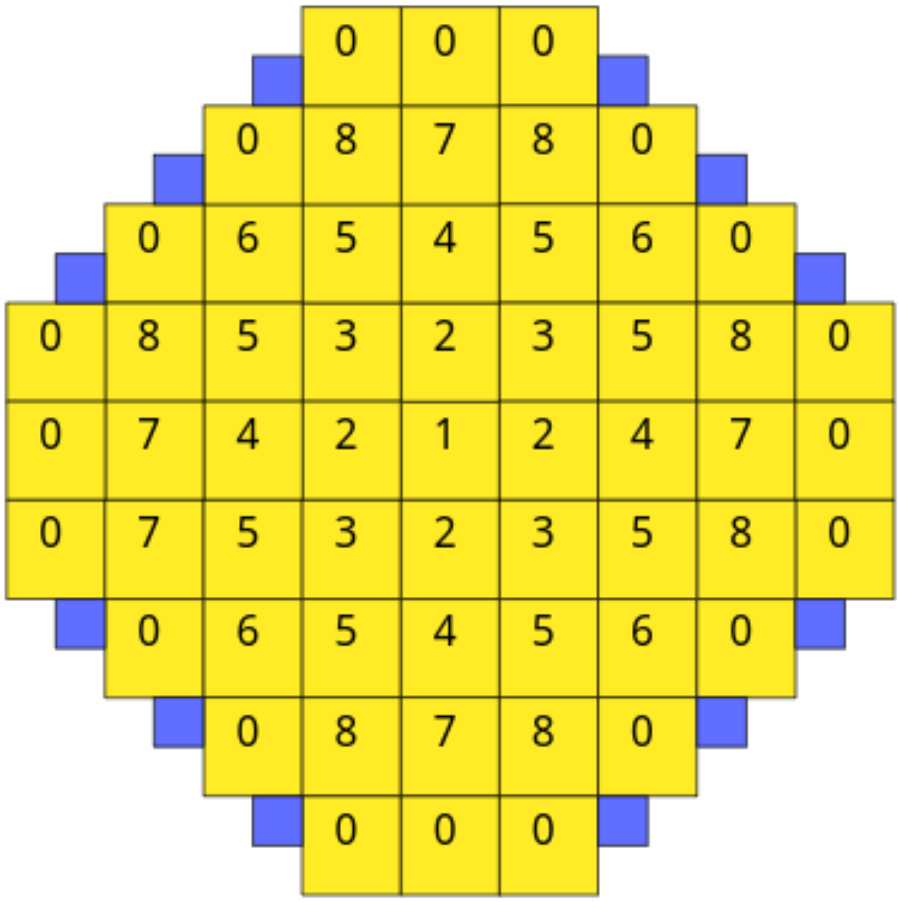

Figure 42: BWRX-300 control rod banks. Yellow squares represent 2x2 supercells, while blue squares represent peripherial assemblies.

These insertions resulted in the core power and flux distributions seen in Figures 43, 44 and 45 for the ABWR, and Figures 46, 47 and 48 for the BWRX-300, presented in the same manner as was done for the RR SMR.

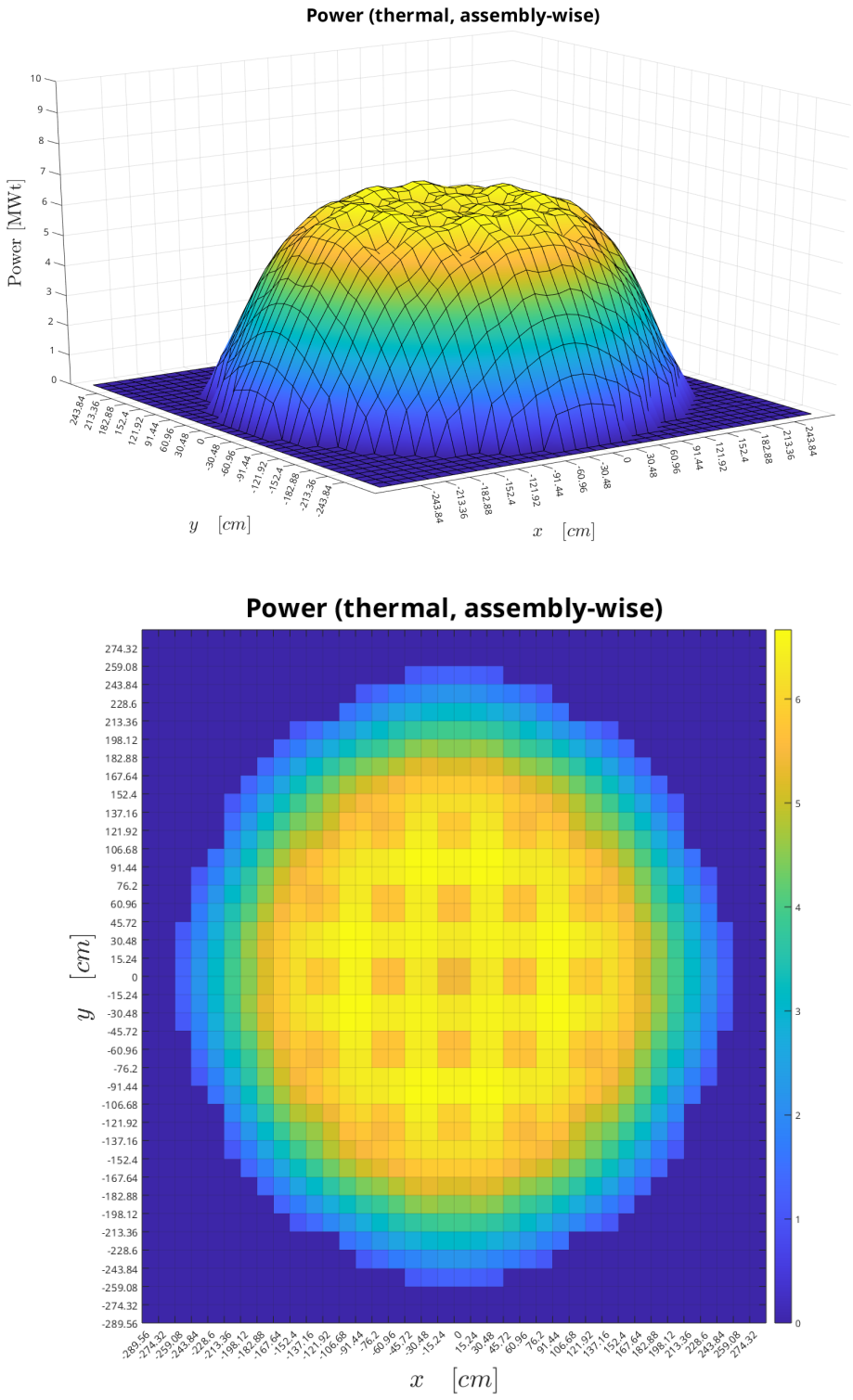

Figure 43: ABWR power distribution in the Serpent model.

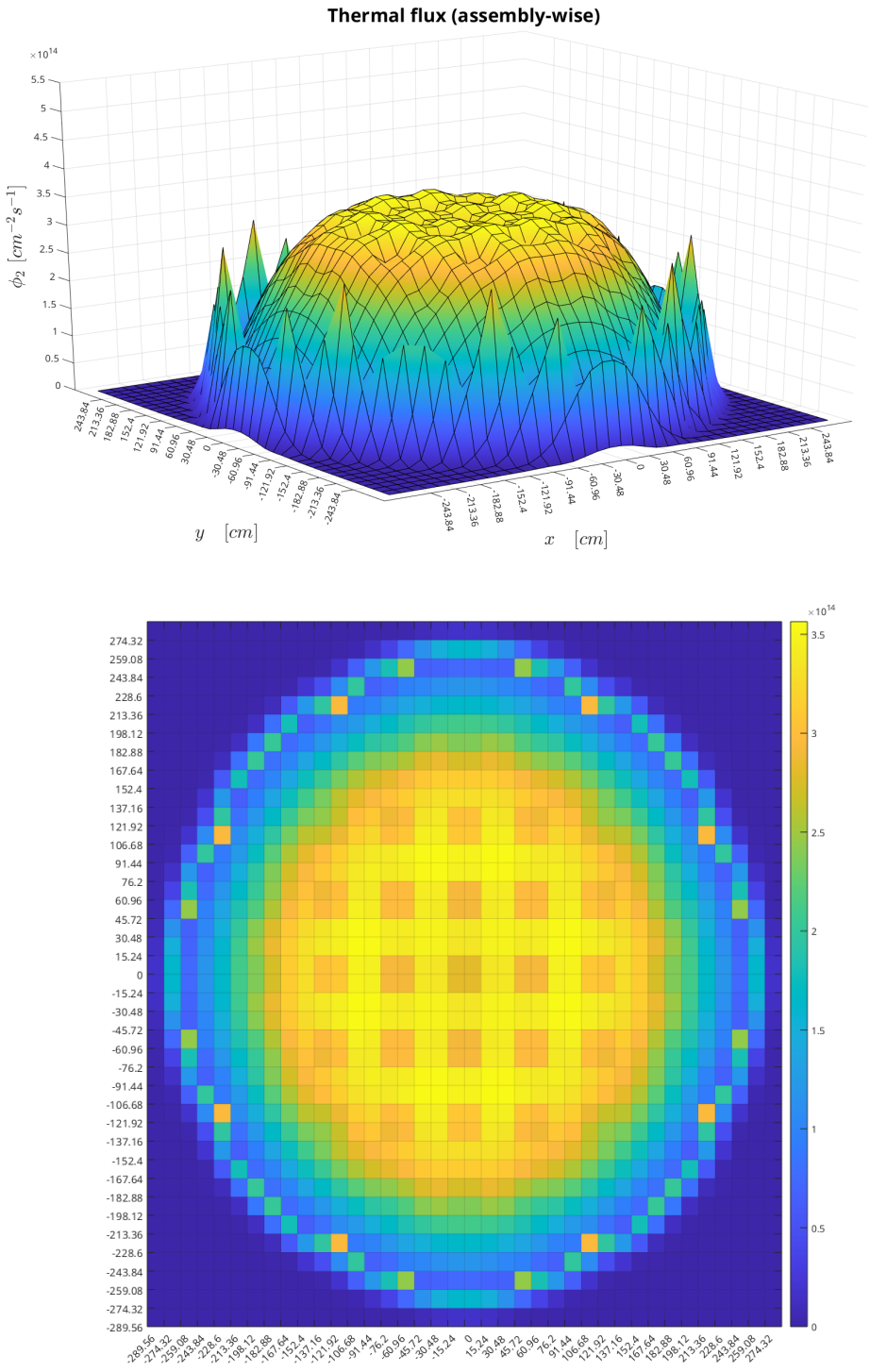

Figure 44: ABWR thermal flux distribution in the Serpent model.

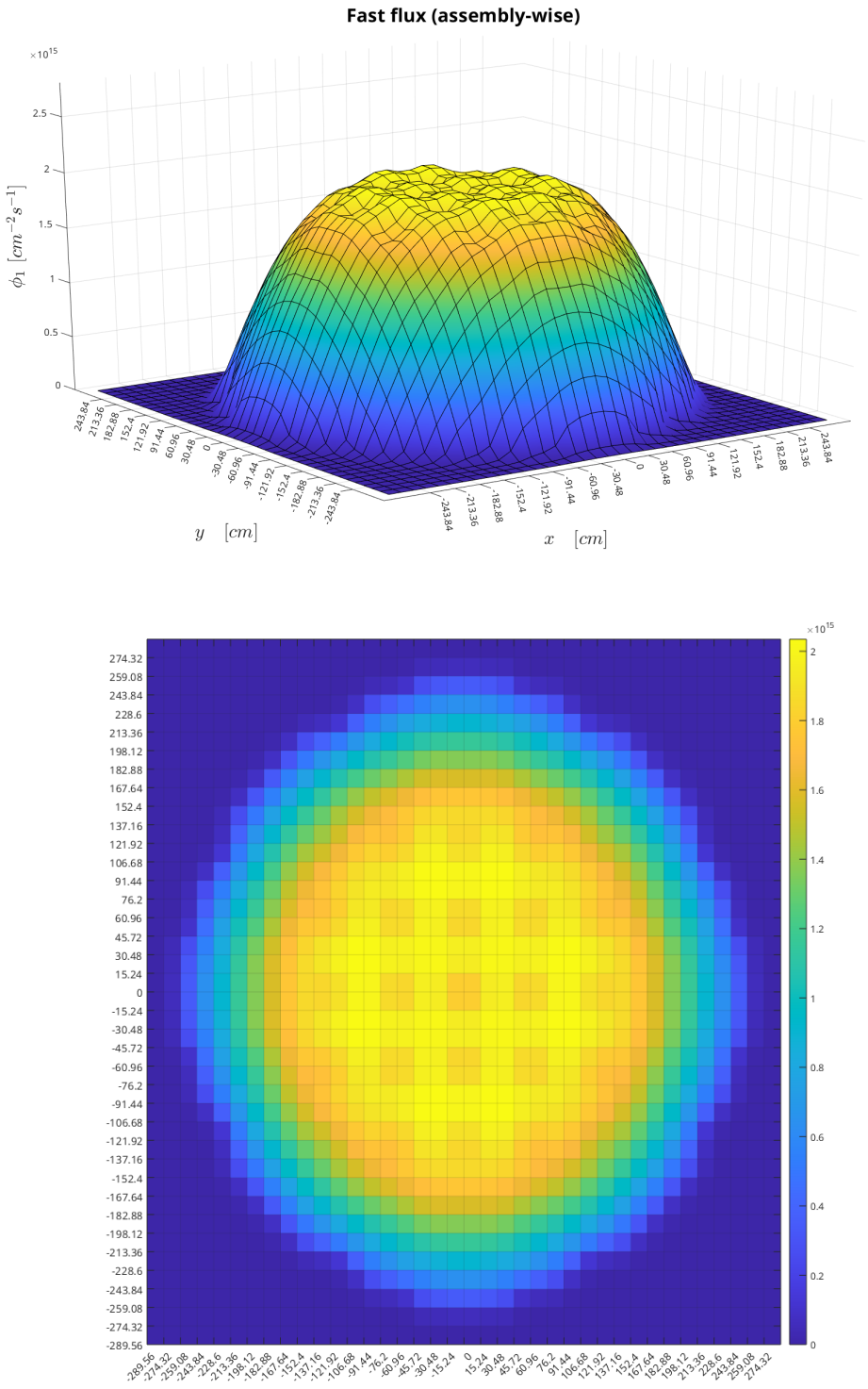

Figure 45: ABWR fast flux distribution in the Serpent model.

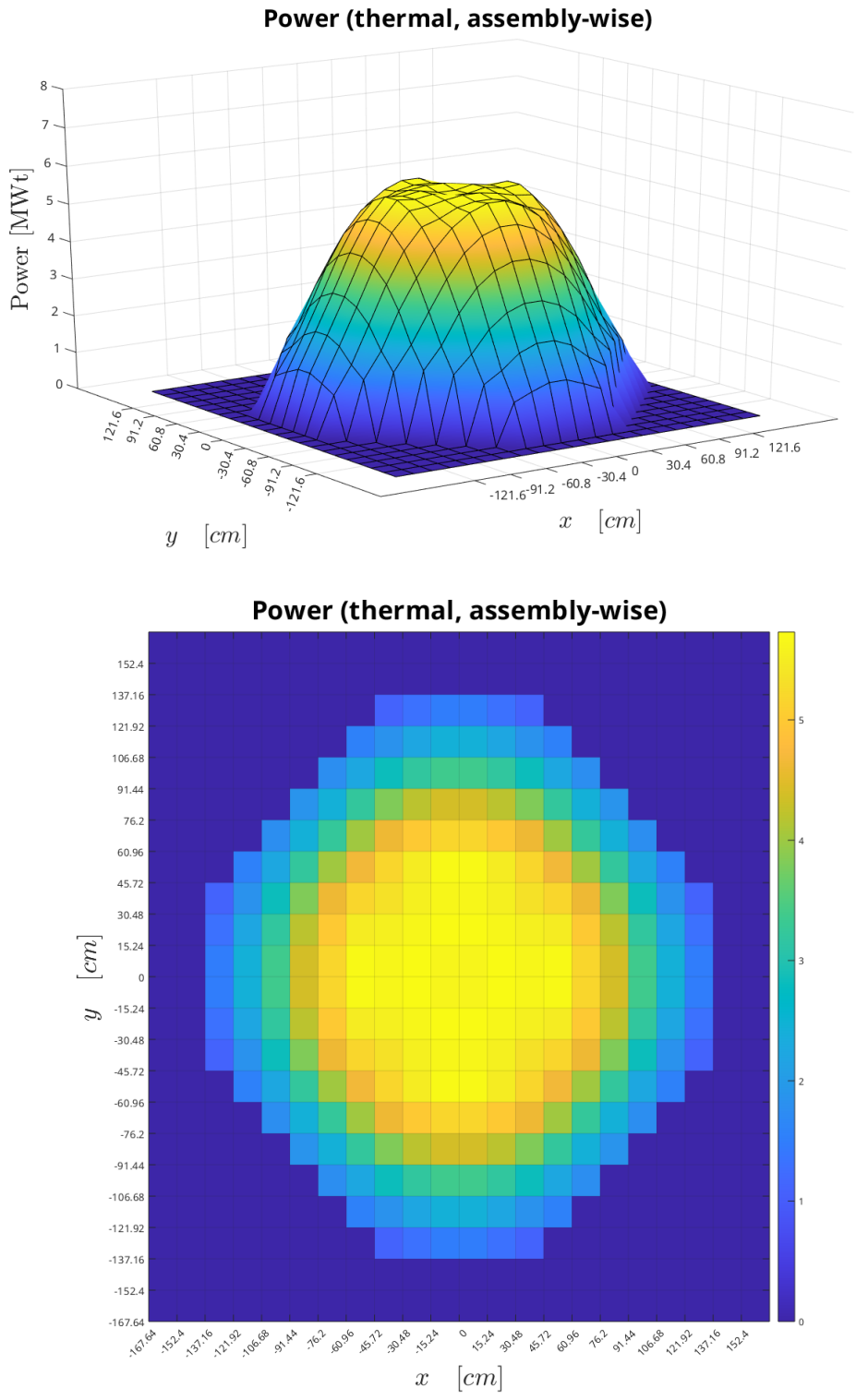

Figure 46: BWRX-300 power distribution in the Serpent model.

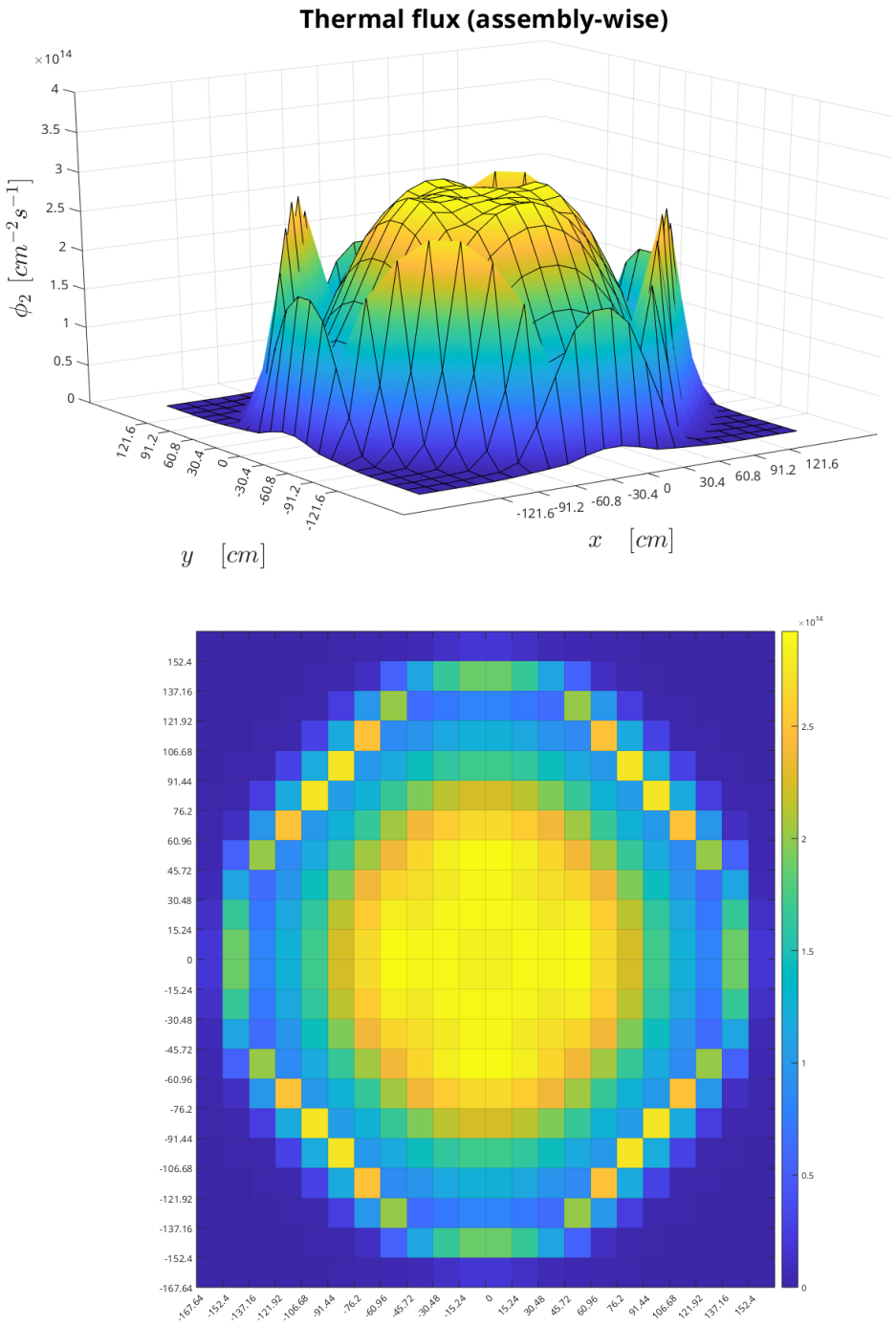

Figure 47: BWRX-300 thermal flux distribution in the Serpent model.

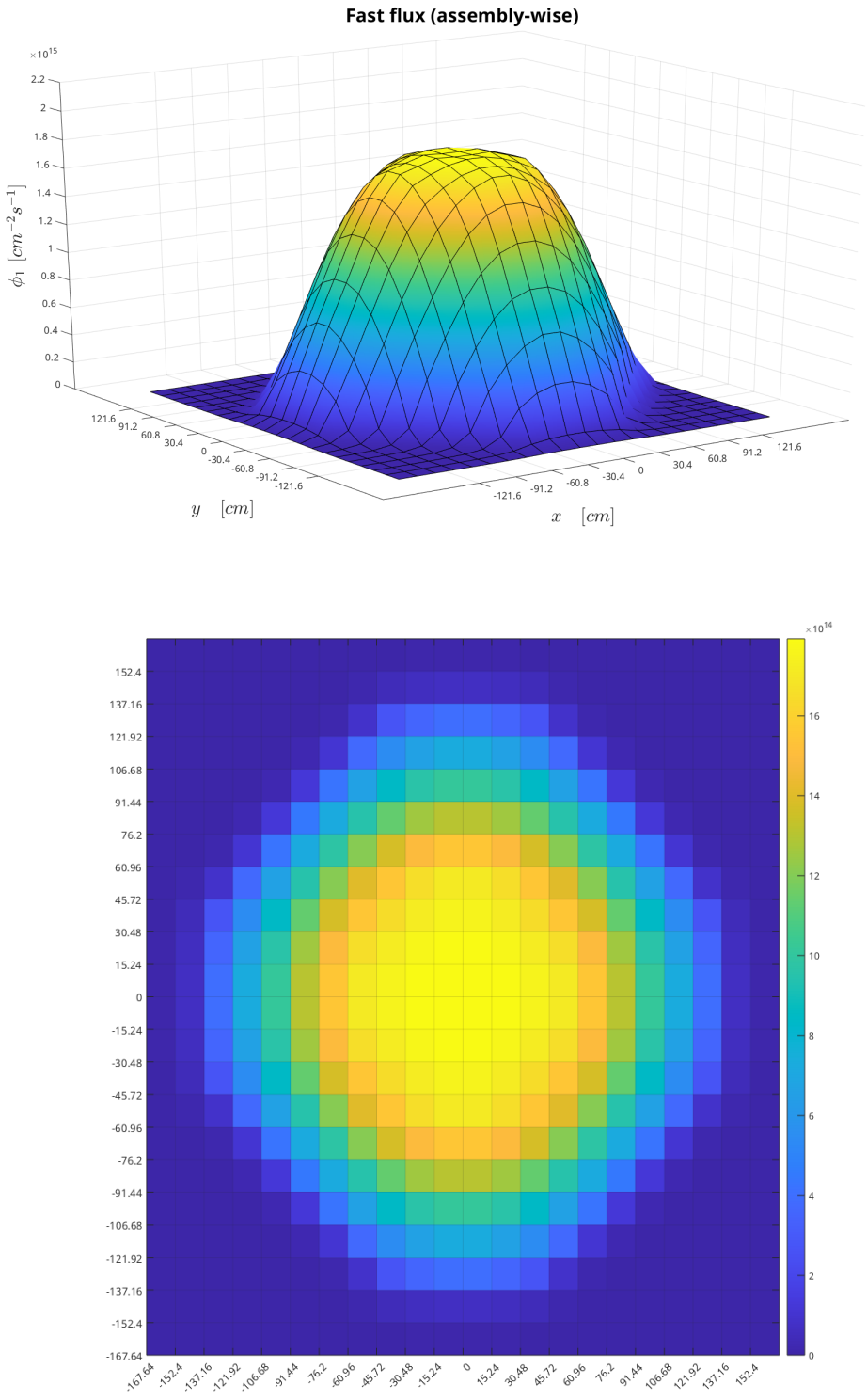

Figure 48: BWRX-300 fast flux distribution in the Serpent model.

5.5 Full model

In the ABWR and BWRX-300 models there are some additional structures surrounding the core. The first one is the core shroud, which was assumed to be at an equivalent distance of 20.955 cm from the baffle in both models [30]. The second structure is the RPV, the diameter of which is specified in [30] to be 7.112 m for the ABWR with a thickness of 174 mm and height of 21 m, and in [11] to be 4 m for the BWRX-300 with a thickness of 136 mm and a height of 27 m. Figures 49 and 50 shows the full models from the side. The full height of the RPVs have not been included in the models, as it was deemed unnecessary. For the ABWR only 14.73 m has been included in the Serpent model, and in the BWRX-300 only 21 m were included. Since the details in Figure 50 are hard to see, Figure 51 instead shows the side-view of the BWRX-300 without the long chimney. Figures 52 and 53 show the active fuel height in the ABWR and BWRX-300 respectively.

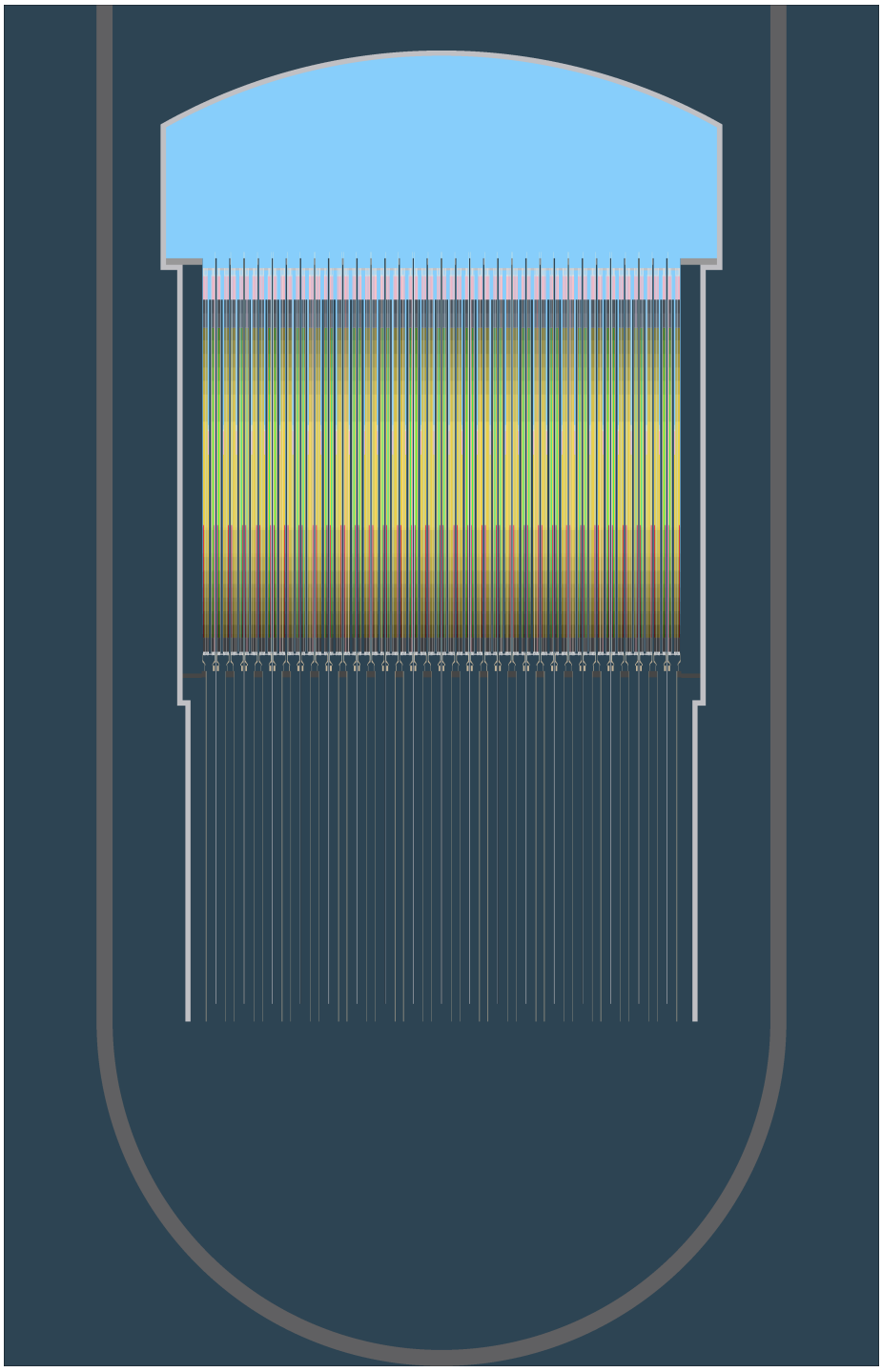

Figure 49: ABWR Serpent full model, side-view.

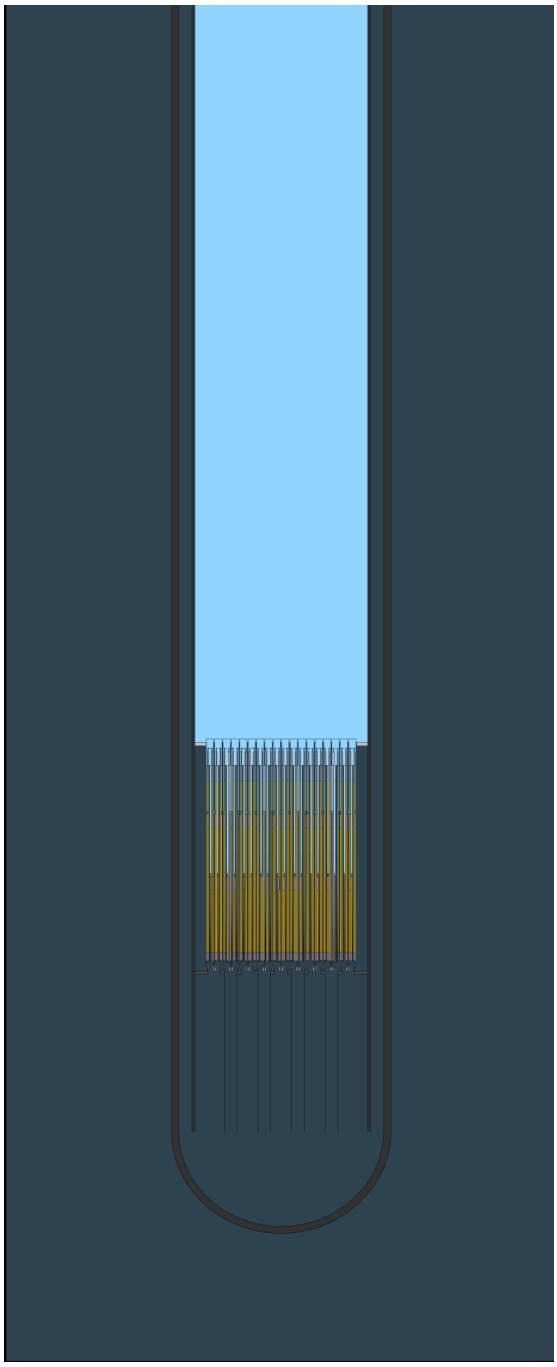

Figure 50: BWRX-300 Serpent full model, side-view.

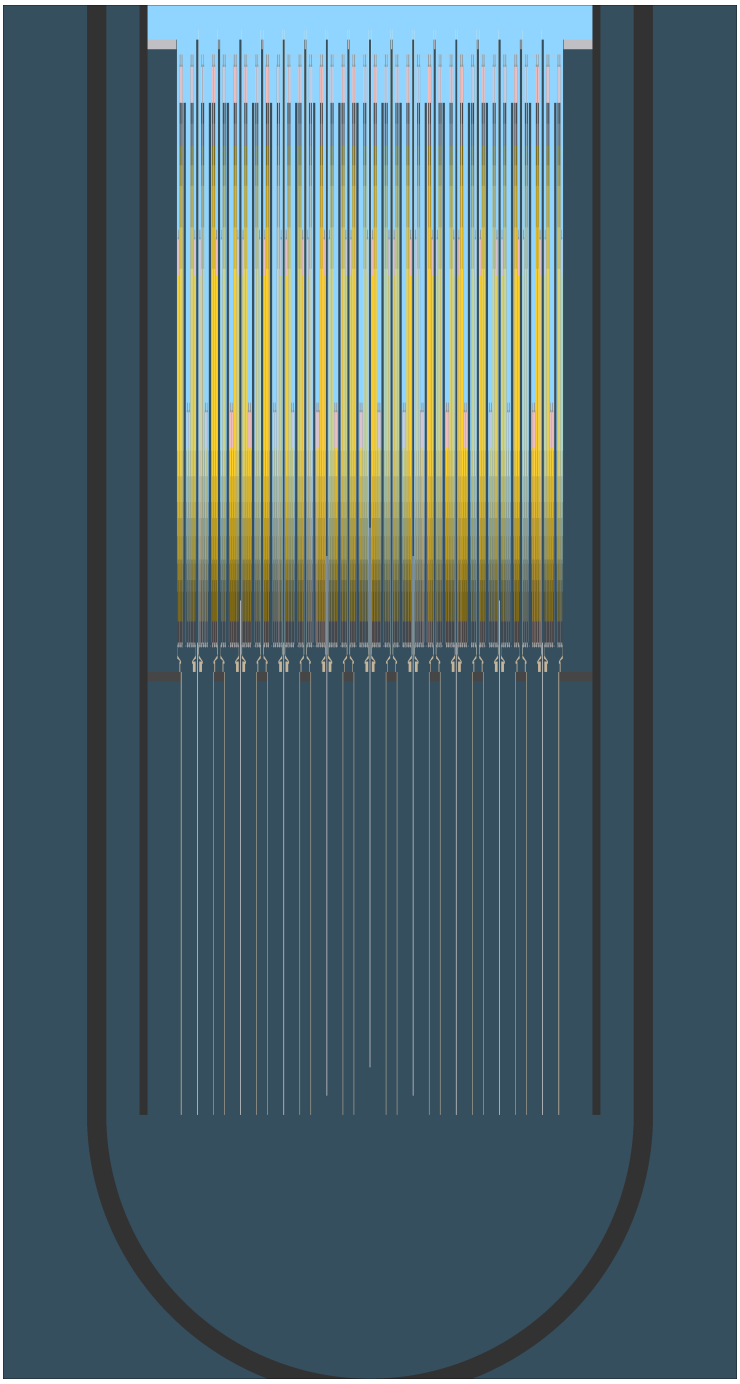

Figure 51: BWRX-300 Serpent model, side-view

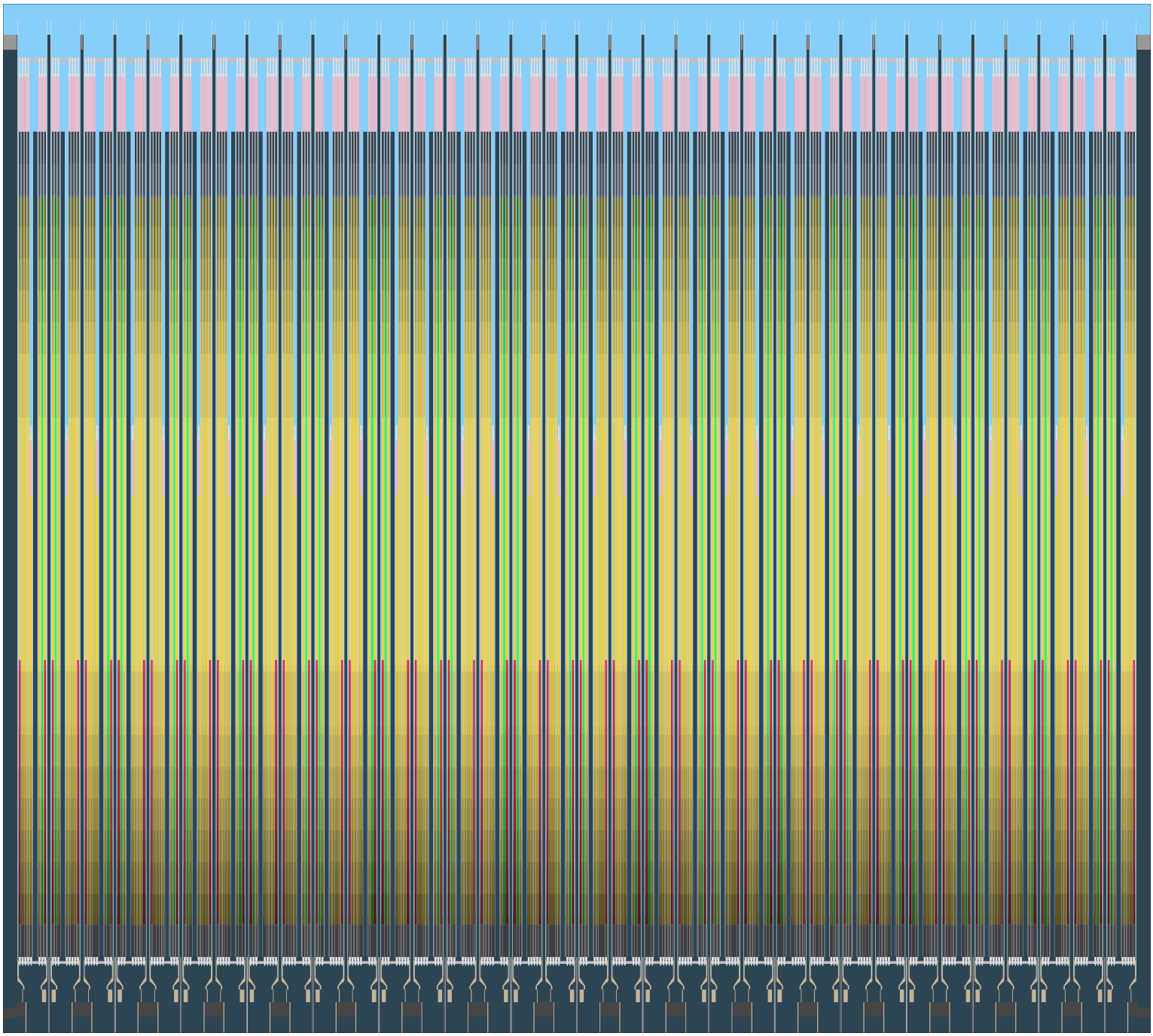

Figure 52: ABWR Serpent model active fuel region, side-view.

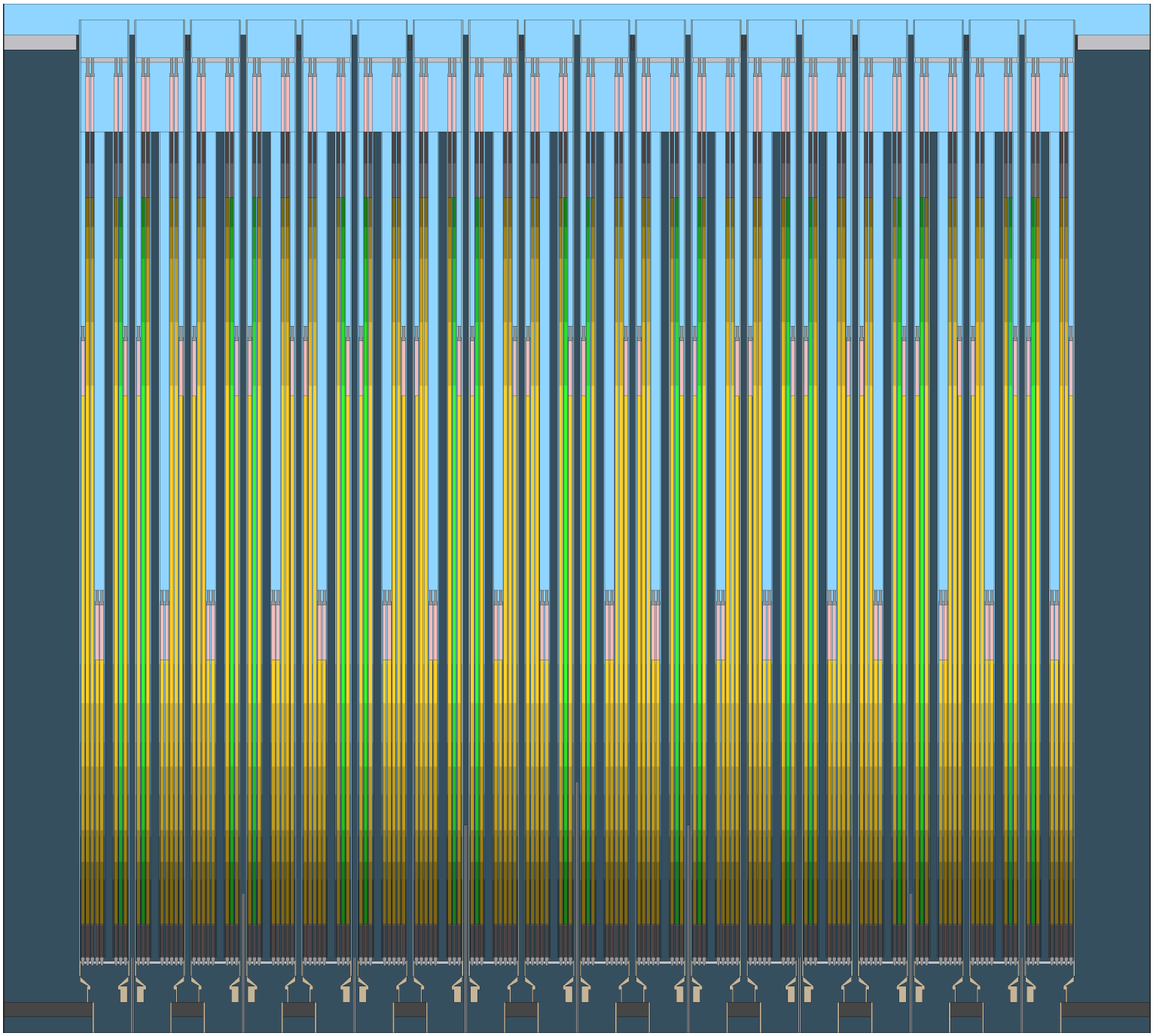

Figure 53: BWRX-300 Serpent model active fuel region, side-view.

These figures show additional details above and below the core which are included in both BWR models, including the control rod guide tubes, core plate, orificed fuel supports, fuel assembly inlet nozzles, lower and top tie-grids, and the top plate. Each of these structures are identical in both models in their design, though they were made to fit each model's geometry. As an example the core plate, which can be seen in Figures 54 for the ABWR and 55 for the BWRX-300, has a smaller diameter and a lower amount of openings for control rods to pass through in the BWRX-300 model, but the general structure and dimensions of these are the same. Some more of the geometrical components such as the top guides can be seen in Figures 56 and 57, and the orificed fuel support in Figure 58.

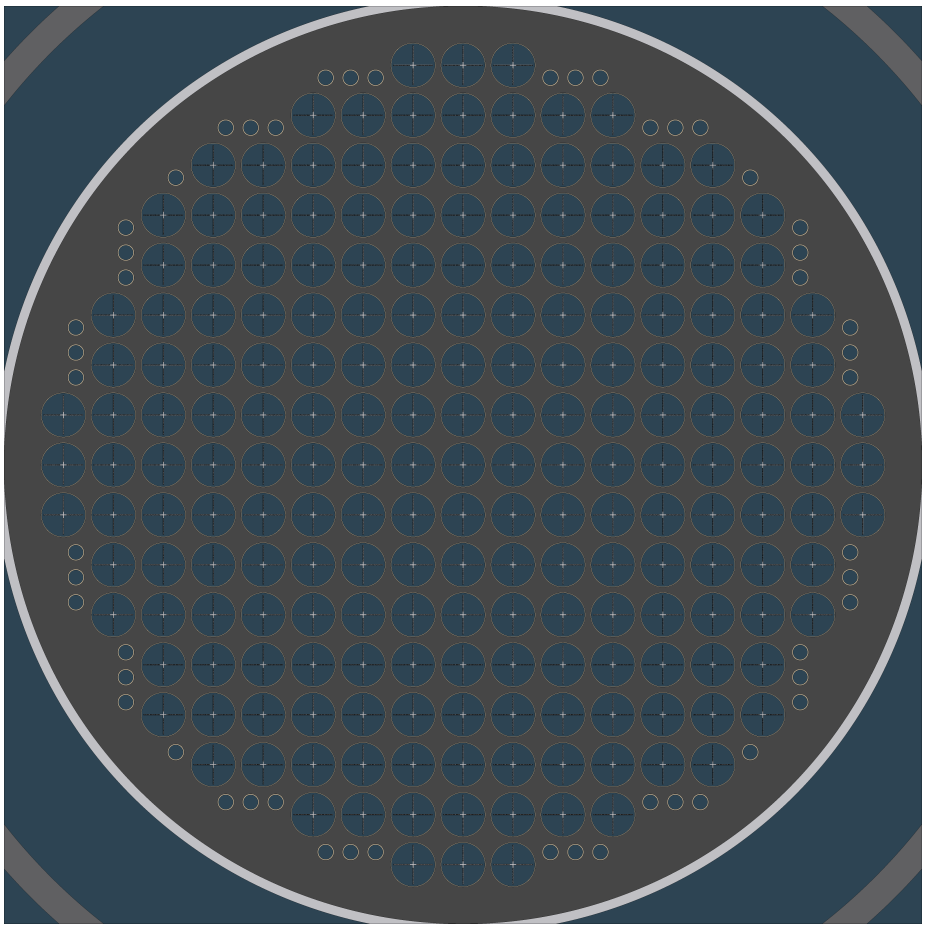

Figure 54: ABWR core plate model in Serpent.

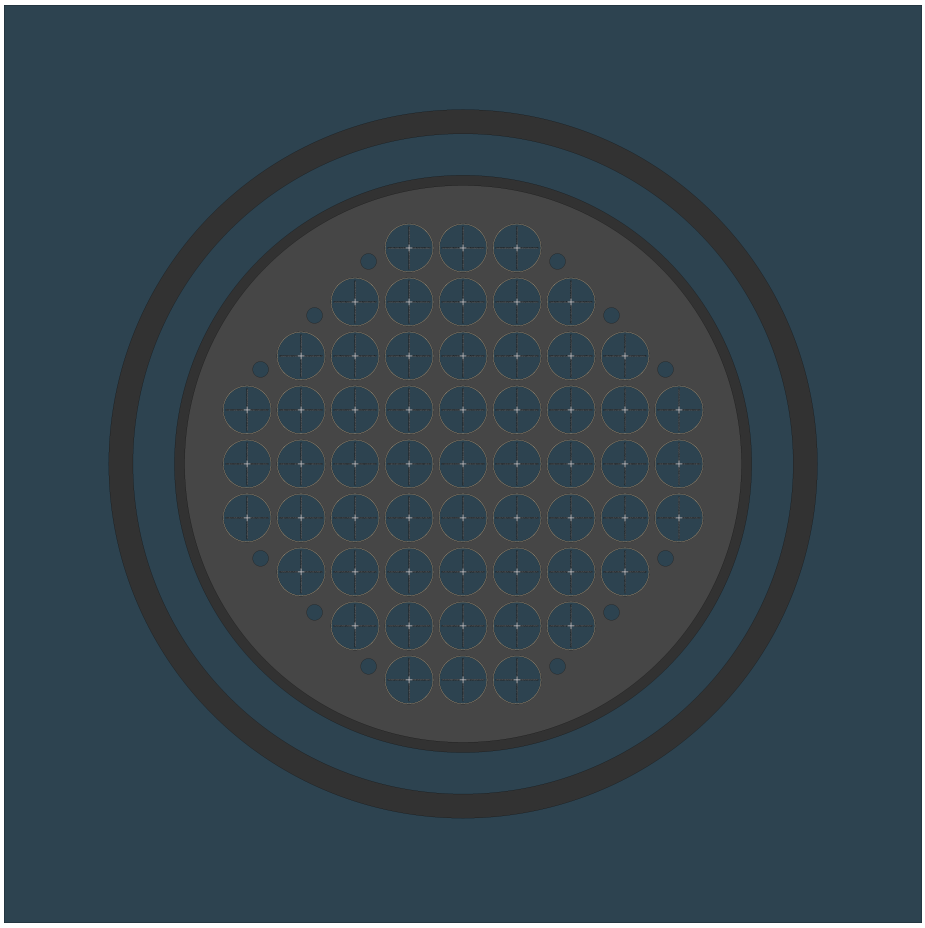

Figure 55: BWRX-300 core plate model in Serpent.

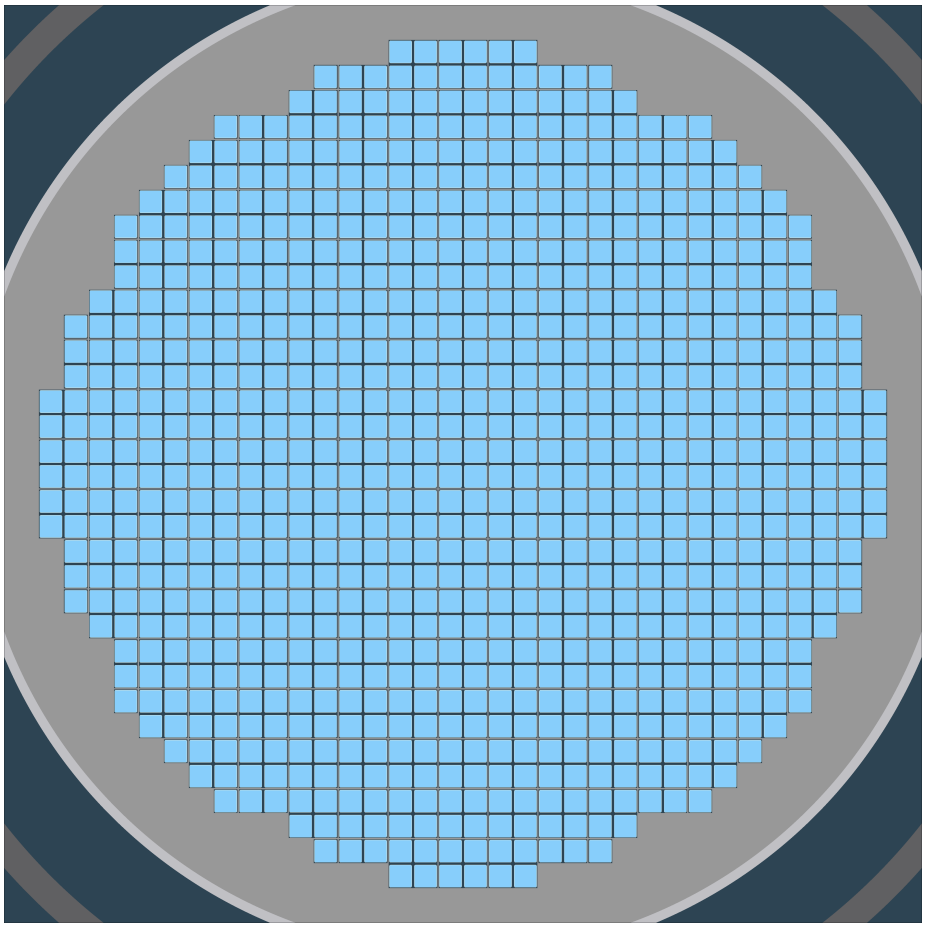

Figure 56: ABWR Serpent top guide model.

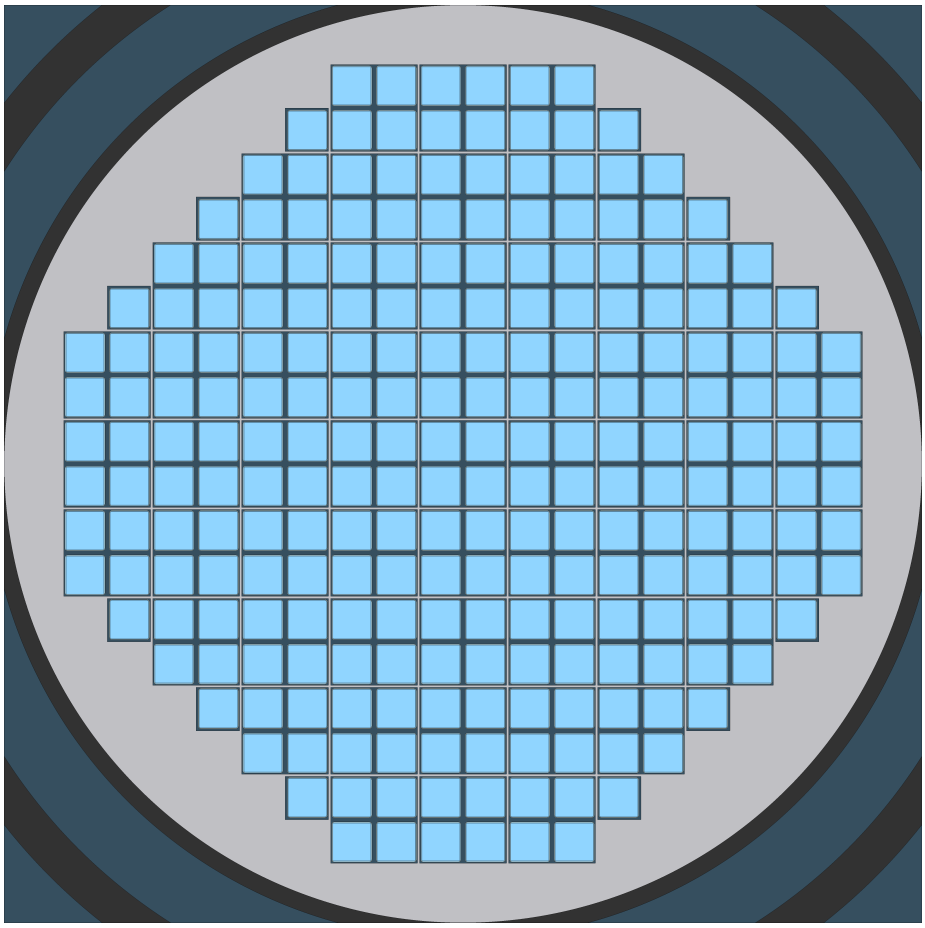

Figure 57: BWRX-300 Serpent top guide model.

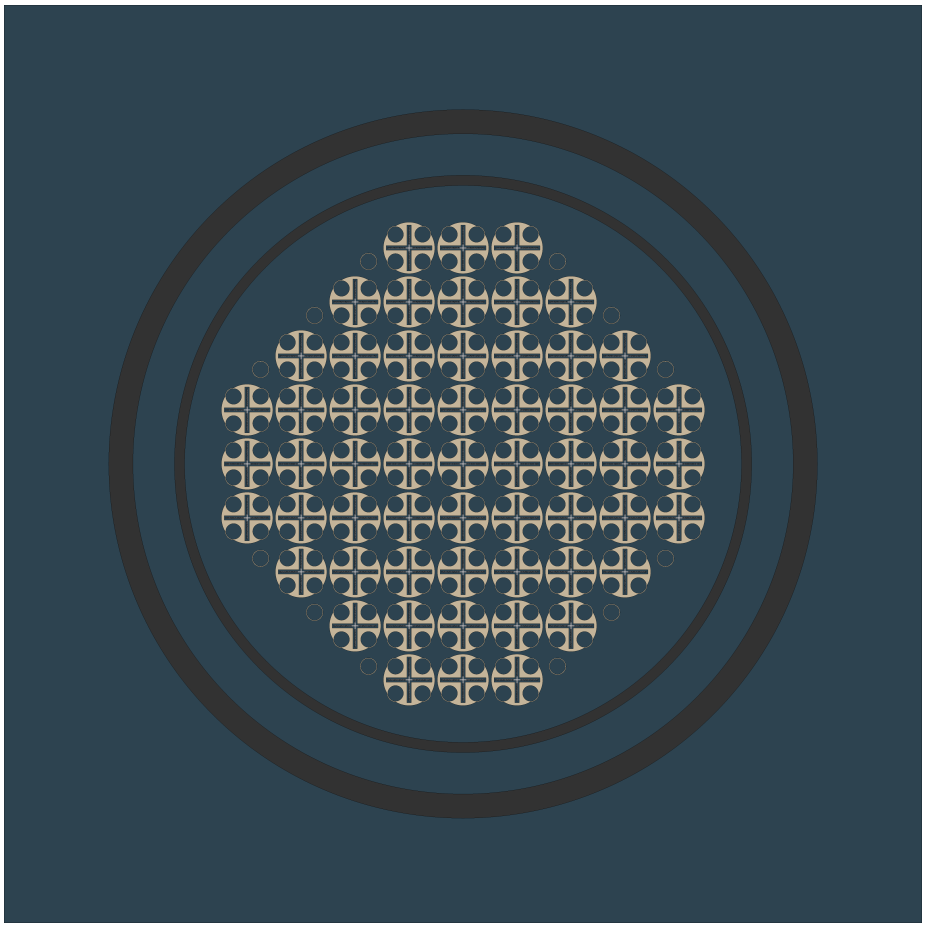

Figure 58: Cross-cut of the BWRX-300 model at the level of the orificed and peripheral fuel supports.

5.5.1 BWR components close to active fuel region

Several structural components located in proximity to active fuel in the BWRX-300 and ABWR models have been designed with a considerable level of geometric detail. These structural components can broadly be divided into components directly underneath the fuel assemblies and components directly above the fuel assemblies. The purpose of this section is to show clearly what these components look like the BWR models, and this is done with the help of pictures. Note that no numbers for the geometric dimensions are provided. This decision was made for the sake of brevity. Note that all components shown in this section are identical in the ABWR model and the BWRX-300 model. The pictures have been generated with Serpent for the ABWR model.

In the lower region, the BWR models contain detailed geometry for LEPs, Lower Tie Grids (LTG) and inlet nozzles. In the upper region, the models contain detailed geometry for Upper Tie Grids (UTG)

In regards to how these geometric models were created, it must be stated clearly that no definitive numbers for the dimensions of these components have been found throughout the publicly available documentation. However, using a large number of sources, where [25] and [29] are two examples, it has been possible to obtain enough constraints on the components to generate reasonable candidates for each of the components.

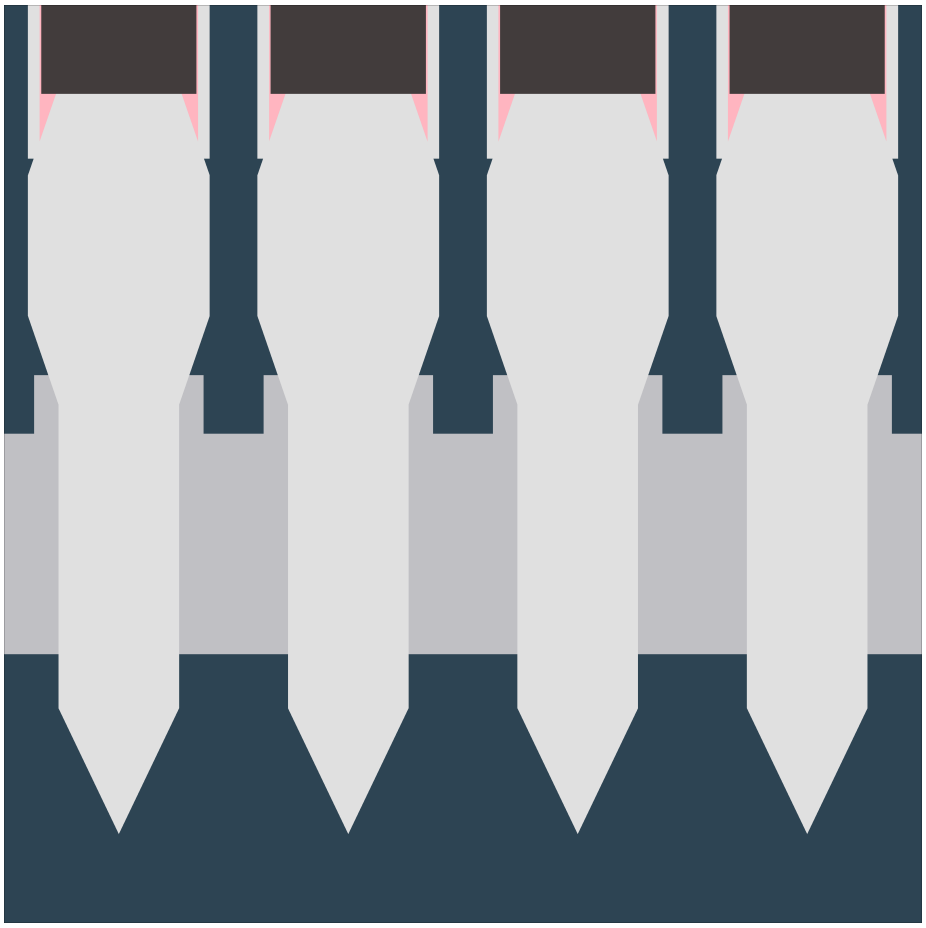

Figure 59: BWR Lower End Plug, side view. It is mentioned that the LEPs shown here have been created directly in Serpent. To accomplish this, several conical and cylindrical surfaces were used to form cells with the union cell operator available in Serpent.

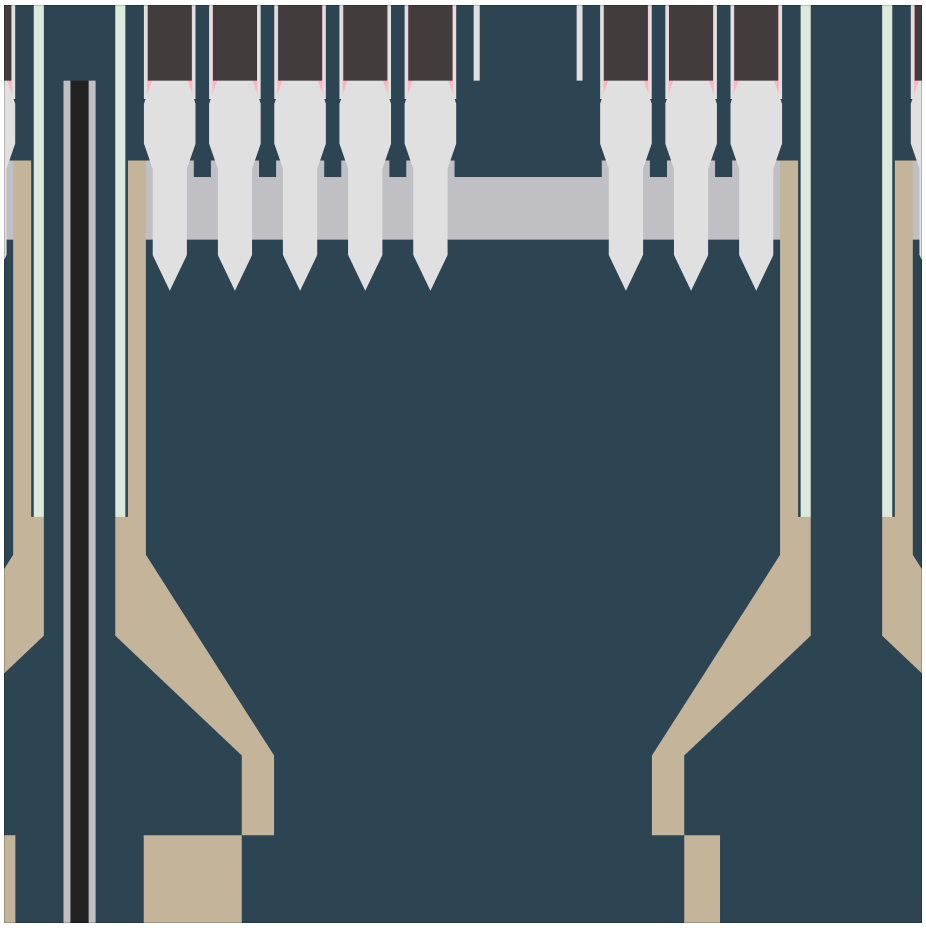

Figure 60: BWR Inlet Nozzle, side view. At the very top of the image the lowest parts of the lower axial blanket can be seen, in dark grey. Below the blanket are the LEPs, which seat into the LTG. The LTG has three distinct layers which cannot be seen in this image. These three layers can be seen in Figures 61, 62 and 63, where each figure shows the three layers in order from top towards the bottom. The top-most layer is located where the LEPs seat into the LTG. The second layer is in the middle of the LTG, below the LEPs seats and above the debris filter. The third layer is the bottom third of the LTG, which includes the debris filter.

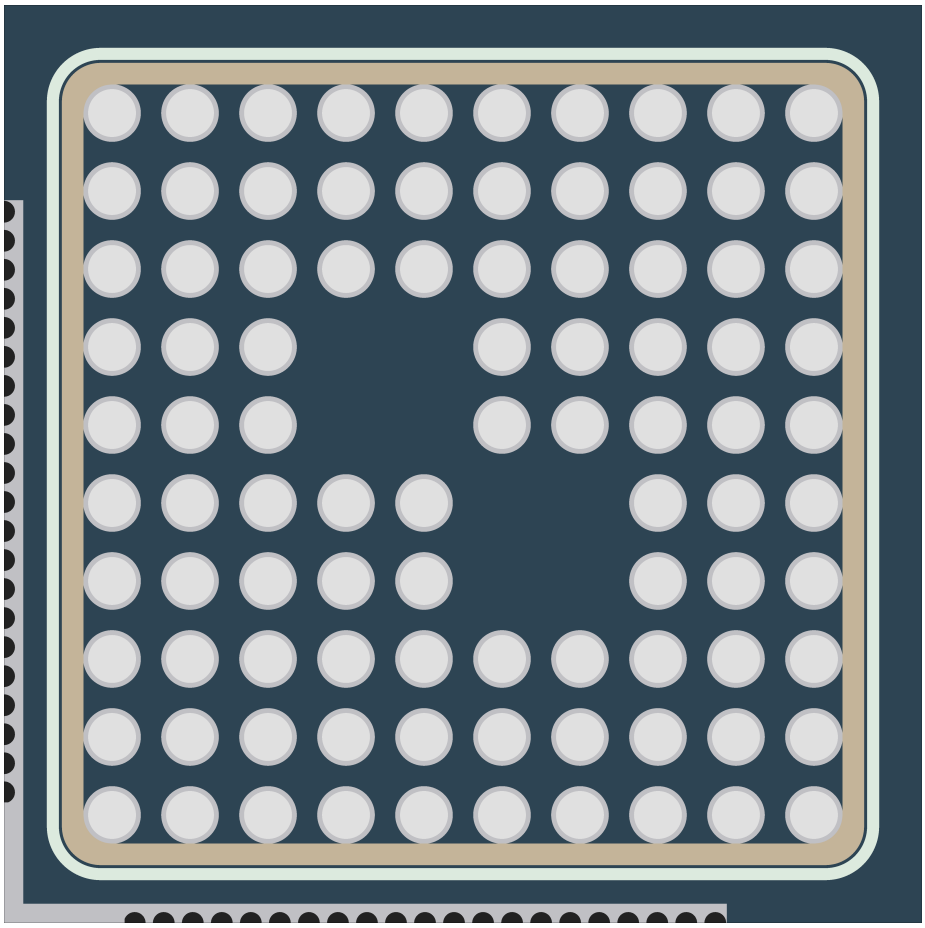

Figure 61: BWR Lower Tie Grid 1. Cross-sectional view of the LTG at the top-most axial height, where LTG only consists of the seats for LEPs. Refer to Figure 60 for clarification on where this cross-sectional plane is located.

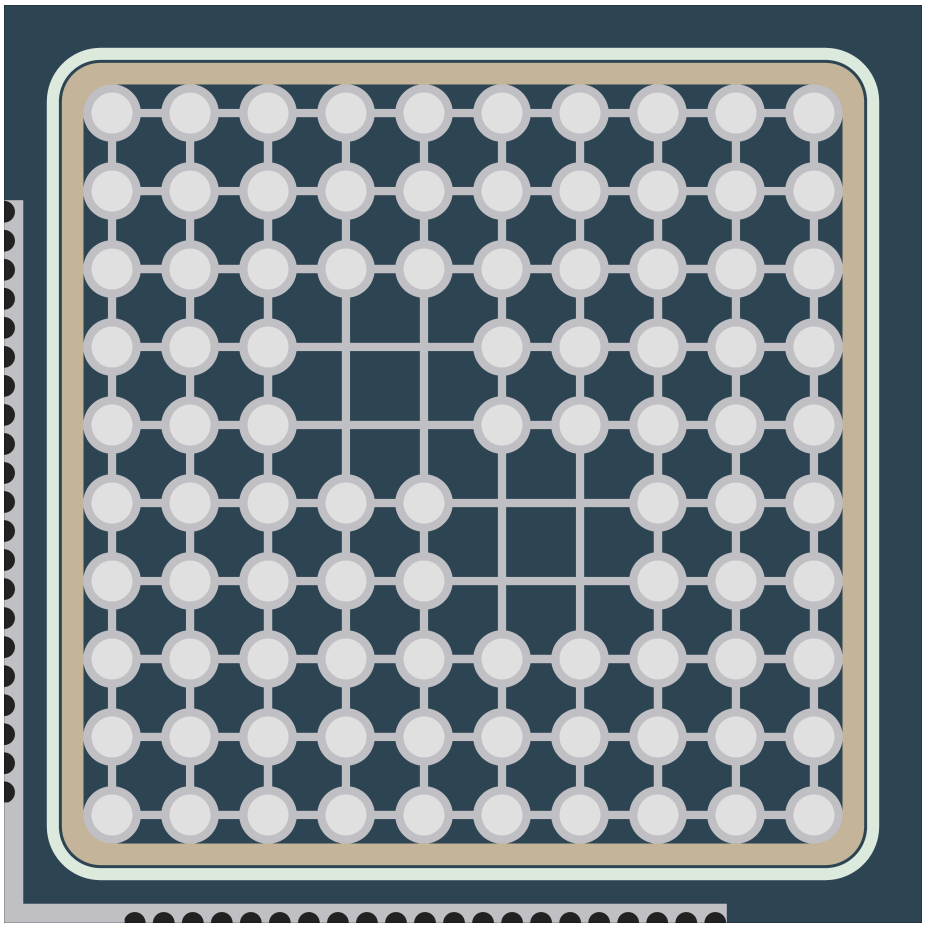

Figure 62: BWR Lower Tie Grid 2. Cross-sectional view of the LTG at the middle axial height, just before the debris filter starts. Refer to Figure 60 for clarification on where this cross-sectional plane is located.

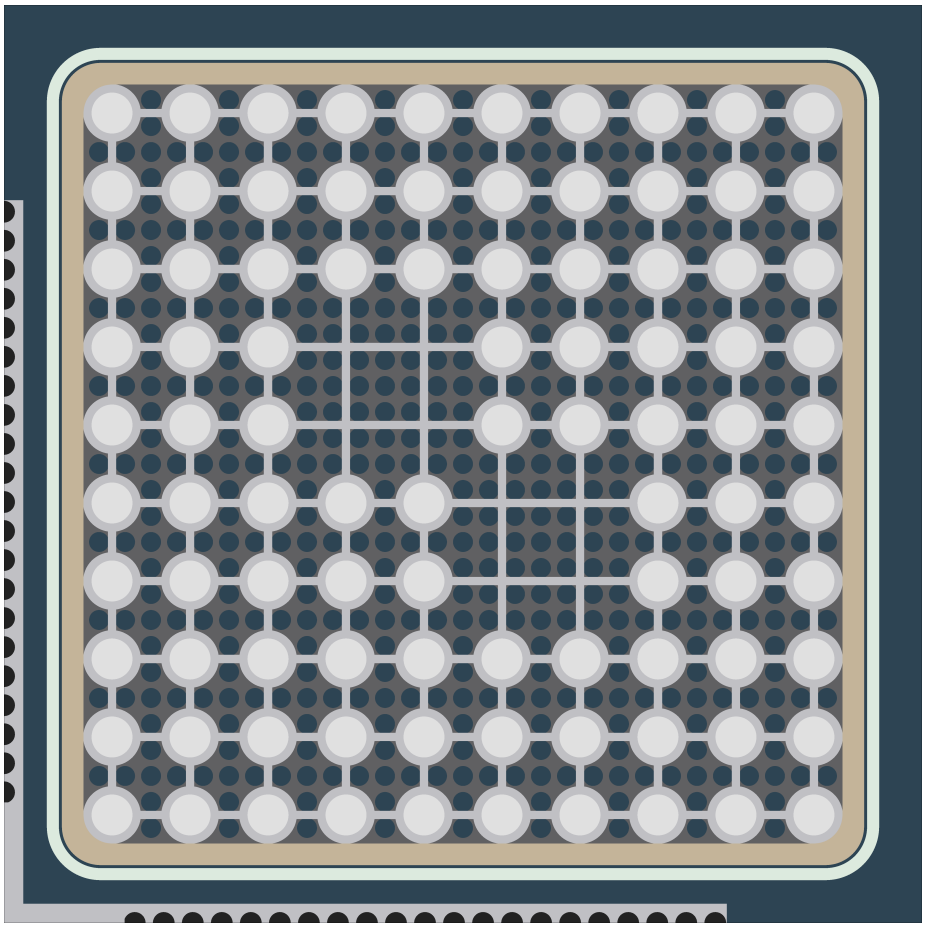

Figure 63: BWR Lower Tie Grid 3. Cross-sectional view of the LTG in the lower-most axial height, where the debris filter is also included. Refer to Figure 60 for clarification on where this cross-sectional plane is located.

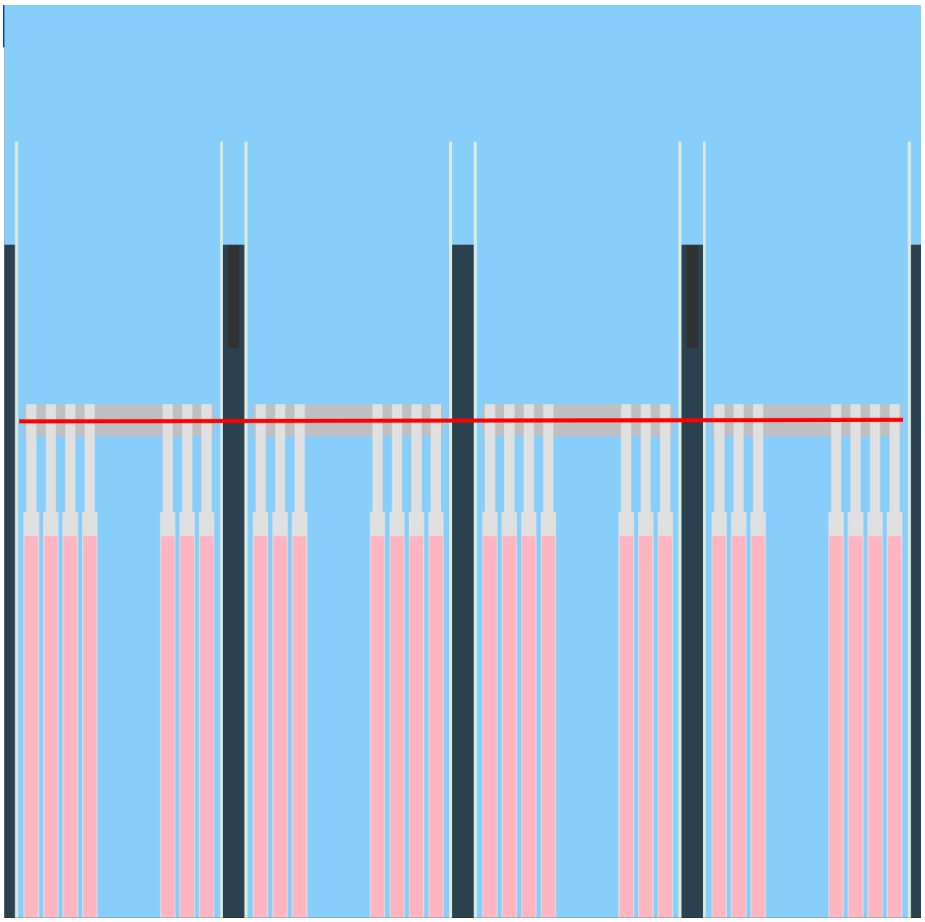

Figure 64: BWR Upper geometry of fuel assemblies. The pink in the fuel rods are the upper gas plenums, above which are the zircaloy-2 upper end plugs. The upper-most section of the fuel assemblies are the upper tie grids. The red line shows the location of the axial plane through the UTGs depicted in Figure 65.

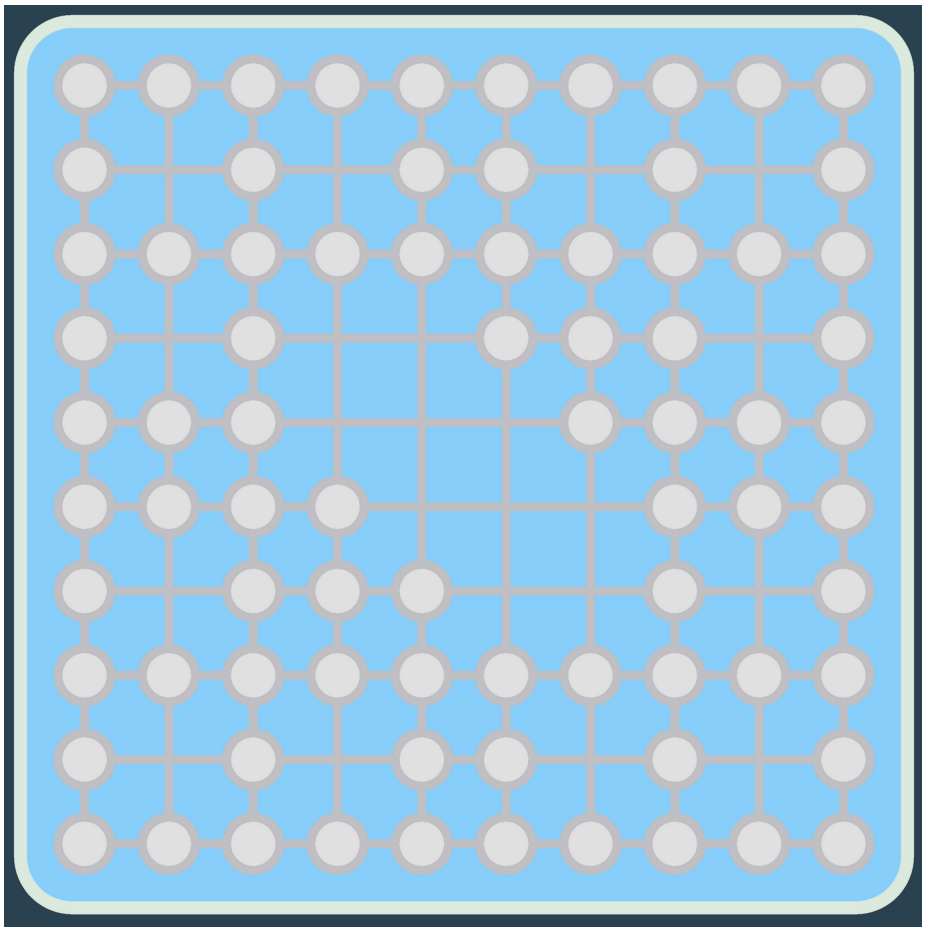

Figure 65: BWR upper tie grid cross-cut. The exact axial level shown in this figure is indicated by the red line in Figure 64.

6 Results and Discussion

6.1 BWRs

The result of the 1 second burnup step for the ABWR and the BWRX-300 Serpent models, normalized to produced energy and extrapolated to 1 year can be found in Table 27. The range for ^{3}H depend on the amount of diffusion through the fuel cladding that is assumed. The normalized ^{14}C production rate in the ABWR was 425 GBq·GW(e)$^{-1}$·a^{-1}, and the production of ^{3}H in the coolant was 1404 GBq·GW(e)$^{-1}$·a^{-1}. Using the method described in Chapter 3, the total estimated ^{3}H in the coolant of the ABWR should be 896 GBq·GW(e)$^{-1}$·a^{-1}. The amount diffusing from the fuel should therefore be 756 GBq·GW(e)$^{-1}$·a^{-1}. The estimated ^{3}H production from ternary fission from the Serpent model is $5.83{\cdot}10^{5}$ GBq·GW(e)$^{-1}$·a^{-1}, meaning the diffusion factor in the ABWR should be approximately 0.13. If a diffusion factor of 0.013 % or 1 % were to be used, the estimated ^{3}H production rate would instead be 216 GBq·GW(e)$^{-1}$·a^{-1} or 5972 GBq·GW(e)$^{-1}$·a^{-1} respectively.

For the BWRX-300, if the same diffusion factor is used as in the ABWR, the estimated normalized production rate of ^{3}H that ends up in the coolant is 924 GBq·GW(e)$^{-1}$·a^{-1}. For the highest or lowest amount of diffusion, the production rate becomes 246 GBq·GW(e)$^{-1}$·a^{-1} or 5982 GBq·GW(e)$^{-1}$·a^{-1} respectively. The normalized ^{14}C production rate was 471 GBq·GW(e)$^{-1}$·a^{-1}.

6.2 PWRs

The result of the 1 second burnup step for the AP1000 and the RR SMR, normalized to produced energy and extrapolated to 1 year, can be found in Table 27. If the same diffusion factor 0.13 % that was used for the BWRs is used, the estimated normalized production rate of ^{3}H that ends up in the coolant for the AP1000 is $3.02{\cdot}10^{4}$ GBq·GW(e)$^{-1}$·a^{-1}. For the lower amount of diffusion of 0.013 %, the normalized ^{3}H production rate amounts to $2.94{\cdot}10^{4}$ GBq·GW(e)$^{-1}$·a^{-1}. If 1 % diffusion through the cladding is assumed instead, the same production rate becomes $3.55{\cdot}10^{4}$ GBq·GW(e)$^{-1}$·a^{-1}. The normalized ^{14}C production rate was 385 GBq·GW(e)$^{-1}$·a^{-1}.

For the RR SMR, the estimated normalized production rate of ^{3}H ending up in the coolant is 911 GBq·GW(e)$^{-1}$·a^{-1} using the same diffusion factor of 0.13% as before. For a diffusion factor of 0.013% or 1 % respectively, the ^{3}H production rate becomes 235 GBq·GW(e)$^{-1}$·a^{-1} or 5956 GBq·GW(e)$^{-1}$·a^{-1}. The normalized ^{14}C production rate was 390 GBq·GW(e)$^{-1}$·a^{-1}.

Table 27: Estimated normalized production rate of ^{3}H and ^{14}C that ends up in the coolant in the different reactor models [GBq·GW(e)$^{-1}$·a^{-1}]. The values range for ^{3}H depends on the amount of diffusion through the fuel cladding [0.013 - 1 %].

Reactor	^{3}H normalized production rate	^{14}C normalized production rate
ABWR	896 [216 - 5972]	425
BWRX-300	924 [246 - 5982]	471
AP1000	$3.02{\cdot}10^{4}$ [$2.95{\cdot}10^{4}$-$3.55{\cdot}10^{4}$]	385
RR SMR	911 [235 - 5956]	390

6.3 Comparison of results and previous studies

As can be seen in Table 27, the normalized production rate of ^{14}C for the AP1000 was estimated to be 385 GBq·GW(e)$^{-1}$·a^{-1}. This was about 48.5 % larger than the discharge rate (atmospheric and liquid) found for PWRs in [3] (see also Table 1) where the median was 259.7 GBq·GW(e)$^{-1}$·a^{-1} for the period 1995-2023, with an inter-quartile range of [167.8-363.4] GBq·GW(e)$^{-1}$·a^{-1}. The ^{3}H production rate of $3.02{\cdot}10^{4}$ GBq·GW(e)$^{-1}$·a^{-1} in the Serpent model was also considerably higher than the discharge rate of $1.83{\cdot}10^{4}$ [$1.46{\cdot}10^{4}$-$2.59{\cdot}10^{4}$] GBq·GW(e)$^{-1}$·a^{-1} from [3] (see also Table 1). The discharge values from European reactors also include PWRs besides the AP1000, and as was stated in [3], the spread in discharge rates between different reactors can be quite significant, as indicated by the associated inter-quartile ranges.

Unfortunately, while there are AP1000 reactors currently in operation, there is not much discharge data easily available. The only measurement that could be found (that was not in Chinese) reported an estimated ^{3}H normalized release rate (gaseous and liquid) of $1.87{\cdot}10^{4}$ GBq·GW(e)$^{-1}$·a^{-1} [31, Table 5, p.25, Table 12, p.31] and ^{14}C normalized release rate of 298 GBq·GW(e)$^{-1}$·a^{-1} [31, Table 5, p.25] which was similar to what was reported for the European PWRs [3]. An article [32], which estimates the ^{3}H release rates specifically for the AP1000 arrives at a best-estimate of $2.81{\cdot}10^{4}$ GBq·GW(e)$^{-1}$·a^{-1} and conservative estimate of $4.10{\cdot}10^{4}$ GBq·GW(e)$^{-1}$·a^{-1}. The estimate that was derived using our developed Serpent model is fairly close to this best estimate.

Another point to keep in mind is the fact that the Serpent model is simplified in one important aspect when it comes to ^{3}H production, namely that the boron concentration is assumed to be constant throughout a full year of operation. This is of course a large simplification as the boron concentration goes down during the operation cycle. According to [6], the boron concentration starts out at 1382 ppm for HZP (hot zero power) conditions, which goes down to 0 ppm at the end of full power operation. The concentration of boron in the the Serpent model was as mentioned previously 940 ppm which is in the higher end of the concentration range. Since ^{14}C is not produced through boron

irradiation, only the ^{3}H is affected by the higher concentration.

The point of the model was not however to achieve completely realistic values, but rather values that were good enough to show the validity of the model so that the RR SMR estimates could be trusted. As for the results of the RR SMR, the normalized ^{14}C production rate of 390 GBq·GW(e)$^{-1}$·a^{-1} is higher than in the AP1000 reactor by about 1.34 %, which is not very significant. Due to the reactor not utilizing boron for reactivity control, the ^{3}H production is naturally lower in the smaller reactor, and in this regard the two reactors are not comparable. It is more appropriate to compare the ^{3}H production rate of the RR SMR to the BWRs.

In contrast, the BWRs show a clearer difference between the large and small reactor for both the ^{3}H and the ^{14}C production. The ^{3}H production, including the diffused ^{3}H from ternary fission, is 896 GBq·GW(e)$^{-1}$·a^{-1} in the ABWR and 924 GBq·GW(e)$^{-1}$·a^{-1} in the BWRX-300 meaning the production is approximately 3 % higher in the BWRX-300 compared to the ABWR. Not counting diffusion from the fuel, the production rate was approximately 140 GBq·GW(e)$^{-1}$·a^{-1} in the ABWR and 170 GBq·GW(e)$^{-1}$·a^{-1} in the BWRX-300, meaning that the ^{3}H production rate in the coolant was approximately 21.6 % higher in the BWRX-300. As for the ^{14}C production rate, it is approximately 10.9 % higher in the BWRX-300, with 471 GBq·GW(e)$^{-1}$·a^{-1} compared to 425 GBq·GW(e)$^{-1}$·a^{-1} in the ABWR. The reason behind the larger difference in ^{3}H production rate compared to ^{14}C can likely be attributed to the fact that the cross-sections for ^{3}H and ^{14}C production scale differently with temperature, and since the BWRs do not have an identical neutron spectrum a small change in number of neutrons at a certain energy could have a large impact on the end results. Comparing what was previously found for the RR SMR to the BWRs, it can be seen that the RR SMR had a normalized ^{3}H production rate between that of the ABWR and the BWRX-300, with a total of 911 GBq·GW(e)$^{-1}$·a^{-1}, of which 160 GBq·GW(e)$^{-1}$·a^{-1} was produced directly in the coolant. The increased production rate in the RR SMR and BWRX-300 compared to the ABWR can therefore be almost entirely attributed to an increased production in the coolant, which was to be expected.

The larger increase in normalized production rates in the small BWR compared to the small PWR can largely be attributed to the fact that the difference in size is much larger in the BWRs than in the PWRs. The BWRX-300 has a core volume of approximately $2.1238{\cdot}10^{7}$ cm^{3} compared to the ABWR's $7.7163{\cdot}10^{7}$ cm^{3}, meaning the core volume of the ABWR is 3.6333 times larger than that of the BWRX-300. The RR SMR has a core volume of approximately $1.5666{\cdot}10^{7}$ cm^{3} compared to the AP1000's $3.0979{\cdot}10^{7}$ cm^{3}, meaning the AP1000 core volume is only 1.9974 times larger than that of the RR SMR. As can be seen upon comparing the normalized production rates of the BWRX-300 and the RR SMR, the core volume does not seem to be the only factor that matters. Despite having a larger physical core volume, the BWRX-300 still has a higher

normalized production rate of ^{14}C and ^{3}H than the RR SMR even though the RR SMR does not use boron. These differences are likely a result of differing operating conditions.

To give an accurate estimate of the discharge rates of the RR SMR and the BWRX-300 from the work so far is a difficult task. On one hand, it is possible to assume that the estimates of the production rates that were obtained and presented in Table 27 are accurate despite the simplifications that were made in creating the models. In such a case, the estimated normalized production rates and the estimated normalized release rates could be said to be equivalent, since essentially all produced ^{14}C and ^{3}H can be released from the reactor system [1, p. 13, 31]. The normalized release rate of ^{14}C and ^{3}H in the BWRX-300 would then be slightly smaller than that of the median release rate of European BWRs, shown in Table 1. For the RR SMR, the ^{3}H release rate will be smaller than the median release rate from European PWRs no matter how one would estimate it. The ^{14}C release rate would however be approximately 50 % larger than that from European PWRs. Figures 66, 67, 68 and 69 show the yearly variation in release rate of ^{14}C and ^{3}H from European PWRs and BWRs [3]. The results of the Serpent models are also indicated as dotted lines in the graphs to see how they relate.

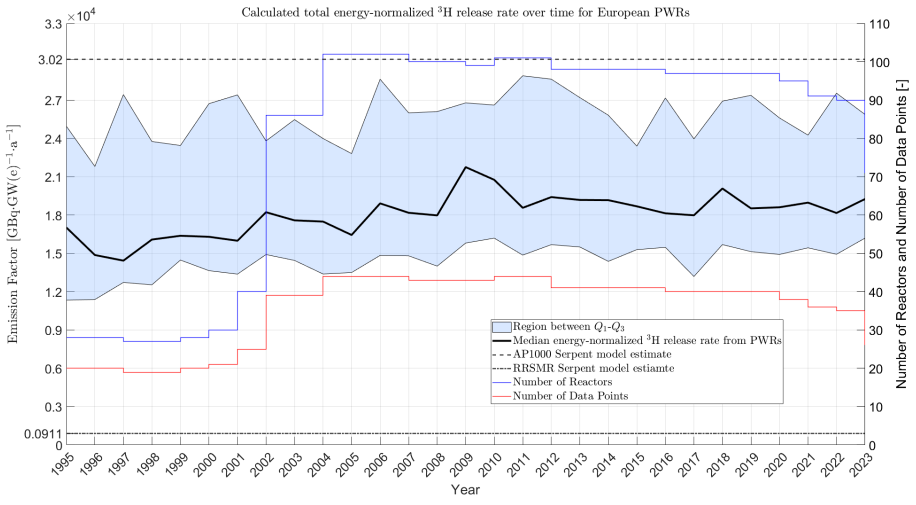

Figure 66: Normalized release rate of ^{3}H (liquid and atmospheric) from European PWRs, median and interquartile range [3]. The results of the Serpent simulations for the AP1000 and the RR SMR are also indicated in the graph.

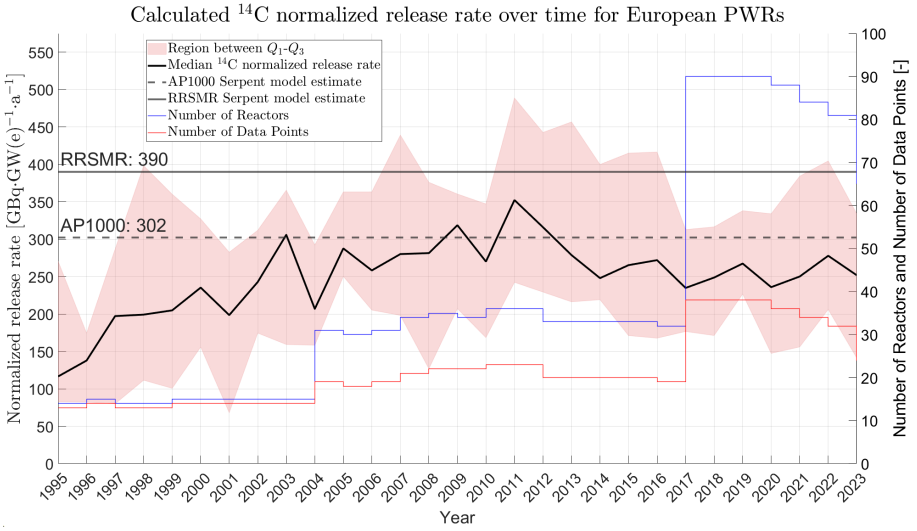

Figure 67: Normalized release rate of ^{14}C from European PWRs, median and interquartile range [3]. The results of the Serpent simulations for the AP1000 and the RR SMR are also indicated in the graph.

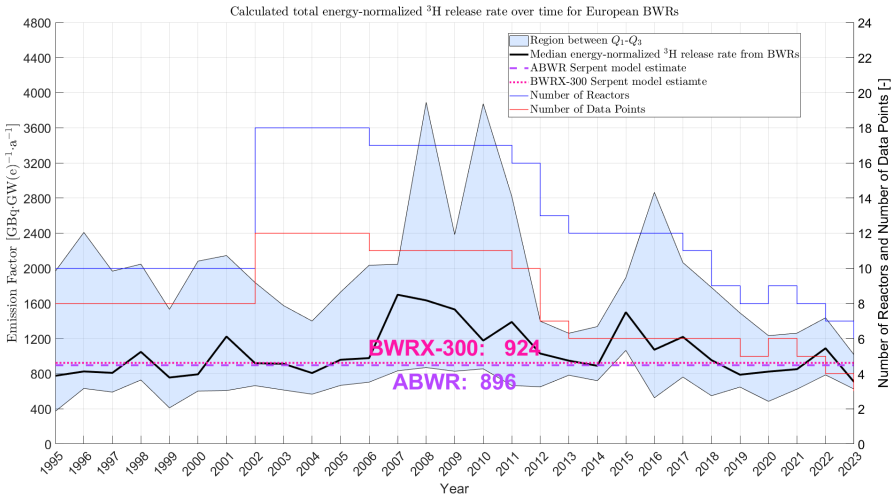

Figure 68: Normalized release rate of ^{3}H (liquid and atmospheric) from European BWRs, median and interquartile range [3]. The results of the Serpent simulations for the ABWR and the BWRX-300 are also indicated in the graph.

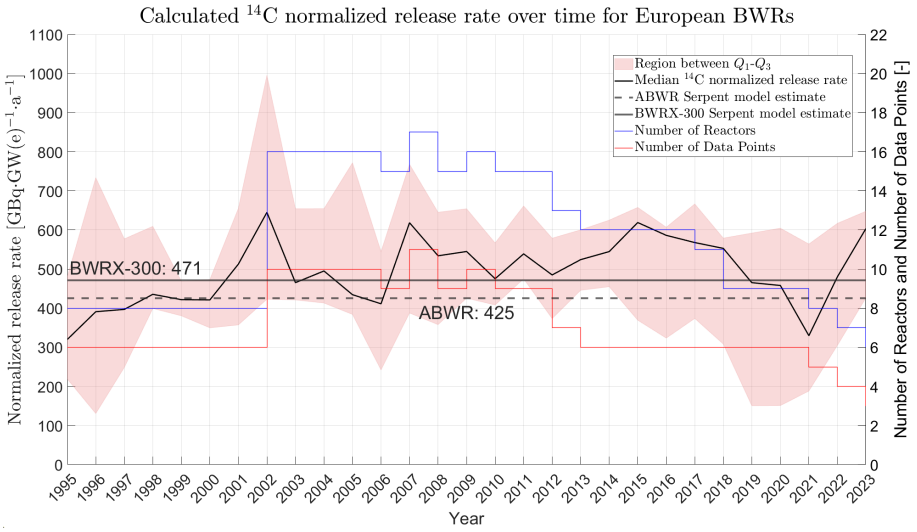

Figure 69: Normalized release rate of ^{14}C from European BWRs, median and interquartile range [3]. The results of the Serpent simulations for the ABWR and the BWRX-300 are also indicated in the graph.

Another way of estimating the release rate is by applying the results to the median release rates of European LWRs seen in Table 1. Since the discharge rate and production rate from the reactors are highly correlated, the normalized discharge rate from the smaller reactors is expected to be larger than conventional reactors by the same percentage as the production rate was. Applying this to the median normalized release rates which were found in the previous study, see Table 1 [3], the estimated normalized release rate of the RR SMR and the BWRX-300 are shown in Table 28.

Table 28: Estimated normalized discharge rate of the RR SMR and the BWRX-300. The values were estimated by applying the factor of increased production rate in the Serpent models to known values from European reactors [3]. These values are used in place of direct comparison to measurements from real AP1000s and ABWRs, as these are not available.

Reactor	^{3}H [GBq·GW(e)$^{-1}$·a^{-1}]	^{14}C [GBq·GW(e)$^{-1}$·a^{-1}]
RR SMR	1031	263.2
BWRX-300	1045	533.2

These results were however based on certain assumptions about the geometry and operating conditions of the reactors. Especially so for the RR SMR, for which there is little information available, but also to some extent for the BWRX-300. The sources of error that are expected to have had the largest impact are:

- The geometries of the RR SMR and the BWRX-300 have been made by filling in the unknown geometrical components with those from other reactors. More so in the case of the RR SMR, since the BWRX-300, at least in terms of the core, is expected to be fairly accurate. The RR SMR however had a severe lack of available information, due to which the entire core design is mostly guess-work.

- The simplified operating cycle. Serpent does not calculate the total production of radionuclides, but rather the inventory at a certain time step which include decay. For a full year of operation, this would have been a significant amount for ^{3}H, due to which the reactors were only run for 1 second to find the instantaneous production instead. Since the value found in this way is simply scaled to a full year of operation, it does not accurately capture the operation cycle of the reactors, though the impact of this on the results is difficult to quantify.

- Since the models are made without thermal-hydraulic calculations, there is a limit to how accurately the physics can be captured. This simplification of the models is therefore expected to have had a significant impact on the results.

- Physical processes such as diffusion, desorption and leakage from the coolant system are difficult to account for. In the estimations above, only diffusion from the fuel was taken into account, and even then, a somewhat simple way of estimating it was adopted.

- Some material compositions, which could affect the end results are simplified, such as for example the coolant water. In reality the reactor coolant has a water chemistry, which unlike the pure H_2O used in the Serpent models contains other elements either added by purpose, or which have diffused, adsorbed or otherwise entered the coolant as it circulated the primary system of the reactor. There is also a possibility that novel design features which have not been taken into account could severely affect the presence of nuclides such as for example ^{14}N and ^{13}C in the coolant, thus increasing the production of ^{14}C.

7 Conclusions

Based on the results of the Serpent simulations conducted in the present report it is plausible that the operational releases per produced energy unit of the BWRX-300 could be slightly higher than in a traditional large BWR, on the order of 3 % for the ^{3}H discharges and 11 % for the normalized ^{14}C discharges. For the RR SMR the situation is slightly more complicated. The ^{14}C discharges are expected to increase by only about 1.34 %, while the ^{3}H discharges, owing to the fact that the RR SMR does not use boron for reactivity control, are expected to instead decrease by at least one order of magnitude. Applying these increases to known median values from European reactors (see Table 1) would result in an estimated normalized release rate of ^{14}C and ^{3}H on the order of 263.2 and 1031 GBq·GW(e)$^{-1}$·a^{-1} from the RR SMR, and 533.2 and 1045 GBq·GW(e)$^{-1}$·a^{-1} from the BWRX-300. It is important to mention however that the yearly variation for individual nuclear reactors is of a larger magnitude than the variation seen between the large and small reactors of this report [3], except in the case of the ^{3}H discharges from the RR SMR.

These results were however based on certain assumptions and approximations of the geometry and operating conditions of the reactors. Especially for the RR SMR, for which little information is available, but also to some extent for the BWRX-300. The impact on the end results is difficult to establish, though the results are expected to be of the right order of magnitude. To further investigate the topic, the Serpent models could be coupled to a thermal-hydraulics solver. Another change that could be made is to use a different software for the activation calculations, since this is not the primary functionality of Serpent. The Serpent models could then be used to find the flux-distribution which could then be used in another program to find the nuclide inventories, such as the ORIGEN code developed by Oak Ridge National Laboratory [33].

8 Acknowledgments

We would like to thank Christophe Demazière for his guidance in creating the reactor models, and using them to obtain results we could trust to be realistic. We would also like to thank NEA for holding an excellent course in Serpent 2 which we were able to attend. Thanks to Kristina Eriksson Stenström for her helpful inputs and commentary throughout working on this report, as well as with proofreading this report.

9 References

[1] IAEA. *Management of Waste Containing Tritium and Carbon-14*. Tech. rep. 421. IAEA, 2004.

[2] Å. Magnusson. *^{14}C Produced by Nuclear Power Reactors - Generation and Characterization of Gaseous, Liquid and Solid Waste*. PhD thesis. Lund University, 2007.

[3] S. Brandt, F. Öhrlund, and K.E Stenström. *^{14}C and ^{3}H releases from Pressurised Water Reactors and Boiling Water Reactors*. Tech. rep. Lund University, 2025. URL: https://lup.lub.lu.se/search/publication/b95b56e0-3b88-46bc-9a5a-adc5f7af5a27.

[4] Vattenfalls pressavdelning. *Vattenfall tar nästa steg för ny kärnkraft vid Ringhals*. Vattenfall. URL: https://group.vattenfall.com/se/nyheter-och-press/pressmeddelanden/2024/vattenfall-tar-nasta-steg-for-ny-karnkraft-vid-ringhals (visited on 05/27/2025).

[5] L. M. Krall, A. M. Macfarlane, and R. C. Ewing. *Nuclear waste from small modular reactors*. In: *Proceedings of the National Academy of Sciences* 119.23 (2022), e2111833119. DOI: 10.1073/pnas.2111833119.

[6] P. Darnowski et al. *Simulations of the AP1000-Based Reactor Core with Serpent Computer Code*. In: *Archive of Mechanical Engineering* 65 (2018). DOI: 10.24425/124484.

[7] Å. Magnusson et. al. *Characterization of ^{14}C in Swedish Light Water Reactors*. In: *Health Physics* 95(2) (2008), S110–S121. DOI: 10.1097/01.HP.0000309765.35223.14.

[8] C. E. Westerly J. E. Philips. *Sources of Tritium*. Oak Ridge National Laboratory, 1980.

[9] R. Capote Noy. IAEA. URL: https://www-nds.iaea.org/exfor/endf.htm (visited on 2025).

[10] Rolls-Royce SMR. *Environment, Safety, Security and Safeguards Case Version 2, Tier 1, Chapter 4: Reactor (Fuel and Core)*. Tech. rep. 2024. URL: https://gda.rolls-royce-smr.com/assets/documents/documents/rr-smr-e3s-case-chapter-4---reactor-fuel-and-core-v2-public-issue-clean.pdf.

[11] GE-Hitachi. *BWRX-300 General Description*. Tech. rep. 005N9751. Version Revision F. 2023.

[12] C. Demazière. Computer program developed as part of the course "Nuclear Power Technology - Past, present and future", Chalmers University of Technology, Gothenburg. 2024.

[13] Westinghouse. *AP1000 Design Control Document Rev.19 - Tier 2 Chapter 4*. Tech. rep. 2011. URL: https://www.nrc.gov/docs/ml1117/ml11171a500.html.

[14] RJ. McConn Jr et al. *Compendium of Material Composition Data for Radiation Transport Modeling*. Tech. rep. PNNL-15870 Rev. 1. Pacific Northwest National Laboratory, 2011. URL: https://www.pnnl.gov/main/publications/external/technical_reports/pnnl-15870rev1.pdf.

[15] NEA/OECD. *Proposed Spent Fuel Cask Geometry OECD Phase II-B Benchmark*. 1994.

[16] M. Holmgren. *X Steam, Thermodynamic properties of water and steam*. MATLAB Central File Exchange. URL: https://se.mathworks.com/matlabcentral/fileexchange/9817-x-steam-thermodynamic-properties-of-water-and-steam (visited on 04/01/2025).

[17] Advanced Reactor Information System (ARIS). *Small Modular Reactor Catalogue*. Tech. rep. IAEA, 2024. URL: https://aris.iaea.org/publications/SMR_catalogue_2024.pdf.

[18] Y. Adolfsson, O. Bäckström, and K. Zander/Scandpower. *Säkerhetsredovisning för drift av slutförvarsanläggning för använt kärnbränsle (SR-Drift) kapitel 8 - Säkerhetsanalys*. Tech. rep. 1091141. Version 3. SKB, 2010.

[19] S.P. Murray. *GNF-A Response to NRC Request for Additional Information Dated 12/23/10 for Model No. RAJ-11 Package*. 2011. URL: https://citeseerx.ist.psu.edu/document?repid=rep1&type=pdf&doi=5bd9ffb8bc96cf200105e4a5a56d940585474d38 (visited on 03/20/2025).

[20] A. Peakman et al. *Development of an equilibrium loading pattern and whole-core fuel performance assessment in the Advanced Boiling Water Reactor (ABWR) with UO2 and U3Si2 fuels*. In: *Progress in Nuclear Energy* 117 (2019), p. 103053. ISSN: 0149-1970. DOI: https://doi.org/10.1016/j.pnucene.2019.103053. URL: https://www.sciencedirect.com/science/article/pii/S0149197019301489.

[21] GE Nuclear Energy. *ABWR Design Control Document, Rev.4*. Hitachi-GE Nuclear Energy, Ltd, 1997.

[22] A. Detkina. *Optimising BWR spent fuel storage using burnup credit method and exploring other solutions for the management of high-level waste*. PhD thesis. University of Liverpool, 2021.

[23] General Electric Company. *General Electric Systems Technology Manual Chapter 2.2: Fuel and Control Rods System*. Tech. rep. 2011.

[24] Ltd Hitachi-GE Nuclear Energy. *The ABWR General Plant Description*. 2007.

[25] N. H. Larsen. *Core Design and Operating Data for Cycles 1 and 2 of Peach Bottom 2*. Topical Report EPRI NP-563. Prepared for the Electric Power Research Institute, Project 1020-1. San Jose, California: General Electric Company, Nuclear Energy Engineering Division, June 1978. URL: https://www.nrc.gov/docs/ML1125/ML11258A302.pdf.

[26] NEA. *Physics of Plutonium recycling*. In: *OECD Publishing* VII (2003).

[27] Righton Blackburns Metals and Plastics. *S20910 (XM-19) Bar & Sheet*. URL: https://www.rightonblackburns.co.uk/datasheets/view/stainless-steel-s20910-xm-19-bar-sheet (visited on 05/2025).

[28] Steelpro Group. *SA508, A508, Low Alloy Steel, Pressure Vessel Steel*. URL: https://steelprogroup.com/nuclear-grade-steel/sa508/ (visited on 03/2025).

[29] GE Hitachi. *UK ABWR Generic Design Assessment - Generic PCSR Chapter 11 : Reactor Core*. Hitachi-GE Nuclear Energy, Ltd, 2017.

[30] GE Nuclear Energy. *ABWR Design Control Document, Rev.0*. Hitachi-GE Nuclear Energy, Ltd, 1997.

[31] Harvey Taylor. *Annual Radioactive Effluent Release Report 2024, Vogtle Electric Generating Plant Units 3&4*. NRC, 2024.

[32] Q. Wang. *Estimation of tritium generation and discharge of the AP1000 reactor based on historical discharge data from the U.S. pressurised water reactors*. In: *Nuclear Technology and Radiation Protection* 38.2 (2023), pp. 80–87. DOI: 10.2298/NTRP2302080W.

[33] Oak Ridge National Laboratory. *ORIGEN*. URL: https://www.ornl.gov/project/origen (visited on 2025).

[34] C. Demazière. *Modelling of Nuclear Reactor Multi-Physics*. Elsevier, 2020. ISBN: 9780128150696. DOI: 10.1016/c2017-0-01631-2. URL: http://dx.doi.org/10.1016/C2017-0-01631-2.

[35] C. Demaziére. *Physics of Nuclear Reactors*. Textbook, Chalmers University of Technology, Gothenburg, Sweden, 2017.

Appendix

A1 Discrepancies in Serpent results with different evaluated nuclear data file libraries.

Initially the Serpent models were run using ENDF/B-VII.1. The results for ^{3}H and ^{14}C production in the coolant with this nuclear data library was within reason, but the ternary fission yield of ^{3}H was about 3-4 orders of magnitude less than expected. When running the models instead with JEFF-3.2, the ternary fission yield of ^{3}H was more reasonable, but the ^{14}C production in the coolant was approximately cut in half compared to running with ENDF/B-VII.1. It was also noticed that all models both large and small, PWR or BWR, had essentially the same normalized ^{14}C production, which was unexpected. The models were then run with a third ENDF library JENDL-4.0 for comparison, which showed similar production of ^{3}H and ^{14}C in the coolant as with ENDF/B-VII.1, and similar ternary fission yield of ^{3}H as with JEFF-3.2.

The present authors are of the opinion that the results obtained with JENDL-4.0 are the most reasonable overall given prior expectations, and therefore all results have been obtained using the JENDL-4.0 library.

As a final note on the topic of the nuclear data libraries, it is mentioned that it remains unclear why these problems have been encountered. It has, however, been conclusively determined that it is in fact the libraries themselves that are the root cause of the problem, since the entire difference seen stem from only changing the nuclear data libraries used, keeping the model geometry and materials definitions used fixed.

A2 Derivation of equation 1

The argument now provided assumes familiarity with reactor theory. For references on reactor theory, see [34, ch. 2][35, ch. 3]. Note that the argument here requires the assumptions specified in sections 2.1 and 2.2.

The argument essentially relies on showing that for a homogeneous cylindrical LWR of (extrapolated) radius R and height $H := \alpha R$, where $\alpha \in \mathbf{R}_+$ operating at critical steady-state conditions, the total net neutron leakage out of the system per unit energy production will increase non-linearly with decreasing reactor size. Note that in this setup the height to radius ratio α is supposed to be fixed, meaning the reactor size is described by a single parameter, namely the radius R, and the non-linearity is supposedly quadratic in R. This extra leakage will in turn mean higher irradiation of the materials surrounding the core, much of which is coolant, per unit energy, thereby generating higher operational releases per unit energy.

Assuming that the electrical power is linear in the thermal power, it suffices

to consider the thermal power. The total thermal power of the reactor can be expressed as

$$\begin{aligned} Power &= \int_{\mathbf{R}_+} \mathrm{d}E \int_V \mathrm{d}^3\vec{\mathbf{r}}\, \kappa(\vec{\mathbf{r}}, E)\Sigma_f(\vec{\mathbf{r}}, E)\phi(\vec{\mathbf{r}}, E) \\ &= V(\kappa\Sigma_f\phi) \end{aligned}$$

where κ, Σ_f and ϕ refer to quantities that are spatially homogenized and energy-condensed over the entire core volume V and over all neutron energies $\mathbf{R}_+$.

The net leakage of neutrons through the core boundary[11] can generally be expressed as the surface integral

$$\text{Leakage} = \int_{\mathbf{R}_+} \mathrm{d}E \oint_{\partial V} \mathrm{d}^2\vec{\mathbf{s}} \cdot \vec{\mathbf{J}}(\vec{\mathbf{r}}, E)$$

This expression for the net leakage cannot be simplified without invoking the assumptions listed above. Invoking those assumptions and using 1G-diffusion theory allows the net leakage to be simplified using the steps

$$\begin{aligned} &\vec{\mathbf{J}}(\vec{\mathbf{r}}, E) = -\vec{\boldsymbol{\nabla}} \cdot D(\vec{\mathbf{r}}, E)\vec{\boldsymbol{\nabla}}\phi(\vec{\mathbf{r}}, E) = -D\nabla^2\phi(\vec{\mathbf{r}}, E) = DB_0^2\phi(\vec{\mathbf{r}}, E) \\ &\implies \int_{\mathbf{R}_+} \mathrm{d}E \oint_{\partial V} \mathrm{d}^2\vec{\mathbf{s}} \cdot \vec{\mathbf{J}}(\vec{\mathbf{r}}, E) = DB_0^2 \int_{\mathbf{R}_+} \mathrm{d}E \int_V \mathrm{d}^3\vec{\mathbf{r}}\, \phi(\vec{\mathbf{r}}, E) \\ &\implies Leakage = V\big(DB_0^2\phi\big) \end{aligned}$$

where D is the diffusion coefficient of the system, and B_0 is the eigenvalue of the fundamental mode of the critical reactor, i.e. B_0^2 is the so-called geometric buckling of the reactor. For the case of a axially finite homogeneous reactor core, the geometric buckling can in this setup be expressed as:

$$B_0^2 = \frac{j_0^2 + \pi^2/\alpha^2}{R^2},$$

where j_0 is the first zero of $J_0(x)$, i.e. the zeroth order Bessel function of the first kind, having the approximate value $j_0 \approx 2.4048$ [35, p. 116, 119, 126, 133–137]

The net leakage out of the system per unit (thermal) energy production can thus be expressed as a function of the geometric parameters α and R as

$$l(\alpha, R) \equiv \frac{Leakage(\alpha, R)}{Power(\alpha, R)} = \frac{D}{\kappa\Sigma_f}\left(j_0^2 + \frac{\pi^2}{\alpha^2}\right)\frac{1}{R^2} \tag{3}$$

Note that equation 3 is identical to equation 1 shown in section 2.2.

[11] per unit time/per neutron generation

A3 Issues with estimating the operational releases of ^{14}C and ^{3}H in the SMRs using equation 1

A question one might ask is that if equation 1 which is derived in Appendix A2 is deemed valid enough to inform us about the scaling of the energy-normalized leakage, couldn't it then also be used to directly estimate the total irradiation of the surrounding coolant, and therefore also the operational releases of ^{14}C and ^{3}H in the SMRs under consideration, also in a trustworthy way? The answer depends on the required precision, but regardless the answer is probably no. It is more important however that the difficult part in this case is to establish the property of trustworthy-ness.

Two issues are now highlighted with the theory underlying the derivation of equation 1, followed by a brief reflection.

The first issue with the mathematical model is that the material properties of the reactor core are modeled as spatially homogeneous throughout the core and as energetically condensed over the entire considered neutron energy range[12]. Using the macroscopic fission cross section Σ_f as an example, the homogenization and condensation procedure corresponds mathematically to

$$\Sigma_f = \frac{\frac{1}{V}\int_V \mathrm{d}^3\vec{\mathbf{r}} \int_0^{5k_bT} \mathrm{d}E\, \Sigma_f(\vec{\mathbf{r}},E)\phi(\vec{\mathbf{r}},E)}{\frac{1}{V}\int_V \mathrm{d}^3\vec{\mathbf{r}} \int_0^{5k_bT} \mathrm{d}E\, \phi(\vec{\mathbf{r}},E)}$$

It is clear from this expression that the operation of homogenization and condensation of any material property incurs on this variable dependencies on for instance the reactor size, which in this setup means dependency on R, and on the critical steady-state flux $\phi(\vec{\mathbf{r}},E)$. This in turn implies dependency on the net neutron leakage i.e. the very quantity being studied in the first place! Furthermore, while the homogenized and condensed materials properties are expected to vary with R slowly when compared to B_0^2 such that equation 1 can still be considered informative, the material properties certainly will not be constant in any exact sense. This can be shown quite easily, by simply considering the constraint imposed on the net neutron leakage per unit (thermal) energy from the condition of criticality, i.e. from the implications following from the condition that $k_{eff} = 1$. By starting from the general definition of the effective multiplication factor [34, eq. 2.38] obtained from the scaled neutron transport equation, we find:

$$\begin{aligned} k_{eff} = 1 &= \frac{\int_V \mathrm{d}^3\vec{\mathbf{r}} \int_{\mathbf{R}^+} \mathrm{d}E\, \nu(\vec{\mathbf{r}},E)\Sigma_f(\vec{\mathbf{r}},E)\phi(\vec{\mathbf{r}},E)}{\int_{\mathbf{R}_+} \mathrm{d}E \oint_{\partial V} \mathrm{d}^2\vec{\mathbf{s}}\cdot\vec{\mathbf{J}}(\vec{\mathbf{r}},E) + \int_V \mathrm{d}^3\vec{\mathbf{r}} \int_{\mathbf{R}^+} \mathrm{d}E\, \Sigma_a(\vec{\mathbf{r}},E)\phi(\vec{\mathbf{r}},E)} \\ &= \frac{V(\nu\Sigma_f\phi)}{\text{Leakage} + V(\Sigma_a\phi)} \implies \\ \implies \mathit{Leakage} &= V(\nu\Sigma_f - \Sigma_a)\phi \end{aligned}$$

[12] Here it's taken as the typical thermal range i.e. $E \in [0, 5k_bT]$, where $5k_bT \approx 0.025$[eV].

Together with the expression of the total thermal power of the reactor, found in section 2.2, we find a new expression[13] for the function defined in equation 1:

$$l(\alpha, R) = \frac{Leakage(\alpha, R)}{Power(\alpha, R)} = \frac{\nu\Sigma_f - \Sigma_a}{\kappa\Sigma_f}$$

This alternative expression for the function $l(\alpha, R)$ serves only one purpose: to make it plainly obvious that for it to equal equation 1, it cannot be true that every quantity appearing in it is to good approximation constant in R [14].

The second issue with the mathematical model has to do with the boundary conditions used. For the establishment of the relation between the critical flux $\phi(\vec{\mathbf{r}}, E)$ and the total net neutron leakage it generates out of the core volume, the proper mathematical derivation involves solving the Helmholtz equation over the specified core geometry. This requires the specification of boundary conditions, and one standard method used in reactor physics is to employ so-called 'extrapolated distance' boundary conditions, which are based on neutron transport theory [35, p. 102-109]. This methodology is a powerful tool which is used to derive many results within reactor physics. In the derivation presented in section 2.2, this kind of boundary condition is necessary to establish the exact analytic relationship between the geometric buckling B_0^2 and the geometric parameters α and R.

The problem with these boundary conditions in this specific case is that they correspond to a spatially convex nuclear reactor core surrounded by a pure vacuum. This is equivalent to setting the incoming neutron current to zero everywhere on the core boundary. All four reactor cores considered in this report are surrounded by a reflector, as nuclear reactor cores typically are. Now, in the derivation of equation 1 the net neutron current across of the core boundary is used, a quantity which is significantly affected by the presence of a reflector. The purpose of any reflector is exactly to reflect back into the core as many neutrons as possible that leave the core through the core boundary. Therefore, the incoming neutron current will be non-zero across the core boundary. Strictly speaking, this invalidates the assumptions underlying the boundary conditions used to derive equation 1.

A reflector region can be included in the mathematical model explicitly by straight-forwardly changing the material throughout the space exterior to the core from a vacuum to a homogeneous non-multiplying medium which in this case is largely water. The interested reader is referred [35, p. 138-147] for treatment of the modified mathematical problem using both 2G and 1G diffusion theory. The reference is provided in favor of a rather lengthy and mostly off-topic discussion about reflectors and boundary conditions, and the discussion is

[13] That this expression equals equation 1 is easily shown equivalent to the familiar result from 1G diffusion theory that $B_0^2(\alpha, R) = \frac{\nu\Sigma_f - \Sigma_a}{D}$

[14] Of course, one could go further by examining more closely how these R-dependencies behave, for instance by using that $\phi(\vec{\mathbf{r}}, E)$ is known analytically in the setup under consideration.

instead moved on to the next topic, namely why any of these issues have been brought up in the first place.

The two issues raised above strikes the current author as being of the annoyingly familiar kind that one encounters in physics when attempting to study a complex problem using a physical model that is too simple for the job.

The resolution of the two problems raised requires one to be able to judge whether or not certain more or less finely detailed inaccuracies of the mathematical model are significant or not in relation to the obtained result. Providing such judgment based on theory alone when it isn't an option to defer to any prior established knowledge[15] is difficult for something as physically subtle as a nuclear reactor core[16].

A third very brief example highlights perfectly the kinds of validity judgement issues that arises; equation 1 treats perfectly cylindrical reactors. This is often a very reasonable approximation as the fuel assembly lattice layout of most LWRs is arranged in such a way as to approximate a cylinder. But the BWRX-300 is an exception, having an octagonal lattice configuration. An octagonal lattice still approximates a cylinder, just less well. The point of this example is that it is difficult to say, using theory alone, precisely how much this matter. What should the value of R be for the BWRX-300?

The problem of estimating the operational releases of ^{14}C and ^{3}H in the two SMRs under consideration could of course be solved in a trustworthy manner from theory alone. This would likely require one to switch over to more powerful theoretical tools than those underlying equation 1, at least if one must achieve results of any significant level of precision. Or one could use some other method for solving the problem.

In the modern age, problems like the one faced here can often be solved by utilizing the speed of modern CPUs and the availability of high-capacity RAM.

This is precisely what high-resolution 3-dimensional full-core Serpent 2 models accomplish in this research project. How Serpent 2 is used for this purpose is the topic of section 2.3.

[15] i.e. when one doesn't already know what the answer is beforehand.

[16] As a precautionary measure against any kind of misunderstanding it is mentioned that this is **not** a critique of theory in general.